DISSERTATION

submitted to the
Combined Faculties for the Natural Sciences and for Mathematics
of the Ruperto-Carola University of Heidelberg, Germany
for the degree of
Doctor of Natural Sciences

Presented by:
M.Sc. Yan Yu
Born in: Hubei, P.R. China

Oral examination: May 10th, 2013

Manipulation of Neuronal Activity with Light-activated Ion Channels

Referees : Prof. Dr. Hilmar Bading
Prof. Dr. Christoph Schuster

Summary

Neuronal activity is required for proper neural development, as well as for the maintenance of neural circuits, adaptation to changing environments, learning and memory formation. Electrical activation of neurons induces transient increases in the intracellular calcium (Ca^{2+}) concentration, which can propagate to the nucleus thereby linking synaptic stimulation to gene regulatory events. However, it is unclear if and how different spatial-temporal patterns of activity give rise to distinct genomic responses. In this thesis I used optogenetic method to investigate activity dependent regulation of signaling pathways and gene expression in cultured hippocampal neurons. The goal was to investigate whether intrinsic activity could be mimicked in a controllable way, and if yes, how this was achieved. Specifically, I used Channelrhodopsin (ChR2), a light-gated, cation-selective, small membrane channel isolated from *Chlamydomonas reidhardtii*. ChR2 can be activated with blue light and functions without any addition of cofactor when expressed in mammalian systems. I used transfection and adeno-associated virus-mediated gene transfer to express ChR2 in cultured hippocampal neurons, which afterwards could be stimulated and activated with blue LED pulses to reliably induce action potential firing and Ca^{2+} transients. A double mutant variant of ChR2, ChR2-ab, was made, characterized and its cellular functions were studied. The results indicated that ChR2-ab inherited the properties from its previous single mutant, being more sensitive, longer opening and bi-stable. Neurons expressing ChR2-ab responded to light exposure with membrane depolarization, which ultimately led to the expression of a previously characterized pool of activity-dependent genes. ChR2-ab-mediated induction of these genes was L-type voltage-dependent Ca^{2+} channel dependent, as it was completely blocked with nifedifine. Similarly, treatment of ChR2-ab-expressing neurons with NMDA receptor blockers MK-801 and APV inhibited the light-evoked induction of *atf3, ifi202b, inhba* and *serpinb2*. When synaptic activity was inhibited with Na^{+} channel blocker TTX to prevent action potential firing, ChR2-ab-mediated gene induction of *atf3, inhba, npas4, nr4a1* and *serpinb2* was also restrained. Expression of CaMBP4, an inhibitor of nuclear Ca^{2+}/CaM complex, revealed that ChR2-ab-mediated gene induction dependent on nuclear Ca^{2+} signaling. Interfering the function of CREB/CBP transcription complex with E1A protein diminished gene expression induced with ChR2-ab. Whole-cell patch-clamp and signaling pathway analysis revealed that neurons expressing ChR2-ab had higher basal activity, with more frequent mEPSC and higher level of pCREB and pERK. However, some ChR2-ab-expressing cells died after light application on day *in vitro* 14. Pharmacological analysis suggested that this was due to activation of extra-synaptic NMDA receptors during ChR2-ab activation. In an alternative strategy to induce activity, ChR2 was targeted to the membrane of endoplasmic reticulum using various targeting sequences with the goal to directly trigger Ca^{2+} release from this internal Ca^{2+} store. Additionally, transcription analysis with catFISH method revealed that a single nuclear Ca^{2+} transient induced with Bicuculline treatment was capable and sufficient to initiate transcription of *arc* gene.

Zusammenfassung

Die Neuronale Aktivität ist für eine ordnungsgemäße Nervenentwicklung, sowie für die Erhaltung neuronaler Schaltkreise, für Adaptation auf sich ändernde Umgebungen und für das Lernen als auch für die Bildung des Gedächtnisses erforderlich. Die elektrische Aktivierung von Neuronen führt zu vorrübergehenden Erhöhungen der intrazellulären Kalziumkonzentration (Ca^{2+}), die zum Zellkern weitergeleitet werden kann, wodurch eine synaptische Stimulation mit der Genregulation verbunden wird. Es ist jedoch unklar, ob und in welcher Art räumliche und zeitliche Aktivitätsmuster zu unterschiedlichen genomischen Antworten führen. In dieser Arbeit habe ich optogenetische Methoden verwendet, um aktivitätsabhängige Regulierungen der Signalwege und der Genexpression in Zellkulturen von hippocampalen Neuronen zu untersuchen. Es war das Ziel herauszufinden, ob intrinsische Aktivität auf kontrollierbare Weise nachgeahmt werden kann, und wenn dies möglich ist, wie dies erreicht werden kann. Dafür verwendete ich Channelrhodopsin (ChR2), ein kleiner licht-gesteuerter, Kationen-sensitiver Membrankanal, welcher aus *Chlamydomonas reidhardtii* isoliert wurde. ChR2 kann mit blauem Licht angeregt werden und kann bei der Expression im Säugertiersystem ohne Zugabe von Cofaktoren seine Funktion ausführen. Ich verwendete Transfektionen und Adeno-assoziierten Virus-vermittelten Gentransfer, um ChR2 in kultivierten hippocampalen Zellen zu exprimieren. Später können diese mit blauem LED-Licht angeregt werden, um zuverlässig Aktionspotentiale und Ca^{2+}-Ströme zu erzeugen. Zusätzlich habe ich eine Doppelmutante von ChR2, Chr2-ab hergestellt, diese charakterisiert und ihre zellulären Funktionen untersucht. Die Ergebnisse zeigen, dass ChR2-ab die Eigenschaften seiner Vorläuferversion beibehalten hat, darüber hinaus empfindlicher ist, zu einer längeren Öffnung des Kanals führt und bistabil ist. Bestrahlt man nun Neuronen, die ChR2 expremieren, mit blauem Licht, so führt dies zur Membrandepolarisierung der Nervenzelle, wodurch letztendlich die Expression von bekannten aktivitätsabhängigen Genen induziert wird. Die ChR2-ab-vermittelte Induktion dieser Gene war abhängig von L-Typ spannungsabhängigen Kalziumkanälen, da diese durch Verwendung von Nifedipine vollständig blockiert werden konnten. Zudem führt die Behandlung mit NMDA-Rezeptor Blocker MK801 und APV in ChR2-ab exprimierenden Neuronen zur Inhibierung der Licht-induzierten Expression von *atf3, ifi202b, inhba* und *serpinb2*. Wenn synaptische Aktivität mit dem Natrium-Kanal Blocker TTX inhibiert wurde, um zu verhindern, dass Aktionspotentiale ausgelöst wurden, wurde die ChR2-ab-vermittelte Induktion der Gene *atf3, inhba, npas4, nr4a1* und *serpinb2* verringert. Die Expression von CaMBP4, einem Inhibitor des nukleären Ca^{2+}/Calmodulin-Komplexes, führte dazu, dass eine ChR2-ab-vermittelte Geninduktion von kernständigem Ca^{2+} abhängig ist. Wenn man mit dem E1A Protein in die Funktionsweise des CREB/CBP Transkriptionskomplexes eingreift, wird die ChR2-ab-induzierte Genexpression zusätzlich verringert. "Whole-cell Patch-Clamp" und eine Untersuchung der Signalwege haben gezeigt, dass Neuronen, die ChR2-ab exprimieren, häufiger mEPSCs (mini excitatory postsynaptic currents) und eine höhere Menge an pCREB und pERK aufweisen und somit eine höhere Basalaktivität haben. Jedoch starben einige ChR2 exprimierende Zellen nach der Anwendung von Licht an Tag *in vitro* 14. Pharmakologische Untersuchungen wiesen darauf hin, dass dies durch die Aktivierung der extrasynaptischen NMDA Rezeptoren während der Aktivierung

von ChR2-ab verursacht wurde. In einem weiteren Ansatz zur Induktion der Aktivität wurde ChR2 durch Verwendung verschiedener Zielsequenzen an die Membran des Endoplasmatischen Reticulums lokalisiert, mit der Zielsetzung eine Ca^{2+} -Freisetzung unmittelbar aus diesen internen Ca^{2+}-Speichern auszulösen. Zusätzlich wurde eine Transkriptionsanalyse mit der catFISH Methode durchgeführt, in der gezeigt wurde, dass ein einziger, durch Bicuculline Behandlung induzierter, kernständiger Ca^{2+} Strom ausreicht, um die Transkription des Gens *arc* zu initiieren.

Acknowledgements

I would like to express my gratitude to all those who gave me the possibility to start and complete this thesis.

First of all, I would like to thank Prof. Hilmar Bading for his great supervision, invaluable support, stimulating suggestions and constant encouragement during the whole process of the work. I also thank Prof. Chrostoph Schuster for kindly accepting to become the second supervisor of this thesis.

I want to thank following institutions for funding my PhD position and research: the Hartmut Hoffmann-Berling International Graduate School of Molecular and Cellular Biology (HBIGS), individual fellowship through the Landesgraduiertenförderung (LGFG), Deutsche Forschungsgemeinschaft (DFG) and European Research Council (ERC).

I thank all the friends and colleagues in the Bading lab. Life without them in the lab would have been much more difficult. Thanks to Ana M. M. Oliveira for lots of great ideas, encouragement and proofreading of my thesis. Thanks to C. Peter Bengtson for his introduction to electrophysiology and calcium imaging methods, his patient instructions, his help for my experiments up there in the E-Phys lab. Thanks to Anna M. H. Hertle for her suggestions, problem-solving discussions at neighboring desk, GCaMP3nls viruses and critical comments on this thesis. Thanks to David Lau for always being willing to answer my questions, for his great help in finding and designing the targeting sequences at the starting phase of the project and proofreading of my thesis summaries. Thanks to H. Eckehard Freitag for providing the firing pattern of Bic induced activity and all the MEA recordings of different ChR2 variants at different culture stages, all the help with rat culture and proofreading my thesis. Thanks to Bettina Buchthal for teaching me the catFISH protocol, for her patience in helping me troubleshooting the experimental problems and comments on my thesis summaries. Thanks to Daniela Mauceri for teaching me all the experimental assays during my PhD and for providing me with the E1A and related viruses. Thanks to Yan-Wei Tan for discussion of my results and all the free-time chats. Thanks to Thekla Hemstedt for helping me with Latex, translating the summary of my thesis and help within and outside the lab. Thanks to Carlos Bas-Orth, Sara Monaco and Stefanie Hayer for being around and helping me with scientific and nonscientific problems. Thanks to Otto Bräunling for all the supports of the daily life in the lab. Thanks to Irmela Meng for her professional and effective administration related work. Thanks to Iris Bünzli-Ehret for providing all the culture for my thesis work. Thanks to Ursula Weiss, Andrea Hellwig, Monika Keusch, Oliver Teubner and Alan Summerfield for their excellent job for supporting my work and life in the lab.

I thank my family for their understanding and endless support. Without them I would not be able to have the chance to study abroad or finish this thesis work.

A special thanks goes to my boyfriend Zhuang Lin for his understanding and supporting. Thanks to him for introducing me the Latex, it is great.

Heidelberg January 2013

Yan Yu

Contents

List of Figures

List of Tables

List of Abbreviations

β-ME	β-mercarptoethanol
AAV	Adeno-Associated Virus
aCSF	artificial Cerebrospinal Fluid
AD	Alzheimer's Disease
AM ester	Acetoxymethyl ester
AMPA	α-amino-3-hydroxy-5-methyl-4-isoxazolepropionic acid
ATR	all-*trans* retinal
Bic	Bicuculline
BSA	Bovine Serum Albumin
Ca^{2+}/CaM	Calcium/Calmodulin complex
CaM	Calmodulin
CaMBP4	Calmodulin Binding Protein 4
CaMKIV	Calcium/calmodulin-dependent protein kinase type IV
CatCh	Calcium translocating channelrhodopsin
catFISH	Cellular Compartment Analysis of Temporal Activity by Fluorescence In Situ Hybridization
CBP	CREB Binding Protein
CDK1	Cyclin Dependent Kinase 1
ChoP	Channelopsin
ChR2	Channelrhodopsin 2
CICR	Ca^{2+} Induced Ca^{2+} Release

CMKII	Ca^{2+}/CaM dependent protein kinase II
CMKIV	Ca^{2+}/CaM dependent protein kinase IV
CNS	Central Nervous System
cpFP	circularly permuted fluorescent protein
CRE	Cyclic-AMP Response Element
CREB	Cyclic-AMP Response Element Binding protein
DEPC	Diethylpyrocarbonate
DIV	day *in vitro*
DMSO	di-methylsulfoxide
DNA	Deoxyribonucleic Acid
EE	Enriched Environment
eEPSC	evoked Excitatory Postsynaptic Current
ER	Endoplasmic Reticulum
ERK	Extra-cellular signal Regulated Kinase
EtBr	Ethidium Bromide
EtOH	Ethanol
FAM	Fluorescein amidite
FISH	Fluorescence In Situ Hybridization
FRET	Fluorescence Resonance Energy Transfer
GABA	γ-aminobutyric acid
GECI	Genetically Encoded Ca^{2+} Indicator
GOF	Gain of Function
HEK-293	Human Embryonic Kidney 293 cell line
hGH polyA	human Growth Hormone polyA
ICC	Immunocytochemistry
IEG	Immediately Early Gene

IEI	Inter Event Interval
INM	Inner Nuclear Membrane
IP_3R	Inositol 1,4,5-triphosphate Receptor
ITR	Inverted Terminal Repeat
Kd	Dissociation constant
LB	Lysogeny Broth
LED	Light-Emitting Diode
LOF	Loss of Function
LTP	Long Term Potentiation
M.W.	Molecular Weight
mEPSC	miniature Excitatory Postsynaptic Current
mOsm	milliosmole
NGS	Normal Goat Serum
NLS	Nuclear Localization Sequence
NMDA	N-methyl-D-aspartate
ONM	Outer Nuclear Membrane
ORF	Open Reading Frame
PBS	Phosphate Buffered Saline
PBST	Phosphate Buffered Saline with Tween 20
PCR	Polymerase Chain Reaction
pCREB	phosphorylated CREB at Ser133 site
pERK	phosphorylated ERK1/2, dually phosphorylated at Thr202 and Tyr204 of ERK1, Thr185 and Tyr187 of ERK2
PFA	paraformaldehyde
PLC	Phospholipase C enzyme
PLCγ1	Phospholipase C, gamma 1
PMT	Photomultiplier tube

Pol II	Polymerase II
PSD	Post-Synaptic Density
Q-PCR	Quantitative Polymerase Chain Reaction
rAAV	recombinant AAV
RNA	Ribonucleic Acid
rpm	round per minute
RyR	Ryanodine Receptor
SCC	Saline-Sodium Citrate buffer
SDS-PAGE	Sodium Dodecyl Sulfate Polyacrylamide Gel Electrophoresis
SFO	Step Function Opsin
SSFO	Super Step Function Opsin
TBST	Tris Buffered Saline with Tween 20
TM	Transmembrane domain
Tm	Melting temperature
TnC	Troponin C
TTX	Tetrodotoxin
VDCC	Voltage-Dependent Calcium Channel
WPRE	Woodchuck Hepatitis Virus (WHP) Posttranscriptional Regulatory Element

Chapter 1

Introduction

1.1 Activity-dependent Gene Expression

Extrinsic activity input plays essential roles in the proper development of neural circuitry during the early stage, in the adulthood to maintain normal function and to form long-lasting memories and other adaptations [8, 108, 145]. In infancy and also in adult, the memories and adaptations are ultimately mediated by experience-driven changes in connectivity of neural network [1]. These changes are central to our everyday lives and are tragically disrupted in numerous neurological, psychiatric, and neurodegenerative disorders [29]. Gene expression is believed to be the central mediator for this connectivity change [137]. Neurons change their gene expression patterns according to the inputs they have received [105, 157]. Many genes are known to be regulated by neural activity and some of them are essential for the formation of the chemical and structural changes according to the activity input. These gene products are believed to affect dendrite development, axon branching, formation of synapses between axon and dendrite, and stabilizing the activity-dependent refinement of the neural circuits [31, 40, 151, 155]. This is important for synaptic plasticity, which is the capability for modification of the strength of neuronal connections [67]. And these kinds of long-lasting changes in the strength of synaptic connections modified by gene transcription are believed to be the cellular mechanism for memory formation [3, 131]. Several cellular signaling pathways are activated according to the neural activity; these signaling pathways often affect the transcription of neuronal genes [2]. Responding to synaptic activity, Ca^{2+} influx through NMDA receptors or L-type VGCC activates Ca^{2+} dependent kinase CaMKII or CaMKKIV, which phosphorylate CREB at Ser 133. Phosphorylated CREB binds to its coactivator CBP/p300 and activates the transcription of its downstream genes. The neural activity-dependent expression of genes is also affected by epigenetic processes such as methylation of DNA or modification of histones [4].

Studies in nonhuman animals suggest that more stimulating environment could aid the treatment and recovery of a diverse variety of brain related dysfunctions, including Alzheimer's disease and those connected to aging, whereas lack of stimulation might impair cognitive development [34, 66, 72, 146]. Brains in richer, more stimulating environments, have increased numbers of synapses, and

the dendrite arbors upon which they reside are more complex [143]. With extra synapses there is also increased synapse activity and so increased size and number of glial energy support cells. The requirement of for activation of transcription for neuronal plasticity is best studied using long-term potential (LTP). LTP is a long-lasting enhancement in signal transmission between two neurons that results from stimulating them synchronously [33]. It is believed to be the major phenomena underlying synaptic plasticity, the ability of chemical synapses to change their strength. Memories are thought to be encoded by modification of synaptic strength, so LTP is widely accepted as the major cellular mechanisms for learning and memory [20, 19].

1.1.1 Synaptic and Extrasynaptic NMDA Receptors

NMDA receptors are cation channels gated by neurotransmitter glutamate and are one of the major Ca^{2+} permeable receptors in neurons [63, 65]. NMDA receptors are vital for normal brain functions [1]. They are central to activity-dependent changes in synaptic strength and connectivity

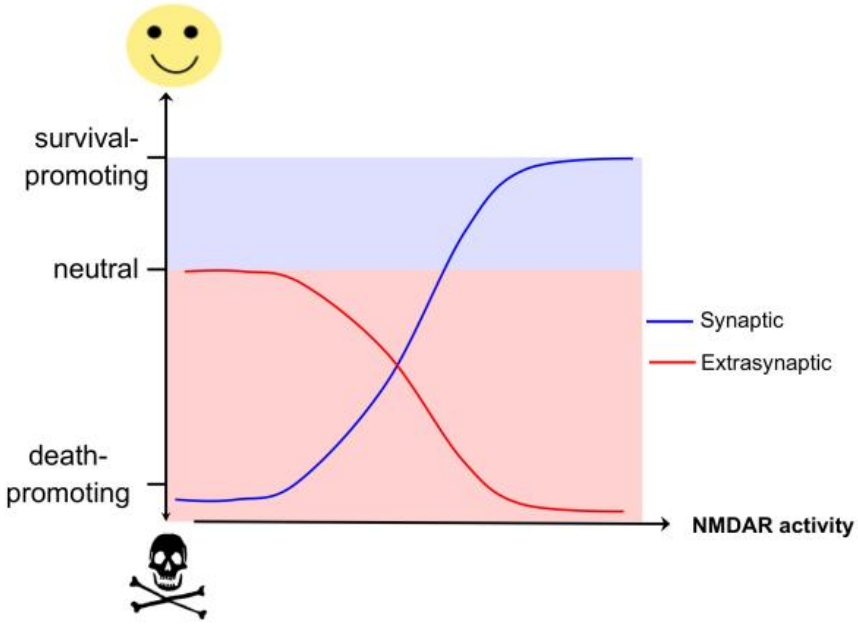

Figure 1.1: Schematic illustration of opposing effects of synaptic and extrasynaptic NMDA receptors on cell survival. Figure is obtained from [59].

which are thought to be underlying the formation of memory and learning [158]. During the development, NMDA receptors switch in sub-type and change their location [35, 138]. There has been a long-standing paradox about NMDA receptors being both neuron-protective and neuron-lethal [58]. Growing evidence suggests that physiological level of synaptic NMDA receptors activation can promote neuron survival and render them more resistant to deleterious insults [106, 157]. Previous data show that hippocampal neurons have two functionally distinct NMDA receptor signaling pathways [59]. Synaptic complexes promote nuclear signaling to CREB, induce BDNF gene expression, and activate an anti-apoptotic pathway; extrasynaptic complexes antagonize nuclear sig-

naling to CREB, block induction of BDNF expression, and are involved in mitochondrial dysfunction and cell death [139]. As illustrated in Figure 1.1, hypoactivity of synaptic NMDA receptors is harmful to neurons. Enhancing synaptic NDMA receptor activity triggers multiple neuroprotective pathways and this promotes neuronal survival. Low levels of activation of extrasynaptic NMDA receptors have no effects on neuronal survival but increasing the level of extrasynaptic NDMA receptor activity activates cell death pathways and exacerbates certain neurodegenerative processes, thus reducing neuronal survival [62]. For instance, the balance between synaptic and extrasynaptic NMDA receptor signaling was reported to control the formation of of mutant huntington inclusions, neurotoxicity and disease severity and progression in dodels of Huntington's disease [102].

1.1.2 CREB

Activity dependent activation of the transcription factor CREB (cyclic-AMP response element binding protein) is heavily implicated in synaptic plasticity, learning and survival [21, 88, 121]. Neural activity induces the phosphorylation of CREB and activates its gene transcription activity [27]. CREB is one of the major transcription activators mediating Ca^{2+} induced gene expression [4]. It was first isolated as a phosphor-protein binding the CRE (cyclic-AMP response element, 5′-TGACGTCA-3′) on the mouse somatostatin gene [95]. Upon discovery, it attracted focus from all fields, especially from neuroscience. Typical isoforms of CREB are αCREB, βCREB and ΔCREB [84, 120]. It plays important role in information storage and mice deficient in α and β forms of CREB have defective long term memory [22]. CREB is known to be generally constitutively expressed and activated via post-translational modifications such as phosphorylation. Phosphorylation of residue serine-133 is particularly important and regarded as a marker for CREB-mediated transcription [47]. CREB phosphorylation on serine-133 can be mediated by a number of protein kinases, including the multifunctional calcium/calmodulin (Ca^{2+}/CaM) dependent protein kinases (CaMK) II and IV [39]. Both CaMK II and IV have an N-terminal catalytic domain and a central Ca^{2+}/CaM binding regulatory domain. Activation of enzymes occurs when Ca^{2+}/CaM complex binds and displaces the auto-inhibitory domain. In addition to phosphorylation at serine 133 site, CREB can also be phosphorylated at serine 142 by CaMKII, which exhibits inhibitory effect on CREB mediated gene expression [130]. As CaMKIV is expressed dominantly in nucleus and efficient in activating CREB, it appears to be a prime candidate for the activation of CREB mediated gene expression by nuclear Ca^{2+} signals [90].

However, CREB phosphorylation on serine 133 does not necessarily indicate that CREB-dependent gene expression is induced [28]. It still needs recruitment of the co-activator CBP (CREB binding protein). CBP and its close relative p300 are vital components of the cellular machinery that regulate gene expression [77]. CBP binds specifically to phosphorylated CREB and can connect sequence-specific transcriptional activators to components of the basal transcription machinery and may disrupt repressive chromatin structures through its intrinsic or associated histone acetyltransferase activity [78]. Downstream of CREB, there are quite a large number of target genes. Among those, *c-fos* is one of the first and most extensively examined genes. *c-fos* has both CRE and SRE (serum response element) and its expression is tightly regulated by neuronal activity [37].

1.1.3 Immediate Early Gene: *Arc*

Neural activity-dependent gene transcription occurs over various time periods, ranging from minutes to days. One of the rapidest gene induction is observed in the transcriptional activation of a group of genes called the "immediate early genes" (IEG) [79]. These genes are activated rapidly and transiently in response to a wide variety of cellular stimuli without any other protein synthesis. They represent a standing response mechanism that is activated at the transcription level in the first round of response to stimuli. Thus IEGs are distinct from "late response" genes, which can only be activated later, following the synthesis of early response gene products [103]. About 40 cellular IEGs have been identified so far. The earliest known and best characterized include *c-fos*, *c-myc* and *c-jun*, genes that were found to be homologous to retroviral oncogenes [96]. In their role as "gateways to genomic response", many IEG products are naturally transcription factors or other DNA-binding proteins. However, other important classes of IEG products include secreted proteins, cytoskeletal proteins, and receptor subunits. One of these genes, *Arc*, encoding the activity-regulated cytoskeleton-associated protein, is transcribed in the rat brain as rapidly as 5 min after the animal has moved from its familiar home cage to a novel environment [142].

Arc is specially required for long-term memory formation and affects all of these forms of synaptic plasticity [123]. *Arc* is found only in vertebrates and is highly conserved [85]. Glutamatergic neurons in the brain express *Arc* in response to an increase in synaptic activity in a range of behavioral stimuli. Localization and stability of the transcript and protein are highly regulated. Arc protein is not found in presynaptic terminals or axons but is highly expressed in dendrites, the postsynaptic density and the nucleus [127]. *Via* regulating AMPA receptor endocytosis and surface inserting, *Arc* modulates synaptic transmission and plays a role in the homeostatic regulation of synaptic strength [30, 115].

Using a very sensitive method, cellular compartment analysis of temporal activity by fluorescent *in-situ* hybridization (catFISH), J.F. Guzowski *et al.* detected *Arc* mRNA in discrete intranuclear foci within minutes of neuronal activation and subsequent disappearance from the nucleus and accumulation in cytoplasm by 30 minutes [53]. Given the critical role in neuronal plasticity and memory formation and its fast transcription start, *Arc* was chosen as a model gene to study the minimal activity requirement for gene transcription initiation in this work.

1.2 Ca^{2+} in Neurons

In neurons, calcium ions (Ca^{2+}) control gene transcription induced by synaptic activity [44]. Ca^{2+} signals are key mediators of numerous adaptive changes in the nervous system that are initiated by electrical activity. It is the principal second messenger which controls diverse cellular mechanisms such as development, morphogenesis, learning and memory and other adaptations to environments [18]. To control multiple processes using a signal second messenger, neurons exploit the spatial and temporal differences of calcium signals associated with electrical activity. The states and histories of neuronal activity are represented by a calcium code that comprises the site of Ca^{2+} entry, and the amplitude, duration and spatial properties of signal-evoked Ca^{2+} transients [17]. The site of

Ca^{2+} entry can determine the biological outcome of calcium signaling, as shown by site-specific differences in the regulation of CREB-mediated transcription [57].

1.2.1 Ca^{2+} Entry

As the best well-known second message, Ca^{2+} plays extraordinarily important and versatile roles in every type of cell. It is responsible for coupling many of external events or stimuli to the cell's responses [32]. Ca^{2+} plays a central role to in the nervous system, as well as mediating other important processes such as activation of the immune system [25]. Its functional range includes such varied processes as secretion, contraction, metabolism, gene expression, apoptosis and learning and memory. During development, it is responsible for controlling numerous biological processes [18], including fertilization, proliferation, cell type specialization. Regular Ca^{2+} spikes sweep through the egg which will initiate internal Ca^{2+} induced Ca^{2+} release during fertilization. This regular pattern of Ca^{2+} spiking stimulates CAMKII, which then acts through CDC25 to dephosphorylate the enzyme cyclin-dependent kinase 1 (CDK1), resulting in cyclin B activation and the completion of meiosis. During the phase of cell proliferation, Ca^{2+} oscillates as the cell cycle does. Spontaneous Ca^{2+} transients trigger specific events such as nuclear envelope breakdown [76] and cell cleavage [26]. In lymphocytes, the signaling from antigen binding to the T-cell receptor will be transduced to phospholipase C, gamma 1 (PLCγ1), which produces both DAG and IP_3 for a prolonged Ca^{2+} elevation to activate proliferation [15].

In the central nervous system, Ca^{2+} plays vital roles in connecting neurons. Synaptic transmitter release from the presynaptic neuron activates the receptors on the postsynaptic membrane, opening of Ca^{2+} channels couples this chemical event to electrical changes of the cell [45]. Activity-induced Ca^{2+} influx into mature neurons affects synaptic function by acting both at the synapse and within the nucleus [11]. Long term potentiation (LTP), the proposed molecular model for learning and memory, will be impaired if Ca^{2+} influx from outside is blocked. Ca^{2+} signal in neurons has very strict spatial and temporal regulation to achieve this versatility [42]. In the case of synaptic specific stimulation, Ca^{2+} responses will be restricted only to those spines [86]. Individual spines can undergo input-specific, Ca^{2+}-dependent synaptic modifications during the process of learning and memory [160]. Between cell membrane, there is a ten thousand folds Ca^{2+} concentration difference: 100 nM in the cytoplasm and 1 mM outside. Ca^{2+} influx coming from outside in some cases is restricted to synapses to achieve the synapse-specific long term potentiation, and sometimes transduced to the nucleus to induce gene expression, global structural changes. Different apartments within neuron have different levels of Ca^{2+} and undergo diverse functions. For example, Ca^{2+} concentration in the endoplasmic reticulum (ER) is 100 μM [50], which is much higher than that in the cytoplasm and therefore ER serves as a good internal Ca^{2+} stores [141].

1.2.2 Ca^{2+} Buffering and Uptaking

Signal Ca^{2+} is derived either from the external medium or from internal stores. Entry of Ca^{2+} from the outside medium is driven by the presence of a large electrochemical gradient across the plasma

membrane. There are many different plasma-membrane receptor channels controlling Ca^{2+} entry from the external medium. Receptor-operated *N*-methyl-D-aspartate (NMDA) and voltage-operated Ca^{2+} channels are the two major sites for Ca^{2+} entry into hippocampal neurons. Differently located receptors or channels can induce various responses. It is well demonstrated that NMDA receptors sitting in the synaptic cleft mediate cell survival signal, while extrasynaptic NMDA receptors lead to neuronal death [139]. L-type Ca^{2+} channels are voltage gated and mainly sit on the cell body and proximal dendrites, which is an ideally position for providing Ca^{2+} signal inducing gene expression.

As mentioned above, Ca^{2+} concentration in the ER is much higher than that in the cytoplasm; this makes ER a perfect internal Ca^{2+} storage. And there are different Ca^{2+} channels on the ER membrane regulating the Ca^{2+} release from it, within which inositol 1, 4, 5-triphosphate receptors (IP_3R) and the ryanodine receptors (RyR) are the major mediators for internal Ca^{2+} release [14, 16, 24, 159]. Immunostaining of cerebellar Purkinje cells revealed that the receptor is expressed in the ER, nuclear envelope, and portions of the Golgi complex, but not mitochondria or plasma membranes [116]. The primary determinants for IP_3R are IP_3 and Ca^{2+}. IP_3 is generated by hydrolysis of phosphatidylinositol-4, 5-bisphosphate by a family of phospholipase C enzymes (PLCβ, PLCγ *et al.*) [148]. The binding of IP_3 increases the sensitivity of the receptor to Ca^{2+}. A special property of IP_3R is that it is also Ca^{2+} sensitive, meaning Ca^{2+} induced Ca^{2+} release (CICR) from these channels, which contributes to the rapid rise of Ca^{2+} levels and the development of regenerative Ca^{2+} waves [41].

In fact, Ca^{2+} is not free to diffuse in the cell, but that there are a lot of Ca^{2+} binding proteins buffering the movement of Ca^{2+}. Most of the Ca^{2+} that enters the cytoplasm is rapidly bound to various cytosolic buffers such as parvalbumin, calbindin and calretinin. Cytosolic buffers are involved in shaping both the amplitude and duration of Ca^{2+} signals. This is particularly important in neurons for that Ca^{2+} signals are largely confined to synapses. There is another family of Ca^{2+} buffers, termed as Ca^{2+} sensors, which respond to an increase in Ca^{2+} by activating diverse processes. The classical sensors are troponin C (TnC) and calmodulin (CaM) [43]; they have four EF hands that bind Ca^{2+} and undergo conformational changes to activate various downstream effectors. In the case of CaM, Ca^{2+}/CaM complexes activate the responsive downstream kinases, such as CaMKII and CaMKIV.

On the other hand, the cytoplasmic Ca^{2+} concentration can not always be so high after an increase. Once Ca^{2+} has carried out its signaling functions, it is removed from the cytoplasm by various pumps and exchangers. Ca^{2+}-ATPase pumps and Na^{+}/Ca^{2+} exchangers on the cell membrane extrude Ca^{2+} to the outside medium. And sarco-endoplasmic reticulum Ca^{2+}-ATPase (SERCA) pumps will return Ca^{2+} to the internal stores. Another important component of Ca^{2+} uptake mechanism is mitochondria. Mitochondria create an electrochemical gradient by excluding protons to synthesis ATP and also for Ca^{2+} uptake through a uniporter which has low sensitivity to Ca^{2+}.

For neurons, this elevated Ca^{2+} clearance is especially important as that neurons often respond to changes in stimulus intensity by varying the frequency of Ca^{2+} waves. Without this Ca^{2+} uptake, a steady level of the same average Ca^{2+} concentration will be maintained and this is much less efficient in signalling transduction, such as initiating gene expression [81].

1.2.3 Nuclear Ca^{2+}

Although remarkable progress has been made in revealing the signaling mechanism that regulates activity-dependent gene transcription, many questions remain to be answered. One is how synaptic signals are sent to the nucleus. Neural activity is received at the synapses, however, the signal is transduced into a nucleus that is located hundreds of microns distant from the synapses. One hypothesis is that the signal is transduced only as a membrane depolarization, which is, the neural activity itself. However, there are many different transcription factors that are activated by activity-dependent Ca^{2+} influx. How cells interpret these Ca^{2+} signals and convert them into specific transcriptional responses remains unclear. One way to circumvent that confusion inside the nucleus would be to send a specific signal to the nucleus only when synapses are activated at a specific input sufficient to modify their gene expression. Elevation of nuclear calcium is required for sustained gene expression induced by neuronal activity [11]. The sub-cellular pattern of Ca^{2+} signals is an important component of how this second messenger regulates cell function [55]. In neurons, Ca^{2+} controls gene transcription induced by synaptic activity. There are two strategies to couple external stimuli to transcription. The first one is that, close to the site of Ca^{2+} entry, it activates cytoplasmic signalling molecules. These then transduce the signal in a Ca^{2+} independently manner to the nucleus. Among those, extra-cellular signal regulated kinase (ERK) signalling cascade is the prime target of these local Ca^{2+} transients. Ca^{2+} influx through NMDA receptors activate ERK pathway and the latter then regulates several transcription factors [37]. Secondly, Ca^{2+} can directly enter the nucleus and function there to activate target gene expression [61]. However, in this case, it is not the same Ca^{2+} at the entering site that goes into nucleus. But that this process is achieved by the CICR from internal stores or the coinciding with back-propagating dendritic action potentials. Nuclear Ca^{2+} stimulates CREB-mediated transcription and, through inducing the activity of the transcriptional co-activator CBP, may modulate the expression of numerous genes including neurotransmitter receptors and scaffolding proteins [9]. Blockade of nuclear Ca^{2+} increase by microinjection of a non-diffusible Ca^{2+} chelator abolished CRE mediated gene expression, demonstrating that nuclear Ca^{2+} is essential for neuronal gene expression.

1.2.4 Imaging Ca^{2+} Signals

Activity-induced Ca^{2+} signals propagate from the starting site to nucleus to initiate gene responses. Therefore, visualization of cytosolic and nuclear Ca^{2+} is of great relevance in understanding the cellular behavior upon different stimuli. For the past decade progressive advances have been made in the design Ca^{2+} sensors. Basically, there are two major groups of Ca^{2+} indicators: synthetic fluorescence Ca^{2+} sensors and genetically encoded Ca^{2+} indicators (GECIs). The synthetic fluorescence Ca^{2+} sensors cover a large range of Ca^{2+} sensors with different fluorescent excitation/emission spectra, dynamics and capacities. Fura-2 is a ratiometric and sensitive indicator dye for measuring intracellular Ca^{2+} [51]. 340/380 nm excitation ratio for Fura-2 allows accurate measurements of the intracellular Ca^{2+} concentration. Fluo-3 and Fluo-4 are visible-light excited. They have an absorption spectrum compatible with excitation at 488 nm by argon-ion laser sources and a very

large fluorescence intensity increase in response to Ca^{2+} binding. X-rhod-1 is a red dye (excitation peak at 576 nm and emission peak at 602 nm) with rather low affinity to Ca^{2+} with Kd of 700 nM.

GECIs are an alternative to synthetic Ca^{2+} indicators. GECIs can be easily targeted to specific cell types or subcellular compartments with tissue specific promoter. As they are expressed by cells, they are compatible with long-term, repeated *in vivo* measurements. GECIs consist of Ca^{2+}-binding domain such as calmodulin or troponin C (TnC), fused to either one or two fluorescent proteins. In GECIs with two fluorescent proteins, Ca^{2+} binding modulates fluorescence resonance energy transfer (FRET) between fluorescent proteins. And in GECIs with single fluorescent protein, the fluorescence intensity of a circularly permuted fluorescent protein (cpFP) is modulated by Ca^{2+} binding-dependent changes in the chromophores environment. GCaMP3, which is used in this thesis, is a GECI with one fluorescent protein. It utilizes permuted enhance green fluorescent protein (eGFP) as the fluorophore and interaction between M13 and calmodulin to sense Ca^{2+} change. GCaMP3 is improved based on GCaMP2 (at M153K and T203V sites, numbers refer to residue sequence of the fluorophore eGFP, [136]) and it is brighter, has greater protein stability, has a large dynamic range and higher affinity for Ca^{2+}. To detect nuclear Ca^{2+} change, GCaMP3 is targeted to nuclei with a nuclear localization sequence (NLS) under CaMKIIα promoter to be specifically expressed excitatory pyramidal neurons.

1.3 Activity-mediated Neuron Protection

Physiological levels of synaptic activation are required for neurons to survival and neural circuits have to maintain stable function in front of various plastic challenges. But unfortunately, many of our normal and vital functions are lost due to decrease of neuronal activity such as Alzheimer's disease (AD), which is characterized by progressive impairment of cognition and emotional disturbance and they are strongly correlated with decreased synapse density in limbic structure like hippocampus and neocortex [75]. Procedures which interfere with electrical activity and compromise NMDA receptor function or nuclear calcium signaling can have deleterious effects on the health of neurons both *in vitro* and *in vivo*. For instance, intraperitoneal injection of the NMDA receptors antagonist MK-801 to block NMDA receptor function *in vivo* in seven day-old rats triggers a wave of apoptotic neurodegeneration in many brain regions within 24 hours. These regions include the parietal and frontal cortex, the thalamus and the hippocampus [68]. Likewise, selectively blocking nuclear calcium signaling prevents cultured hippocampal neurons from building up anti-apoptotic activity upon synaptic NMDA receptor stimulation. On the other hand, neuronal activity can boost neuroprotection. Enhancing neuronal firing, especially synaptic NMDA receptor activity, is neuroprotective: cultured hippocampal neurons which have experienced periods of action potential bursting causing calcium entry through synaptic NMDA receptors are more resistant to cell death-inducing conditions [62]. Moreover, stimulating synaptic activity *in vivo* by exposing rats to enriched environments reduces spontaneous apoptotic cell death in the hippocampus and protects against neurotoxic injuries [149]. Activity-dependent neuroprotection is induced by calcium entry through synaptic NMDA receptors and requires that calcium transients invade the cell

nucleus [107]. A pool of activity-regulated genes have been identified which provide neurons with a robust neuroprotective shield against cell death [157].

1.4 Optogenetics and ChR2

Optogenetics refers to the integration of optics and genetics to achieve gain- or loss-of-function (GOF or LOF) of well-defined events within specific cells of living tissue [147]. The very original aspects of the conceptual inspiration for optogenetics can be traced back to the 1970s [36]. But due to some fundamental caveats for a possibility for optical control of nervous system, it took quite a long time for its experimental implementation. The integration of the idea into neuroscience research only started blooming when ChR2 was identified as a directly light-gated cation channel [99] at the beginning of the 21st century.

1.4.1 Optogenetic Toolbox

Organisms ranging from archaebacteria to human beings capture energy and/or information contained within environmental sources of light by using photoreceptors called rhodopsins, which consist of seven-transmembrane-helix proteins, called opsins, covalently linked to retinal. On the basis of primary sequences, the corresponding opsin genes classified into two groups: microbial (type I) and animal (type II). Type I genes are found in archaea, eubacteris, fungi and algae, whereas type II proteins are expressed in animals, including human beings. The type II proteins indirectly influence transmembrane ion currents by coupling to G-protein based signal transduction pathways. Different from the animal type of rhodopsin, the type I proteins (microbial rhodopsin) are not coupled to G-protein-based signal transduction pathway but themselves include direct-light-activated regulators of transmembrane ion conductance, such as the light-driven ion pumps called bacteriorhdopsins and halorhodopsins (BRs and HRs) and the light-driven ion channels (ChRs) [73]. BR is highly expressed in haloarchaeal and serves as part of an alternative energy-production system. BRs pump protons from the cytoplasm to the extracellular medium to form a proton-motive force to drive ATP synthesis. They can support hyperpolarization when expressed in neurons [112]. HRs are light-driven inward chloride pump and can support the quieting of neural activity in response to yellow light [89]. ChRs are light-driven inward nonspecific cation channels and can support neural depolarization [98]. ChRs are rapidly introduced in neuroscience research and expression of ChRs in neurons can support action potentials with brief, millisecond pulses of blue light [99]. These specific proteins make a toolkit for optogenetic manipulation of nervous system.

1.4.2 Identification of ChR2

Channelrhodopsins (ChRs) are a subfamily of retinylidene proteins (rhodopsins) that function as light-gated ion channels [98]. ChRs are derived from algae that have shown experimental utility in optogenetics. They serve as sensory photoreceptors in unicellular green algae, controlling

phototaxis, i.e. movement in response to light [124]. Expressed in cells of other organisms, they enable the use of light to control electrical excitability, intracellular acidity, calcium influx, and other cellular processes. Channelrhodopsin-1 (ChR1) and Channelrhodopsin-2 (ChR2) from the model organism *Chlamydomonas reinhardtii* are the first discovered ChRs. Several other variants have been cloned subsequently from other algal species, and many more are expected to be identified in the future. It was found that ChRs could be expressed in mammalian neurons to mediate precise and reliable control of action potential firing in response to light pulses, without the need for exogenous retinal in vertebrate systems.

The nucleotide sequences of ChR2, together with that of ChR1, were uncovered in a large-scale EST sequencing project in *C. reinhardtii*. Both sequences were submitted to GenBank by three different groups ([124, 132] and direct submission by Peter Hegemann group). Although with different names, both sequences were found to function as single-component light-activated cation channels in a heterologous system [98, 99]. The name "channelrhodopsins" was coined to highlight this unusual property, and the sequences were renamed accordingly. Meanwhile, their roles in generation of photoreceptor currents in algal cells were characterized by John Spudich group [124].

1.4.3 Engineering of ChR2

To date, optogenetic application of microbial opsin genes benefited substantially from molecular modification. Through a combination of molecular engineering and genomic discoveries of new light-sensitive proteins, the toolkit of neuron modulators is rapidly improving in specificity and versatility. With its specific fast depolarization function in neurons, ChR2 is the most widely studied and used in neuroscience research field. With molecular mutagenesis studies, ChR2 function has been engineered to have faster or extended open-state lifetimes, shifted absorption spectra, reduced desensitization, and increased expression and photocurrent magnitude.

Wild type ChR2 is a direct light-switched cation-selective ion channel. It opens rapidly after absorption of a photo to generate a large permeability for monovalent and divalent cations. ChR2 desensitizes in continuous light to a smaller steady-state conductance. Recovery from desensitization is accelerated by external H^+ and negative membrane potential, whereas closing of the ChR2 ion channel is decelerated by intracellular H^+ [99]. After detailed sequence comparisons with the well-characterized BR, Karl Deisseroth group found out the residue C128 (cysteine residue at 128 site of ChR2 protein sequence) to be critical for determining the channel kinetics [13]. Single point mutation of cysteine to alanine or serine at 128 site (ChR2-C128A/S, C128A is used in this work and termed as ChR2-a) produced a bi-stable neural state switches. ChR2-a opens longer upon blue light activation but the photocurrent is relatively lower compared to wild type ChR2. ChR2-a has faster activation kinetics and superior inactivation by green light, granting it as a step-function opsin (SFO), and is very useful for light-controlled induction of immediate early genes [118]. Structure analysis revealed that the photocycle of ChR2 is largely influenced by the putative hydrogen bond between C128 and D156 [10]. Mutation at D156 to alanine has similar effect to C128A, with increased light sensitivity but slowed kinetics. Biophysical characterization

revealed that the the kinetics of ChR2 slows down considerably at depolarized membrane potential [97]. E123T substitution of ChR2 (ChR2-e) abolishes this voltage sensitivity and speeds up channel kinetics [52]. Because the single channel conductance of ChR2 is very small, high expression levels are required to fire neurons reliably. With a screening of a large number of ChR2 point mutants, Andre Berndt and colleagues discovered a dramatic increase in photocurrent amplitude after threonine-to-cysteine substitution at position 159 ([12], ChR2-T159C, termed as ChR2-b in this work). ChR2-b generates very large photocurrents and sensitizes neurons to very low light intensities. Due to the relatively small photocurrent, many optophysiological experiments are limited. Combination of E123T and T159C produced a double mutant (ChR2-be) enabling reliable and sustained optical stimulation of hippocampal pyramidal neurons up to 60 Hz. Another variant of ChR2 called calcium translocating channelrhodopsin (CatCh [74], ChR2-c in this work) having a point mutation at L132C mediates an accelerated response time and a voltage response that is about 70 fold more light sensitive than that of wild type. ChR2-c has enhanced Ca^{2+} permeability leading to its superior properties. An increase in Ca^{2+} concentration elevates the internal surface potential, facilitating activation of voltage-gated Na^{+} channels and indirectly increasing light sensitivity. The different variants of ChR2 made/used in this thesis work are listed in Table 2.2.

1.5 Gene Delivery with AAV

Adeno-associated virus (AAV) is a single stranded DNA, non-pathogenic (replication defective), non-enveloped virus. Depending on the co-infection of an unrelated helper virus (e.g. adenovirus, herpesvirus, human cytomegalovirus, or papillomavirus) AAV is classified to the *Parvoviridae* family, the genus *Dependovirus*. Wild-type AAV contains a DNA genome of approximately 5 kb, which is packaged into an icosahedral, non-enveloped capsid. AAV genome contains three functional regions: two open reading frames (ORF) including *rep* for un-structural proteins and *cap* for structural capsid proteins and the inverted terminal repeats (ITR). ITRs form two T-shaped structures at the 5 and 3 ends of the AAV genome, serve as origin of replication and play a key role in viral genome integration into the host genome as well as in the subsequent rescue of viral DNA from the integrated state. *Rep* codes for a family of multifunctional nonstructural proteins that are involved in viral/vector genome replication, transcriptional control, integration and encapsidation of AAV genomes into preformed capsids. *Cap* codes for the three capsid proteins, VP1, VP2, VP3, which share most of their amino acid sequences except for the N-terminus. Differences among the capsid protein sequence of the various AAV serotypes results in the use of different cell surface receptors for cell entry. In combination with alternative intracellular processing, this gives rise to distinct tissue tropisms for each AAV serotype.

1.5.1 Advantages and Drawbacks

Due to lack of pathogenicity, AAV receives a lot of interest from gene therapy researchers. It can infect dividing and also non-dividing cells and has the ability to stably integrate into the host cell

genome at a specific site, the 19th chromosome in human without any known side-effects. Another advantage of AAV is that it presents very low immunogenicity, and no cytotoxic response has been clearly defined. Recombinant forms of AAV (rAAV) were quickly developed once the latent form and nonpathogenic nature of AAV were discovered. On the other hand, AAV shows some disadvantages. The cloning capacity of the vector is relatively limited (3-4 kb). Large genes are, therefore, not suitable for use in a standard AAV vector. AAV mediated transgene expression is delayed, often it takes 1 to 3 weeks.

1.5.2 AAV Serotypes

Tissue specificity of AAV infection is determined by the capsid serotype. So far, 14 AAV serotypes and multiple variants have been described. Humans are the primary hosts of nine serotypes (AAV1-9) with approximately 80% of the human population testing positive for the most common subtype, AAV2 [140]. AAV2 is the one which has been most extensively examined so far and rAAVs are most commonly derived from it. AAV2 presents natural tropism towards skeletal muscles, neurons, vascular smooth muscle cells and hepatocytes. The primary cell receptor for AAV2 is heparan sulfate proteoglican (HSPG) [129]; also some other co-receptors are defined, like Vβ5 integrin [128], hepatocyte growthfactor receptor (HGFR)and fibroblast growth factor receptor 1 (FGFR-1) [111]. AAV serotypes other than AAV-2 have shown superior transduction efficiencies for various tissues. For example, AAV-1 is reported to be more efficient than AAV-2 in transducing muscle, arthritic joints, pancreatic islets, heart, vascular endothelium, CNS and liver cells, while AAV-3 is well suited for infecting cochlear inner hair cells, AAV-4 for brain, AAV-5 for CNS, lung, eye, arthritic joints and liver cells, AAV-6 for muscle, heart and airway epithelium, AAV-7 for muscle and AAV-8 for muscle, pancreas, heart and liver. For research and clinical usage, the recombinant AAV genome has the wild-type *rep* and *cap* ORFs, which constitutes 96% of the wild-type genome, replaced with a transgene-expression cassette. When the rAAV vectors are produced, the rep, cap and helper virus elements are supplied *in trans* via co-transfection of a number of helper plasmids. rAAV vectors appear to have a tropism for neuronal cells when injected into the central nervous system (CNS), but can also infect some non-neuronal cell types at much lower efficiencies [91].

In this thesis work, I use rAAV with a mosaic capsid (rAAV1/2) which consists of a mixture of unmodified capsid proteins from two different serotypes: AAV1 and AAV2. AAV1 and AAV2 *cap* genes share more than 80% identity at the amino acid level. During viral assembly, the two serotype capsid proteins are theoretically mixed in each virion at ratios of the contributing helper plasmids. The capsid proteins are provided in equal proportions using separate helper plasmids during the packaging process: AAV1 helper (pH21) and AAV2 (pRV1) helper. The AAV1 helper includes the AAV2 *rep* gene and AAV1 *cap* gene while the AAV2 helper carries AAV2 *rep* gene and AAV2 *cap* gene. Since AAV2 capsid proteins would be incorporated into the chimeric virion, we could purify those viruses by heparin affinity chromatography. The mosaic viruses show high infection efficiency and specific neuron tropism.

1.6 Motivation

During development, neuronal activity mediates the formation of the nervous system and neural circuits. In postmitotic neurons, activity continues playing a pivotal role as it mediates activity-dependent morphogenesis, adaptation to the environment, and neuronal protection. Recently it was shown that synaptic activity can boost neuroprotection through induction of a pool of calcium-regulated genes [156] or inhibition of pro-cell-death gene like *p53* [80]. Conversely, interference with synaptic activity can have deleterious effects on the health of neurons and functions of the whole system. In Alzheimer's disease (AD), the strongest anatomical correlate of the degree of clinical impairment is the synapse loss. This loss is thought to be due to the partial blockage of N-methyl-D-aspartate (NMDA)receptors activity and NMDA receptors mediated calcium influx by amyloid-beta (Aβ) oligomers [119]. Loss of neurons in limbic structures, such as the hippocampus and the amygdala, and associated regions of the cerebral cortex are reported to be strongly correlated with the onset of AD. Additionally, similar synaptic degeneration and cell loss are also observed in aged rats [110]. Intriguingly, recent results show that activated neurons are better able to withstand aging and AD [133]. Indeed, synaptic activity can induce rapid dendritic morphogenesis in CA1 hippocampal neurons [87]. Likewise, stimulating synaptic activity *in vivo* by exposing rats to enriched environment (EE) produced a robust increase in hippocampal synapse numbers in adult mice [46]. Modulating neuronal activity is a promising way to initiate downstream effects against degeneration of synapses and cell death [87, 156]. Therefore, it would be very encouraging to try to restore activity of specific groups of neurons before the onset of those symptoms in neurodegenerative disorders and aging. The discovery and introduction of channelrhodopsin2 (ChR2) into the field of neuroscience inspired our activity-restoring strategy. ChR2 is a light-gated, cation-selective, small membrane channel isolated from *Chlamydomonas reinhardtii*. The direct gene products are apoproteins Channelopsin 2 (Chop2) that form ChR2 when reconstituted with the chromophore all-*trans*-retinal (ATR). Chop2 has a 7-transmembrane helix and a long C-terminal extension. Expression of the N-terminal transmembrane fragment is sufficient for the formation of a functional channel in mammalian cells when ATR is present [99]. An advantage of the genetically encoded modulator, ChR2, is that it can be easily targeted to certain types of cells with tissue-specific promoters. Furthermore, ChR2 is fully functional without any additional cofactors when expressed in neurons *in vitro* and *in vivo*. Integration of ChR2 into the plasma-membrane does not alter the intrinsic properties of the host neuron. This channel is activated with blue light with the maximal excitation wavelength at 460nm, which is easily obtained with a standard green fluorescence protein (GFP) filter setup, and it will give reliable, millisecond-timescale control of neuronal spiking, as well as control of excitatory and inhibitory synaptic transmission [23]. ChR2 has been broadly used to activate the neural circuitry in vitro and in vivo [7]. In this thesis, ChR2 is used as a tool to introduce increased neuronal activity to neurons and analyze the potential beneficial downstream effects, including activated signaling pathways, induction of gene expression and neuron protection. ChR2 is also targeted to intracellular membrane system to directly induce Ca^{2+} transients there. Neural activity is induced in another pharmacology way using Bic, a competitive antagonist of $GABA_A$ receptors, to induced synchronized bursting of action potentials and analyze the minimal activity requirement for gene transcription initiation.

Chapter 2

Materials and Methods

2.1 Cloning

2.1.1 Subcloning into AAV Vector

DNA plasmids coding for ChR2 and its mutants were from: Karl Deisseroth, Department of Bioengineering and Howard Hughes Medical Institute, Stanford University, California, USA, for the hChR2; Thomas G. Oertner, Friedrich Miescher Institute for Biomedical Research, Basel, Switzerland, for the ChR2-C128A mutant; Peter Hegemann, Institute of Biology, Experimental Biophysics, Humboldt-University, Berlin, Germany, for the ChR2-T159C mutant.
To adapt these DNAs into our AAV expression system, the coding sequences were subcloned into the AAV expression vector with CaMKIIα promoter. As shown in Figure 2.1, ChR2 was subcloned into the AAV vector with the BamHI and NheI restriction sites. Primers used for amplifying ChR2 fragment were: forward primer P55, 5′-GCGGATCCGTATGCCAAGTAGG-3′ and reverse primer P71, 5′-CGGCTAGCTACCGCGCCAG-3′. HA, eGFP and mCherry tags were used for different purposes. The AAV vector had a human growth hormone polyA (hGH polyA) for stabilizing mRNA , Woodchuck Hepatitis Virus Posttranscriptional Regulatory Element (WPRE) to enhance expressing level and two inverted terminal repeats (ITRs) for virus wrapping.

2.1.2 Point Mutation

Overlap extension PCR method was used to make double mutant on the base of another existing mutant we got from other labs. The idea of overlap extension PCR method was to design the point mutation in two opposite directional primers. In the case of introducing C128A point mutation to ChR2-T159C sequence, primers were P79, 5′-GAATGAGAATGACCGG*GGC*GGTGAGAAG-3′ and P80, 5′-CTTCTCACC*GCC*CCGGTCATTCTCATTC-3′, where the *italic nucleobases* were the coding for Cysteine (C) to Alanine (A) mutation. In combination with another two primers at the beginning and end of the fragment (P55, 5′-GCGGATCCGTATGCCAAGTAGG-3′ and P71,

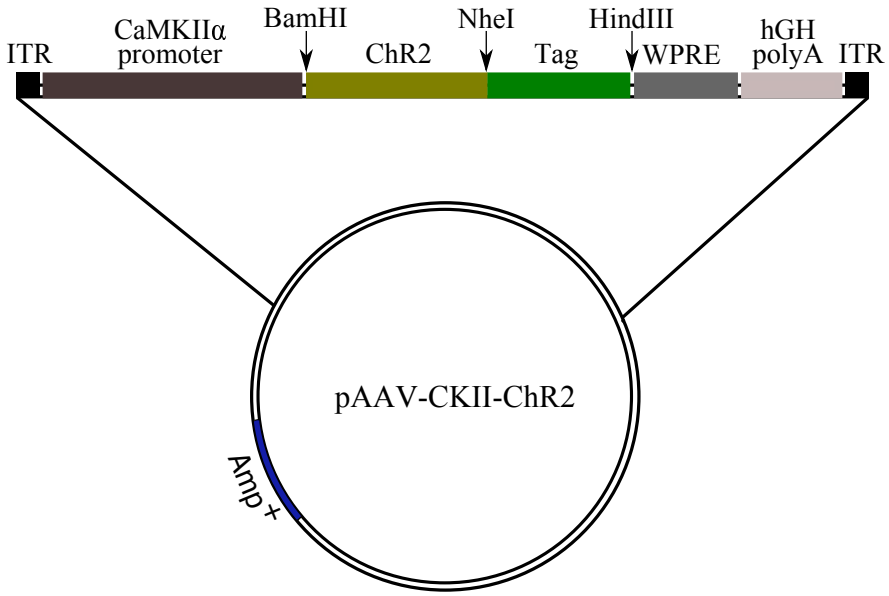

Figure 2.1: Schematic representation of AAV vector map carrying ChR2 coding sequence. ChR2 and fluorescent tag (mCherry or eGFP) is under the control of alpha-Ca^{2+}/calmodulin-dependent protein kinase (CaMKIIα) promoter and followed by Wookchuck Hepatitis Virus posttranscriptional Regulatory Element (WPRE) and human Growth Hormone polyA (hGH polyA). The whole fragment is flanked with two inverted terminal repeats (ITR). Amp^+ gives resistance to ampicillin and serves as a selective marker.

5′-CGGCTAGCTACCGCGCCAG-3′ for ChR2. Underlined nucleobases were BamHI and NheI restriction sites, respectively.), two PRC fragments were produced in the first round of PCR, cutting at the mutated point with some overlap. In the second round of PCR, products from the first PCR were used as template and the primers for whole ChR2 (P55 and P71) were used to get the whole coding sequence with the introduced point mutation. The detailed process for construction was presented in Figure 2.2. PCR machine used in this work were: Peltier Thermal Cycler-200 from MJ research and C1000™ Thermal Cycler from Bio-Rad.

Phusion® (Finnzymes, Thermo Scientific) high-fidelity DNA polymerase was used for all the PCR reactions in this work to ensure accuracy of the sequence. Nevertheless, all plasmids after cloning were sequenced by GATC Biotech. The PCR composition setup and program setting for the PCRs were shown in Table 2.1.

After each PCR, products were mixed with 6x loading buffer and loaded in a 1% agarose gel for electrophoresis, at 120 V for 30 min. Product band size was checked under UV light and expected band was collected for gel extraction and purification.

Both the PCR products from the 2nd PCR and the AAV vector were digested with BamHI and NheI. The entire purification product and 2 µg of vector were used in this digestion. They were digested according to enzyme manual in the 1x Tango buffer at 37°C for 2 h. The digestion products were loaded in an agarose gel and the bands of interest were cut out for a gel extraction.

Purified fragments from gel extraction were used in the following ligation. For each reaction, the mole ratio between insert and vector was 3:1. Quick ligation system (Fermentas) was used. A

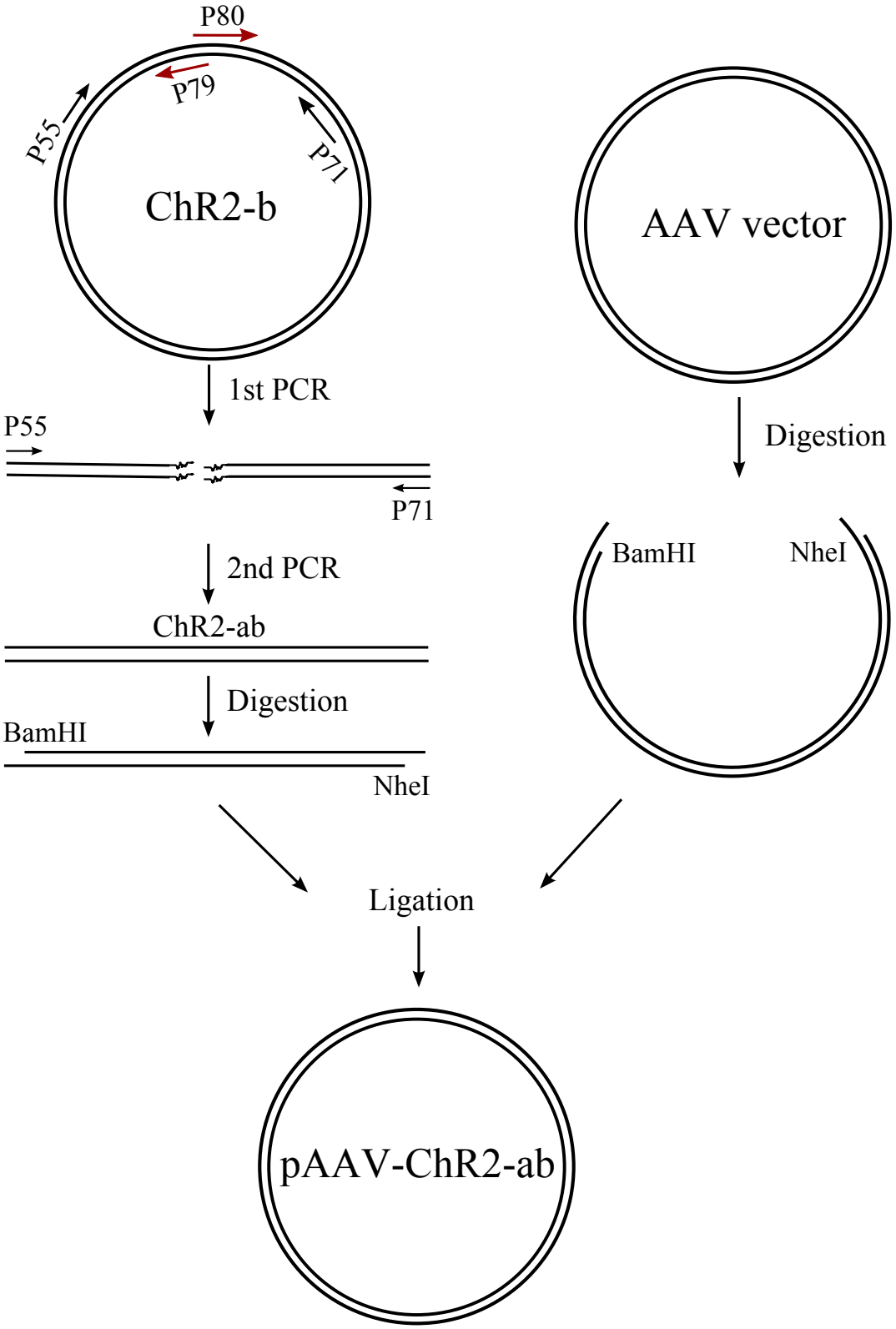

Figure 2.2: Schematic representation of overlap extension PCR method to generate point mutation. ChR2-b coding sequence is used as template and 4 primers, P55, P79, P80 and P71, are used. C128A (a) point mutation is designed in primers P79 and P80. Two DNA fragment products from the first round of PCR are used as template for the second PCR with primers P55 and P71 to create ChR2 whole fragment harboring double mutants (ChR2-ab). ChR2-ab and target vector are digested with BamHI and NehI separately and ligated to generate pAAV-ChR2-ab construct.

Table 2.1: Overlap extension PCR

PCR setup		PCR program		
Component	Volume (µl)	Step	Temperature	Time
Template[a]	1	1	98°C	30 sec
Phusion® HF buffer (5x)	10	2	98°C	10 sec
dNTP mix (10 mM)	2	3	x°C[b]	30 sec
Primer For[c] (20 µM)	5	4	72°C	30 sec
Primer Rev[c] (20 µM)	5	5	Go to step 2 for 30 cycles	
Phusion® DNA polymerase (2 U/µl)	0.5	6	72°C	10 min
H_2O	up to 50	7	4°C	for ever

[a] Totally 100 to 200 ng template DNA was used for PCR. Template DNA was adjusted to be 200 ng/µl. For the 1st PCR, ChR2-b plasmid was used as template for getting both fragments. Purified products from the first round of PCR were used as template for the 2nd PCR with the equal mole ratio.
[b] Different annealing temperature was used according to the melting temperature (Tm) of the primers.
[c] Forward and reverse primers were used accordingly. For making C128A on base of T159C, P55+P79 and P80+P71 were used for the 1st PCR; P55+P71 for the 2nd PCR.

20 µl total volume including the insert, vector, 10 µl 2x quick ligation buffer and 400 U T4 ligase (NEB) was incubated at room temperature for 0.5 h.

DH5α competent cells were transformed with the ligation product. Briefly, DNA and competent bacteria cells were mixed, put on ice for 0.5 h and then heat shocked at 42°C for 90 sec. The bacteria were cooled down on ice for 3 min. 800 µl antibiotic-free lysogeny broth (LB) was added and the bacteria were amplified at 37°C for 1 h with shaking at 225 rpm (CERTOMAT® R, B. Braun Biotech International). The bacteria were spun down at 800 rpm for 5 min and plated on antibiotic (kanamycin, $Kana^+$, 50 µg/ml or ampicillin, Amp^+, 100 µg/ml) containing LB agar plates. Plates were incubated at 37°C overnight. Colonies from the plates were picked up and dissolved in 15 µl of LB. 1 µl of it was used as the template for PCR with primer to check whether the interested fragment was incorporated in the new construct. The positive colonies which had a band at the expected size were amplified for plasmid miniprep and then digested with BamHI and NheI to check the correct insertion. Positive colonies were sent for sequencing.

In this work, mutants of ChR2 were coded as in Table 2.2

2.2 AAV Production

2.2.1 HEK Cell Culturing

Human embryonic kidney 293 (HEK-293, American Type Culture Collection, CRL1573) cells were used for AAV production. These cells were cultured in flasks with DMEM-complete medium (Table 2.3), split in the dilution of 1:5 and passaged every 3 to 4 days. For splitting, culturing medium was removed and the cells were washed twice with phosphate buffered saline (PBS). After

Table 2.2: ChR2 mutants

Name	Mutation	Properties
wt	Wild type	Cation selective ion channel.
a	C128A	Step function opsion (SFO), long opening.
b	T159C	Larger permeability.
ab	a+b	Longer opening with larger current.
c	L132C	CatCh, Ca^{2+} trnslocating channelrhodopsin.
be	b+E123T	High-efficient ChR2.
ad	a+D156A	Super SFO.

removing PBS, 0.05% Trypsin-EDTA (Gibco®) was added directly to the cells and the flask was incubated at 37°C for 5 min. After trypsin digestion, the same volume of DMEM-complete was added to the flask to stop the enzyme digestion procedure. Cells were then suspended and collected in falcon tube. The cell solution was spun at 800 g, at room temperature for 5 min. After spinning, the medium was removed and the cells were resuspended in fresh DMEM-complete, with a flamed pipette Pasteur to get signal cell solution, and plated in a new flask. All the medium used should be pre-warmed at 37°C.

Table 2.3: Dulbecco's Modified Eagle Medium-complete (DMEM-complete), 500 ml

Solution[a]	Volume (ml)	Note
DMEM	500	include 4.5 g/l glusoce
FBS/FCS	50	heat inactivated[b]
NEAA	5	non essential amino acids, 100x
Sodium pyruvate	5	100 mM, 100x
Pen/Strep[c]	2.5	

[a] All from GIBCO®.
[b] FBS (fetal bovine serum) or FCS (fetal calf serum) was incubated at 56°C for 30 min.
[c] Penicillin G sodium, 10,000 unite/ml; streptomycin sulfate, 10,000 µg/ml in 0.85% saline.

2.2.2 HEK Cell Transfection with Ca^{2+}-phosphate

Ca^{2+}-phosphate transfection protocol was used to transfect HEK293 cells for producing virus. The cells were seeded into 150 cm dishes (TC Dish 150x20 NUNC) containing DMEM-complete. At transfection start point, cells should be about 70% confluent. 3 hours before the transfection, DMEM-complete was replaced with pre-warmed IMDM-complete (Table 2.4). All transfection reagents were warmed up to room temperature before use. Five 150 cm dishes were used for producing one virus. And for one virus, the following reagents were used: 12 ml sterile H_2O; 1650 µl

2.5 M $CaCl_2$; 62.5 µg AAV transgene plasmid with genes of interest, 125 µg adenoviral helper plasmid (pFdelta6), 31.25 µg AAV helper (pH21, with cap gene for AAV serotype 1 and rep gene for AAV serotype 2) and 31.25 µg AAV2 helper (pRVI, with cap and rep genes for AAV serotype 2); this pre-mixture was prepared in an order as H_2O, $CaCl_2$ and then plasmids; the mixture was filtered through a 0.2 µm syringe filter into a small sterile bottle. 13 ml 2x HeBs (HEPES buffered saline, see Table 2.5) were added to the mixture while vigorously vortexing for 15 seconds. Very fine and white precipitate formed after 2 min. 5 ml of this transfection mixture was added drop-wise in a circular motion to each plate. Plates were swirled carefully and returned to incubator with 5% CO_2 supply at 37°C. 16 to 20 hours later, Ca^{2+}-phosphate precipitation was checked and could be seen under microscope. The transfection medium was changed back to pre-warmed DMEM-complete. Cells were then put back into the incubator.

Table 2.4: Iscove's Modified Dulbecco's Medium-complete (IMDM-complete), 500 ml

Solution	Volume(ml)
IMDM	500
FBS/FCS, h.i.[a]	50

[a] h.i., heat inactivated, FBS (fetal bovine serum) or FCS (fetal calf serum) was incubated at 56°C for 30 min.

Table 2.5: 2x HeBs

Component	Concentration (mM)
HEPES	50
NaCl	280
Na_2HPO_4	1.5

[a] Adjust pH to 7.05. It is very critical for successful transfection.
[b] Sterile filtered through 0.22 µm Millipore filter, aliquote and store at -20°C.

2.2.3 Virus Harvesting

About 60 hours after transfection, cells were washed with pre-warmed PBS once, harvested in 25 ml PBS/plate by scraping and pelleted by centrifugation at 800 g for 5 min. Pellets were resuspended in 150 mM NaCl/20 mM Tris (pH 8.0), 50 ml/virus and frozen at -20°C. On the next day, cell pellets were thawed at room temperature and lysed by treating them with 50 U/ml Bensonase and 0.5% sodium deoxycholate for 1 hour at 37°C with mixing every 10 min. Cell debris was removed by centrifugation at 3000 g for 15 min, 4°C.The supernatant was transferred into a new tube and frozen at -20°C for purification.

2.2.4 Virus Purification

Heparin column was used to purify the virus. Virus sample was defrosted at room temperature and centrifuged at 3000 g for 15 min, 4°C to get rid of any possible debris. Heparin column was pre-equilibrated with 10 ml 150 mM NaCl/20 mM Tris (pH 8.0) with help of a pump at 1 ml/min flow rate. 50 ml sample solution from each virus was then loaded onto the column at 1 ml/min rate using a 60 ml syringe. The column was washed with 20 ml 100 mM NaCl/20 mM Tris (pH8.0) also at the rate of 1 ml/min. Following wash and elution steps were done manually as the volume was much smaller. The column was washed with 1 ml 200 mM NaCl/20 mM Tris (pH8.0) and then 1 ml 300 mM NaCl/20 mM Tris (pH8.0) at a rate about 1 ml/min. Then it was eluted with 1.5 ml 400 mM NaCl/20 mM Tris (pH8.0), 3 ml 450 mM NaCl/20 mM Tris (pH8.0) and 1.5 ml 500 mM NaCl/20 mM Tris (pH8.0). Eluted virus was collected in a 15 ml sterile tube. The purified virus solution was concentrated using Amicon Ultra-4 (Millipore) concentrators at 2000 g for 2 min and then washed twice with 3.5 ml PBS. After concentration, around 250 µl virus solution was left in the concentrator and transferred into a 1.5 ml tube. Finally, the virus was sterilized by filtration through a 0.2 µm/13 mm diameter syringe filter.

2.2.5 Virus Testing

Ready-to-use virus was firstly check by the purity of capsid proteins. Briefly, 5 µl virus was lysed with sample buffer and loaded to a 12% SDS-PAGE (Sodium Dodecyl Sulfate Polyacrylamide Gel Electrophoresis). Protein separation was performed by electrophoresis with constant current at 30 mA for 1 h. Then the gel was stained with coomassie blue superstain solution (Table 2.6) at room temperature for 45 min and destained (Table 2.6) for about 3 hours till the bands were clear.
Virus was further tested in cultured hippocampal neurons to check the infection efficiency and toxicity to neurons. Normally, cells were infected on day *in vitro* (DIV) 4, fixed on DIV 10. The infection efficiency was calculated as virus positive cell to total cell number.

Table 2.6: Coomassie blue superstain & destain solution

Superstain		Destain	
Component	(w/v or v/v)	Component	(v/v)
Coomassie blue R250	0.1%	Acetic acid	10%
Acetic acid	10%	Isopropanol	10%
Methanol	50%		

2.3 Hippocampal Culture

2.3.1 Hippocampal Culture Preparation

Dissociated hippocampal neuronal cultures were prepared from new-born wild type C57BL/6 pups. Hippocampi were dissected free from the rest of the brain in a mixture solution from Ky/Mg solution (Ky/Mg, Table 2.7) and dissociation medium(DM, Table 2.8) at 1:9 volume ratio (e.g. 5 ml Ky/Mg and 45 ml DM, referred to as Ky/Mg/DM). Hippocampal tissue was then dissociated by enzyme solution (Papain latex 10 Units/ml and 3.7 mM L-Cysteine in Ky/My/DM) for 20 min at 37°C. During incubation, the tube was stirred every 5 min to make it homogenous and to avoid it become yellow. This enzyme incubation was done twice with an enzyme solution change in between. Enzyme activity was stopped by trypsin inhibitor solution (1% , w/v trypsin inhibitor in Ky/My/DM). Inhibition was performed 3 times with complete inhibition solution change in between and each time was incubated at 37°C for 5 min. After enzyme inhibition, hippocampi were washed 3 times with growth medium (GM, Table 2.10) and then triturated by pipeting to get single cell suspension. This cell suspension was diluted in Opti-MEM (supplemented with 20 mM Glucose) to get a concentration about 0.8 hippocampus/2 ml. Cells were plated on poly-D-lysine/laminin (BD Biosciences) coated 35-mm plastic dishes (2 ml/dish, containing 12-mm diameter glass coverslips or not according to different experiment design). 2.5 hours after plating, medium was replaced with fresh neurobasal-A/growth medium (Table 2.10, 2 ml/dish) and put back to a 37°C incubator supplied with 5% CO_2.

2.3.2 Hippocampal Culture Maintenance

AraC (cytosine β-D-arabinofuranoside, Sigma-Aldrich, C1768) was added on DIV 3 at a final concentration of 2.8 μM to inhibit the proliferation of non-neuronal cells. On DIV 8, GM was changed to transfection medium (TM: 10% MEM, ITS containing 7.5 μg/ml Insulin, 7.5 μg/ml Transferrin, 7.5 ng/ml Sodium selenite, 50 Units/ml Penicillin, 50 mg/ml Streptomycin, in SGG. See Table 2.11). If the experiments last longer than 10 days, medium was half changed every other day from DIV 10 on.

Table 2.7: Ky/Mg solution (Ky/Mg)

Component[a]	Final concentration	Stock concentration	For 80 ml
Kynurenic acid	10 mM	Powder	158.56 g
$MgCl_2$	100 mM	2 M	4 ml
HEPES	5 mM	1 M	0.4 ml
Phenol Red	0.5%	100%	0.4 ml
NaOH	12.5 mM	1 N	1 ml
H_2O			up to 80 ml

[a] All chemicals are from Sigma-Alrich Chemie GmbH, München, Germany.

Table 2.8: Dissociation Medium (DM)

Component	Final concentration	Stock concentration	Volume (ml) for 250 ml
Na_2SO_4	81.8 mM	1 M	20.45
K_2SO_4	30 mM	0.25 M	30
$MgCl_2$	5.85 mM	1.9 M	0.77
$CaCl_2$	0.25 mM	1 M	0.063
HEPES	1 mM	1 M	0.25
Glucose	20 mM	2.5 M	2
Phenole Red	0.2%	100%	0.5
H_2O			up to 250

Table 2.9: Salt Glucose Glycine Solution (SGG)

Component	Final concentration	Stock concentration	Volume (ml) for 500 ml
NaCl	114 mM	5 M	11.4
$NaHCO_3$	0.22%	7.5%	14.6
KCl	5.29 mM	3 M	0.882
$MgCl_2$	1 mM	1.9 M	0.264
$CaCl_2$	2 mM	1 M	1
HEPES	10 mM	1 M	5
Glycine	1 mM	1 M	0.5
Glucose	0.54%	45%	6
Sodium pyruvate	0.5 mM	0.1 M	2.5
Phenole Red	0.2%	100%	0.5
H_2O			up to 500

Table 2.10: NB-A/Growth Medium (GM)

Component	Volume (ml)
Neurobasal A-medium	97
B27	2
Rat serum	1
Glutamin(200 mM)	0.25
Pen/Strep	0.5
H_2O	up to 100

sterile filtered through 0.22 µm Millipore filter and store at -4°C.

Table 2.11: Transfection Medium (TM)

Component	Volume (ml)
SGG	88
MEM (without glutamine)	10
ITS	1.5
Pen/Strep	0.5
H_2O	up to 100

sterile filtered through 0.22 μm Millipore filter and store at -4°C.

2.4 Transfection and Infection

2.4.1 Neuron Transfection with Lipofectamine2000

Lipofectamine™ 2000 transfection was carried out to transfect hippocampal neurons. For a 35 mm dish containing 4 coverslips, 5 μl Lipofectamine™ 2000 (Invitrogen™) was diluted in 100 μl TM, and the mixture was vortexed to get homogenous solution. 1.6 μg plasmid DNA was diluted in another 100 μl TM and pipetted up and down. The Lipofectamine and DNA mixture made above were mixed together and left at room temperature for 30 min. Then another pre-warmed 800 μl TM was added to each tube to get the final transfection solution. Growth medium was replaced with the transfection solution. Cells were put back to the incubator for 2.5 to 3 hours. Then, the transfection solution was removed and 2 ml fresh TM was added to the dish. Constructs were expressed for 24 h or 48 h before stimulation or imaging experiments.

2.4.2 Neuron Infection with AAV

Infection of cultured neurons was normally performed on DIV 4. For the infection, virus was first aliquoted with certain amount into a 1.5 ml eppentube. Then some culturing medium was put into the tube and mixed well with virus. The virus solution was put back into cells.

2.5 Q-PCR

To determine the mRNA levels of activity related genes in mouse culture, quantitative PCR (Q-PCR) was performed using TaqMan® Prob-Based Gene Expression Analysis technology with a sequence detection system model 7300 Real Time PCR machine (Applied Biosystems®).

2.5.1 RNA Extraction

All RNA related work was done under RNase-free condition. Total RNA was extracted using RNeasy Plus Mini Kit (Qiagen) with additional on-column DNaseI digestion (RNase-Free DNase Set, Qiagen) during RNA purification. Briefly, cell samples were lysed with lysis buffer (RLT) supplemented with 1% β-mercaptoethanol (β-ME). For each 3.5 cm dish, 600 µl + 6 µl β-ME was used and β-ME was always added in freshly. Cells were then scraped thoroughly, collected into the tube and mixed by vortexing for 30 sec. Equal volume (600 µl for each) of 70% Ethanol was added to the homogenized lysate and mixed well by pipetting. The sample was transferred on to an RNeasy spin column placed in a 2 ml collection tube and spun for 15 sec at 13,000 rpm (round per minute). The flow through was discarded. The column membrane was washed with 350 µl RW1 once and spun down. The on-column DNaseI digestion was performed at room temperature for 15 min with 80 µl DNase solution (10 µl DNaseI stock in H_2O plus 70 µl RDD buffer, final DNaseI concentration: 340 Kunitz units/ml) directly to the RNeasy spin column membrane. After digestion, the column was washed once with 350 µl RW1 and twice with 500 µl wash buffer RPE. The column was placed into a new collection tube and centrifuged for 2 min to get rid of all the wash solutions. For elution, the column was placed into a new, RNase free 1.5 ml tube; 30 µl RNase-free water was directly added to the column membrane and centrifuged for 1 min at 13,000 rpm. The eluted RNA was used for reverse transcription afterwards or stored at -80°C for later use.

2.5.2 cDNA Synthesis

For cDNA synthesis, 1.2 µg of total RNA, random primers were used to do the reverse transcription with High Capacity cDNA Reverse Transcription Kit (Applied Biosystems®). Reverse transcription was done in 20 µl volume. 1.2 µg RNA was dissolved in RNase-free H_2O to a total volume of 10 µl and reverse transcription mixture in 10 µl also. The reagents and reverse transcription program were as shown in Table 2.12 and 2.13, respectively.

Table 2.12: cDNA synthesis mixture, 20 µl

Solution	(µl)
RNA template	1.2 µg in 10 µl
RT buffer (10x)	2
dNTP (100 mM, 10x)	0.8
Random primers (10x)	2
Reverse transcriptase (50 U/µl)	1
RNase inhibitor (40 U/µl)	0.5
RNase-free H_2O	3.7

Table 2.13: cDNA synthesis program

Step	Temperature	Duration
1	25°C	5 min
2	37°C	120 min
3	85°C	5 sec
4	4°C	for ever

After reverse transcription, the products were diluted 1:6 in RNase-free H_2O and used for Q-PCR or stored at -20°C for later use.

2.5.3 Q-PCR

For Q-PCR assay, the diluted cDNA from above was used with TaqMan® Universal PCR Master Mix (Applied Biosystems®). Ready to use probe sets designed by TaqMan® Gene Expression Assays, Applied Biosystems® were used to perform the quantitative PCR. The setup of the reaction mixture and Q-PCR program was show in Table 2.14 and 2.15, respectively. Data reading was in the 4th step at 60°C.

Table 2.14: Q-PCR Mixture, 20 µl

Solution	(µl)
Master mix, 2x	10
Probe, 20x	1
cDNA	9

Table 2.15: Q-PCR program

Step	Temperature	Duration
1	50°C	2 min
2	95°C	10 min
3	95°C	15 sec
4	60°C	1 min
5	Go to Step 3 for 50 cycles	
6	Stop	

Each cDNA sample was assayed in duplicate and a mean cycle time value was calculated. The expression level of the target mRNA in mouse was normalized to the relative ratio of the expression of Gusb mRNA.

2.5.4 List of Probes

The Q-PCR probes used were listed in Table 2.16. They were all FAM (6-carboxyfluorescein) labeled, and were designed and purchased from TaqMan® probe-based gene expression analysis, Applied Biosystems®.

2.6 Western Blot

2.6.1 Western Blot

Hippocampal neuron or HEK293 cell whole cell extract were prepared in 1x sample buffer (3x sample buffer: 9%SDS, 187.5 mM Tris, pH 6.8 and 30% glycerol in w/v. Add 10% β-ME and bromophenol blue before use.) and boiled for 5 min at 95°C before loading. Proteins were separated with 8%-12% SDS-PAGE (Table 2.17) with constant current at 30 mA per gel (Running buffer: 190 mM glycine, 25 mM Tris, 0.1% SDS and pH 8.8) and transferred to nitrocellular membrane (Waterman) with constant voltage at 20 V for 1.5 h (Transferring buffer: 150 mM glycine, 20 mM Tris, 0.1% SDS and 20% Methanol). Membrane was blocked in 5% milk in PBST (0.1%Tween-20 in PBS, 137 mM NaCl, 2.7 mM KCl, 10 mM $Na_2HPO_4 \cdot 2\,H_2O$, 2 mM KH_2PO_4, pH 7.4) at room temperature for 1 h. Membrane was incubated with the primary antibodies at 4°C overnight. On

Table 2.16: Q-PCR probes

Acronym	Gene name	Assay ID
Arc	activity regulated cytoskeletal-associated protein	Mm00479619_g1
Atf3	activating transcription factor 3	Mm00476032_m1
Bcl6	B-cell leukemia/lymphoma 6	Mm00477633_m1
Bdnf	brain derived neurotrophic factor	Mm00432069_m1
Btg2	B-cell translocation gene 2, anti-proliferative	Mm00476162_m1
cfos	FBJ osteosarcoma oncogene	Mm00487425_m1
Dnmt3a1	DNA methyltransferase 3 alpha, isoform 1	Mm00432870_m1
Dnmt3a2	DNA methyltransferase 3 alpha, isoform 2	Mm00463987_m1
Egr1	early growth response 1	Mm00656724_m1
Gadd45b	growth arrest and DNA-damage-inducible 45 beta	Mm00435123_m1
Gadd45g	growth arrest and DNA-damage-inducible 45 gamma	Mm00442225_m1
Gusb	glucuronidase, beta	Mm00446953_m1
Ifi202b	interferon activated gene 202B	Mm00839397_m1
Inhba	inhibin beta-A	Mm00434338_m1
Npas4	neuronal PAS domain protein 4 (Nfx)	Mm00463644_m1
Nr4a1	nuclear receptor subfamily 4, group A, member 1, Nur77	Mm00439358_m1
Puma	BCL2 binding component 3	Mm00519268_m1
Serpinb2	serine (or cysteine) peptidase inhibitor, clade B, member 2	Mm00440905_m1

the next day, after 4 times wash with PBST, secondary antibody was incubated at room temperature for 30 min. The membrane was then washed for 30 min using PBST with an interval of 5 min. ECL detection was performed according to the manual (Amersham). The film was developed with a Kodak developing machine.

Table 2.17: SDS-PAGE

	Upper/Stacking gel, 3.7% (10 ml)	Lower/Resolving gel (20 ml) 8%	10%	12%
H_2O	6.25 ml	9.6 ml	8.2 ml	6.9 ml
4x Buffer[a]	2.5 ml	5 ml	5 ml	5 ml
30% ProtoGel[b]	1.25 ml	5.3 ml	6.7 ml	8 ml
10% APS[c]	100 µl	100 µl	100 µl	100 µl
TMEDE	10 µl	10 µl	10 µl	10 µl

[a] 4x upper gel buffer: 0.5 M Tris-HCl, pH 6.8 and 0.4% (w/v) SDS;
4x lower gel buffer: 1.5 M Tris-HCl, pH 8.8 and 0.4% (w/v) SDS.
SDS is from SERVA and both buffer should be stored at 4°C.
[b] 30% ProtoGel from National Diagnostics.
[c] 10% (w/v) ammonium persulfate (APS) in H_2O.

2.6.2 List of Antibodies

The primary and secondary antibodies for western blot used in this thesis are listed in Table 2.18 and Table 2.19, respectively.

Table 2.18: Primary antibodies-Western Blot

Name	Host species	Company	Dilution
BDNF	rabbit polyclonal	Santa Cruz, sc-546	1:1000 in 5% milk/PBST
c-Fos	rabbit polyclonal	Santa Cruz, sc-253	1:5000 in 5% milk/PBST
CREB	rabbit monoclonal	Cell Signaling, 9197	1:1000 in 5% BSA/TBST
phospho-CREB (Ser133)	rabbit polyclonal	Upstate, 06-519	1:1000 in 5% BSA/PBST
ERK1/2	rabbit polyclonal	Cell Signaling, 9102	1:4000 in 5% BSA/PBST
phospho-ERK1/2	mouse monoclonal	Cell Signaling, 9106	1:2000 in 5% BSA/PBST
tubulin	mouse monoclonal	Sigma, T9026	1:400000 in 5% milk/PBST

Table 2.19: Secondary antibodies-Western Blot

Name	Host species	Conjugate	Company	Dilution
Mouse	goat IgG (H+L)	HRP	JIR, 115-035-003	1:5000 in 5% milk/PBST
Rabbit	goat IgG (H+L)	HRP	JIR, 115-035-144	1:1000 in 5% milk/PBST

Peroxidase-conjugated affini-pure goat IgG.
JIR: Jackson ImmunoResearch.

2.7 Immunocytochemistry

Immunocytochemistry (ICC) was used to compare the protein level in individual cells within the same or in different conditions.

2.7.1 Immunocytochemistry

Neurons were fixed with 4% paraformaldehyde (PFA) /4% sucrose at room temperature for 15 min and permeablized with cold methanol at -20°C for 6 min. Cells were then blocked with 10% normal goat serum (NGS) in PBS at room temperature for 1 h. Primary antibodies were diluted in 2% BSA/ 0.1% Triton-X-100/PBS. Incubation with primary antibodies was performed at 4°C overnight. Secondary antibody was diluted in 2% BSA/ 0.1% Triton-X-100/PBS and it was incubated at room temperature for 1 h. Nucleus was counter stained with Hoechst 33258 (Serva) at a final concentration of 2 µg/ml for 5 min, room temperature. After several times PBS washes, coverslips were mounted on slides.

Immunochemistry results were examined with either Leica SP2 confocal microscopy or Leica DM IRBE inverted microscope. The setting up for the confocal microscope was: 40x objective/NA1.25 oil, Zoom 1, 512 x 512 format, 8 bit resolution, xyz scan mode, 400 Hz speed, 1.0 airy pinhole, line average 1, frame average 1. The whole nucleus was scanned with z-scan at a ΔZ of 1μm. For the intensity analysis, z-scan was used to get the maximal projection. Nucleus was identified according to the Hoechst staining and the same regions of interest were used to get the mean intensity value from staining projection.

2.7.2 List of Antibodies

For ICC, all antibodies used in the work were listed in Table 2.20 and Table 2.21. Antibodies were diluted in 5% BSA/PBST and 50 µl was applied to each coverslips upside down with cell side facing the antibody on parafilm.

Table 2.20: Primary antibodies-Immunocytochemistry

Name	Species	Company	Dilution
CaM	mouse monoclonal	Upstate, 05-173	1:500
c-Fos	rabbit polyclonal	Santa Cruz, sc-253	1:500
phospho-CREB (Ser133)	rabbit polyclonal	Upstate, 06-519	1:500

Table 2.21: Secondary antibodies-Immunocytochemistry

Name	Host species	Conjugate	Company	Dilution
Mouse	goat	Alexa594	Invitrogen	1:500
Rabbit	goat	Alexa594	Invitrogen	1:500
Mouse	goat	DyLight488	Dianova	1:500
Rabbit	goat	DyLight488	Dianova	1:500

2.8 Ca^{2+} Imaging

2.8.1 Live Ca^{2+} Imaging

For Ca^{2+} imaging, we used Fluo-3 acetoxymethylester (Fluo-3, AM, C51H50Cl2N2O23, MW-1129.86, 50 g package, Invitrogen, F-1242) as a Ca^{2+} indicator. DIV 10-12 cultured mouse hippocampal neurons (uninfected or infected on DIV 4) grown on glass coverslip (Roth) were loaded with Fluo-3 at a concentration of about 3 M in CO_2 independent SGG for 20 min at room temperature. Then the coverslip was washed with fresh SGG and then transferred to a custom made chamber with fresh SGG, sitting at room temperature for 20 to 30 min for AM digestion. Calcium imaging was carried out with Leica SP2 confocal microscope. The setting up was as follows: 40x

objective/NA1.25 oil, Zoom 1, 512 x 512 format, 8 bit resolution, xyt scan mode, 400 Hz speed, 1.0 airy pinhole, frame average 1, line average 4 for image, and 1 for time lapse imaging. Virus infected cells were excited with 594 nm laser at 10 30% to see the red fluorescence from mCherry and 30% 488 nm laser for the Ca^{2+} indicator Fluo-3. Emission fluorescence was collected at 600 650 nm for mCherry and 500 550nm for Fluo-3. Time lapse imaging was set with a Δ T of 1.635 sec and totally 200 frames were recorded at the basal Ca^{2+} level recording. Bic or CCh was introduced at frame 120 (about time point 196 sec). To calibrate the fluorescence signal (F), Fluo-3 was saturated by adding 50 µM ionomycin (Fmax, Sigma-Aldrich Chemie GmbH, München, Germany) to SGG solution (containing 2 mM Ca^{2+}) and then quenched with $MnCl_2$ (Fmin). Ca^{2+} concentration was expressed as a function of the Fluo-3 fluorescence Kd * [(F-Fmin)/(Fmax-F)]. The Kd for Fluo-3 was 390 nM at room temperature according to the data sheet. After imaging, data were analyzed offline with ImageJ software (NIH). For the virus infected groups, only mCherry positive cells were analyzed and included in the presented results.

2.8.2 List of Ca^{2+} Indicators

In the study, list of Ca^{2+} sensors (Table 2.22) were used and they were purchased from Molecular Probes™.

Table 2.22: Ca^{2+} Indicators

Indicator	Kd[a] (nM)	Ex[b] (nm)	Em[c] (nm)	Stock (mM)	Working (µM)
Fluo-3	325	506	526	1.46	3.8
Fura-2	140	335/363[d]	510	1	1
X-rhod-1	700	576	602	0.6	0.6

[a] Dissociation constant (Kd) were determined at 22 °C by Molecular Probe™ in 100 mM KCl, 10 mM MOPS, pH 7.2 and 10 mM CaEGTA.
[b] The excitation wavelength used and it is the maximum absorption wavelength.
[c] The maximum emission wavelength.
[d] Fura-2 is a ratiomatric Ca^{2+} sensor and two excitation wavelengthes are used for measuring the free Ca^{2+} concentration.

All the Ca^{2+} indicators were in the form of AM (acetoxymethyl) ester. The AM esters were first reconstituted in DMSO (di-methylsulfoxide) with 20% (w/v) non-ionic detergent Pluronic F-127 to a stock concentration and diluted to working concentration on use. After designed experimental Ca^{2+} imaging, except for Fura-2, the maximum and minimal fluorescence (Fmax and Fmin) were measured. Free Ca^{2+} concentration was calculated using the following equation:

$$Ca^{2+}{}_{\text{free}} = \text{Kd} \cdot \frac{\text{F} - \text{F}_{\text{min}}}{\text{F}_{\text{max}} - \text{F}} \tag{2.1}$$

2.9 Electrophysiology

Whole-cell patch-clamp recordings were made at room temperature from cultured hippocampal neurons plated on coverslips after a culturing period of 12 to 14 days. Coverslips were secured with a platinum ring in a recording chamber (Open Access Chamber-1, Science Products GmbH) mounted on a fixed-stage upright microscope (BX51WI, Olympus). Differential interference contrast optics, infrared illumination, and a Neo sCMOS camera (ANDOR™ Technology) connected to a contrast enhancement unit (Argus, Hamamatsu) and Andor iQ2 sofeware were used to view neurons on a video monitor. Recordings were made with a Multiclamp 700A amplifier, digitized through a Digidata 1322A A/D converter (Axon Instruments), and acquired by using Clampx 10.3 software (Molecular Devices). All membrane potentials were corrected for the calculated junction potential of -11 mV (JPCalc program by Dr. Peter H. Barry). Patch electrodes (World Precision Instrument, Glass thin wall filament 3IN, TW150F-3, 0.1F s/n) were made from a single stage glass microelectrode puller (Model PP-830, Narishige). The settings for the puller were: heat 1, 78.2°C and heat 2, 49°C. Glass pipette capacitance filled with internal solution in aCSF was 3.5 to 4.5 MΩ.

2.9.1 Extracellular Solution & Drugs

Standard aCSF (artificial Cerebrospinal Fluid) was used as extracellular solution for electrophysiological recording. The composition of the aCSF was as in Table 2.23. Osmolarity was measured with a osmometer VAPRO®5520 (Viescor). After preparation, the aCSF was saturated with carbogen (95% oxygen and 5% carbon dioxide) bubbling for 20 min. Cells were recorded with constant aCSF perfusion.

Table 2.23: Artificial Cerebrospinal Fluid (aCSF)

Component	Concentration (mM)	M.W. (g/mol)	10x Stock (g/l)	Osmoliarity (mOsm)
NaCl	125	58.44	73.05	250
KCl	3.5	74.54	2.61	7
$CaCl_2 \cdot 2\,H_2O$	2.4	147.02	3.53	7.2
$MgCl_2 \cdot 6\,H_2O$	1.3	203.03	2.64	3.9
$NaH_2PO_4 \cdot H_2O$	1.2	137.99	1.66	2.4
Glucose $\cdot H_2O$	10	198.17		10
$NaHCO_3$	26	84.01		52
Sum				332.5

Glucose and $NaHCO_3$ are added to the 1 liter of 1x aCSF freshly with the amount of 1.98 g and 2.18 g , respectively.

Pharmacological drugs used during the electrophysiological recording were prepared as stock solution and diluted into aCSF according to Table 2.24. So these drugs were applied as the perfusion

system onto cells.

Table 2.24: Drugs

Drugs	Concentration (μM)	Stock (mM)	Dilution
TTX	0.5	1	1:2000
Gabazine	5	10	1:2000
Cyclothiazide	20	100	1:5000
AMPA	10	5	1:500

2.9.2 Internal Solution

Internal solution was prepared according to Table 2.25. It was used after filtration through a non-sterile PVDF filter, 0.22 μm, 13 mm (Rotilabo®-Spritzenfilter, Roth®).

Table 2.25: Internal Solution

Component[a]	Concentration (mM)	M.W. (g/mol)	For 49.29 ml[b] (mg)	Osmoliarity (mOsm)
K^+-methylsulfate	133	150.2	984.65	266
HEPES	10	238.3	117.46	10
NaCl	8	58.4	23.03	16
KCl	12	74.56	44.10	24
$ATP-Mg^{2+}$	4	507.18	100	8
$GTP-3Na^+$	0.5	523.18	12.89	2
$Phosphocreatine-2K^+$	10	287.3	141.61	30
Sum				326

[a] Each component should be dissolved individually to avoid any precipitation. Final pH value should be between pH 7.35 and 7.45.

[b] This is the final volume for using a whole bottle of $ATP-Mg^{2+}$ containing 100 mg of it.

2.9.3 Blue Light Stimulation

For simultaneous patch recording and ChR2 activation, the blue light from a 470 nm LED through the objective was controlled by Clampx 10.3 software with digital output. The protocol used were either single flash (10 ms duration) or flashes in bursts (10 ms pulse duration at 20 Hz for 1 sec).

2.9.4 Mini Recording

Miniature excitatory postsynaptic currents (mEPSCs) were recorded in the presence of TTX (1 μM, Biotrend, Cologne, Germany). All voltage clamp recordings were performed at a holding potential of -70 mV. mEPSC events were detected using the software MiniAnalysis (Synaptosoft) with a 5 pA amplitude threshold and all mEPSCs were proof-verified manually. Access resistance (Ra) and membrane resistance were regularly monitored during voltage clamp recording to be in the range of 10 - 28 and 150 - 650 MΩ, respectively. If changes larger than 30% occurred, the data was rejected from analysis. Cumulative probability curve was generated from more than 300 mEPSCs. Mean values for mEPSC parameters between groups were analyzed using ANOVA and a post-hoc Turkey's test. All results presented were as mean ± s.e.m.

2.10 Cellular Compartment Analysis of Temporal Activity by Fluorescence In Situ Hybridization (catFISH)

Expression of immediate early genes (IEG) is induced in brain neurons by synaptic activity and is frequently used to monitor neuronal activation. Cellular compartment analysis of temporal antivity by fluorescence in situ hybridization (catFISH) uses fluorescence in situ hybridization (FISH) of IEG RNAs to fixed cultured neurons, and confocal microscope to identify the activity requirement for IEG transcription initiation. The temporal resolution properties of catFISH derive from the time course of IEG transcriptional activation (and subsequent termination) and the translocation of the nascent mRNA to the cytoplasm. Cells active shortly before fixation (2 to 15 min) are distinguished by the presence of one or two areas of intense intranuclear fluorescence; these foci typically disappear within 20 min and the mRNA becomes prominent within the cytoplasm. This cytoplasmic RNA signal is used to identify neurons active 30 to 45 min earlier. Thus, the subcellular location of an IEG RNA signal can be used to discriminate cells activated by two distinct experiences separated by 30 min.

Activation of mouse IEG *Arc* was examined in this study. The plasmid pBSII(SK)-mArc was from Paul F. Worley lab (Johns Hopkins University, School of Medicine, Baltimore, Maryland). The protocol was based on the "catFISH, Neuroanatomical Methods, Current Protocols in Neuroscience" [54], with minor modification.

2.10.1 Plasmid Linearization and Purification

The template plasmid, pBluescript II SK (+)-Arc (pBSII(SK)-Arc)had cDNA for mouse or rat *Arc* gene between EcRI and XhoI restriction sites. This plasmid had T3 and T7 RNA polymerase promoter sequences at the two sides of *Arc* gene (Figure 2.3). Riboprobes were generated from linearized plasmids by *in vitro* transcription using fluorescein-labeled dUTPs. So the combination of EcoRI digestion and T7 polymerase transcription would produce the antisense probe. Similarly,

XhoI digestion and T3 polymerase transcription would produce the sense probe.

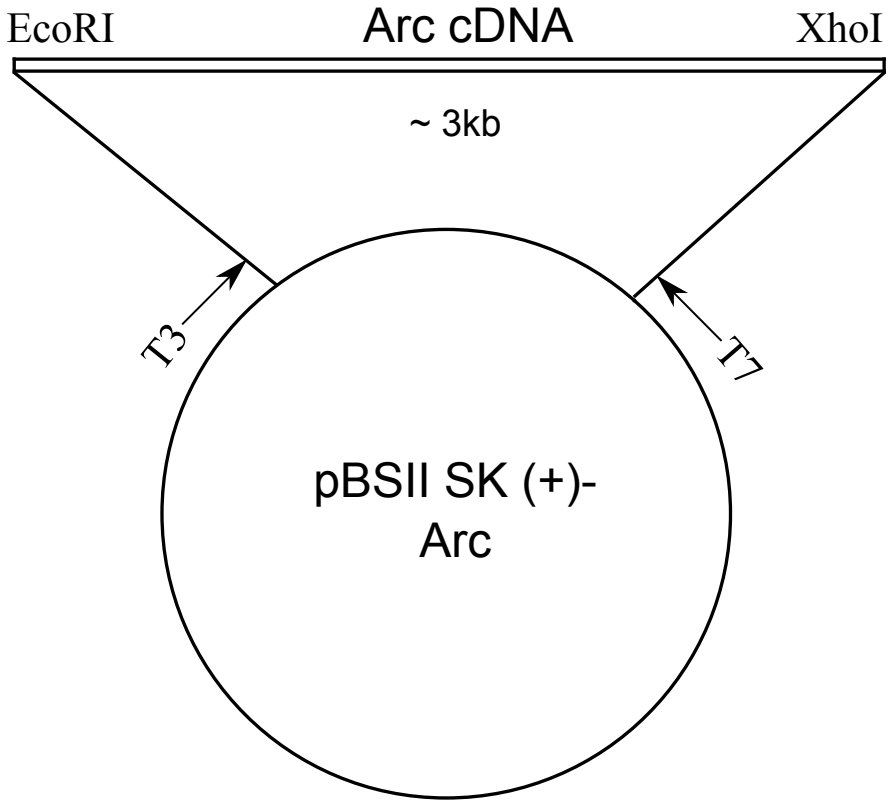

Figure 2.3: *Arc* cDNA in pBSII SK(+) vector. Coding sequence of *Arc* gene was cloned in pBluescript SII SK(+) vector flanked with EcoRI and XhoI restriction sites and T3 and T7 RNA polymerase promoters at each end (from Paul F. Worley, Johns Hopkins University,Baltimore). Restriction enzyme digestion and RNA polymerase are used for *in vitro* synthesis of RNA: EcoRI digested plasmid followed with T7 RNA polymerase *in vitro* transcription produce the anti-sense RNA probe against *Arc* mRNA; XhoI digestion and T3 RNA polymerase transcription make the sense RNA probe.

4.5 µg of the template DNA was digested with EcoRI and XhoI, respectively. An example digestion setup was shown in Table 2.26.

After the digestion, linearization result was tested by running a 1% agrose gel together with the non-digested plasmid. The rest of the linearization product was purified with Phenol/Chloroform method. The cut constructs were filled up to 200 µl with DEPC-treated H_2O and the same volume (200 µl) of Phenol/Chloroform buffer (Tris-buffered 50% phenol, 48% chloroform, 2% isoamyl alcohol solution, so called "25:24:1" solution) was added in. The mixture was mixed with vortex and centrifuged with speed 1300 g at room temperature for 10 min. The supernatant was transferred to a new RNase free tube and the 25:24:1 solution treatment was repeated once again. About 200 µl (as much as possible) supernatant was collected and mixed with same volume of Chloroform. The solution was mixed with vortex and centrifuged at 1300 g, room temperature for 10 min. The supernatant after Chloroform treatment was mixed with 1 µl of glycogen (20mg/ml), 0.1 volume of

Table 2.26: DNA Linearization

Component	60 µl Reaction (µl)
DNA	45[a]
Red Buffer (10x)	6
Enzyme[b]	2
H_2O	up to 60 µl

[a] DNA concentration was adjusted to 100 ng/µl.
[b] EcoRI and XhoI digestion were made separately and parallely.

3 M Na-acetate and 2.5 volumes of absolute ethanol. This mixture was put on dry ice for the DNA to precipitate for 10 to 15 min. After a few seconds of warm up, it was spun down in a 4°C cooled centrifuge at 1400 g for 20 min. This time, the supernatant was discarded and the pellet was washed with 650 µl 70% ethanol twice, both with centrifugation at 4°C , 1400 g for 10 min. The pellet was dried up at room temperature and resuspended with 25 µl DEPC-treated H_2O. Concentration of the purified DNA probe was measured with a photometer (Pharmacia Biotech Ultraspec 2000 Spectrophotometer).

2.10.2 RNA Probes

For the *in vitro* transcription, SP6/T7 Transcription Kit (DIG RNA Labeling Kit (SP6/T7), Roche 11175025910) and T3 polymerase (Roche 11031163001) were used to get the antisense and sense RNA probe for *Arc* gene. The procedure was as follows.

Step 1 1 µg purified template DNA or 4 µl control DNA (vial 3 or 4) and DEPC-treated H_2O was added into a RNase-free tube to the final volume of 13 µl.

Step 2 Following reaction mix (Table 2.27) was prepared on ice.

Table 2.27: *In vitro* Transcription

Reagent	Vial	Volume (µl)
NTP labeling mixture, 10x	7	2
Transcription buffer, 10x	8	2
RNase inhibitor	10	1
RNA Polymerase T7 or T3[a]	12	2

[a] T3 RNA polymerase was purchased separately.

The mixture was mixed gently and briefly spun down.
The tube was incubated at 37 °C for 2 h to do the *in vitro* transcription.

Step 3 After the transcription, 2 µl DNase I, RNase-free was added to remove template DNA.
This was incubated at 37°C for 15 min.

Step 4 The whole reaction was stopped with adding 2 µl 0.2M EGTA (pH 8.0).

After *in vitro* transcription, the products were purified further with columns and the final RNA probe concentration was measured.

2.10.3 Fixation and Prehybridization

After different treatments, cells were fixed with ice-cold 4% PFA (pH 7.2 to pH 7.6) for 10 min. The fixation, following washing and prehybridization steps were summarized in Table 2.28.

Table 2.28: catFISH-Fixation & Prehybridization

Procedure	Solution	Time (min)
Incubation	4% PFA,ice-cold	10
	1x PBS	2
	1x PBS	2
	70% EtOH	1
	95% EtOH[a]	1
Rinse	2x SSC[b]	2
Incubation	Acetic anhydride solution	10
Rinse	DEPC-H_2O	several times
Incubation	1:1 acetone/methanol solution, ice-cold	5
Rinse	2x SSC	5
Incubation	1x Prehybridization solution	30

[a] Point to stop. Coverslips could be stored in 95% EtOH for several days.
[b] SSC: saline-sodium citrate buffer.

For the prehybridization, 1x prehybridization solution (Sigma P1415, 2x concentrate. Diluted 1:1 with deionized Formamide to prepare 1x pre-hybridization solution immediately before use.) was applied to each coverslip on parafilm in the chamber. Some Whatman 3 MM filter paper was saturated with 2x SSC / 50% deionized formamide and put at the bottom of the chamber. Coverslips were incubated in this humid chamber for 30 min at room temperature.

2.10.4 Hybridization

After the prehybridization, coverslips were rinsed in 2x SSC. A final concentration of 1 ng/µl RNA probe (both antisense and sense, separately) were prepared in 1x hybridization solution (Sigma H7140, 2x concentrate. Diluted 1:1 with deionized Formamide to prepare 1x hybridization solution

immediately before use.). The probe was denatured by being heated for 5 min at 90 °C and followed immediately by rapid cooling in an ice bath. Hybridization was performed in the humid chamber in a 56°C oven overnight for at least 16 hours.
Following hybridization, coverslips were washed (Table 2.29) to remove unbound probe or probe which had loosely bound to imperfectly matched sequences. During all the subsequent washing steps, coverslips were gently agitated.

Table 2.29: Wash after Hybridization

Procedure	Solution	Time (min)
Wash	2x SSC[a]	5
	2x SSC	5
	2x SSC	5
Treatment	10 µg/ml RNasaeA in 2x SSC, 37°C	15
Wash	2x SSC	10
Treatment	10 U/ml DNase I[b], 37°C	15
Wash	2x SSC	10
	0.5x SSC	10
	0.5x SSC, 56°C	30
	0.5x SSC	10
Treatment	2% H_2O_2 in 1x SSC	15
Wash	1x SSC	5
	1x SSC	5
	1x SSC	5
	TBS	5

[a] At room temperature if not stated.
[b] DNaseI treatment is needed for transfected or infected conditions only.

2.10.5 Signal Detection

FISH signals were detected with horseradish peroxidase (HRP) conjugated antibody to digoxigenin and amplified using a Cyanine-3 Tyramide Signal Amplification kit (TSA kit, PerkinElmer, NEL704A). Briefly, coverslips were blocked with TNB blocking buffer (0.1 M Tris-HCl, pH 7.5; 0.15 M NaCl; 0.5% Blocking reagent supplied by the TSA kit) at room temperature for 30 min. HRP conjugated DIG antibody (Anti-Digoxigenin-POD, Fab fragments from sheep, Roche 11207733910) was applied to coverslips at 1:100 dilution, 4 °C overnight. On the next day, coverslips were washed three times with TNT wash buffer (0.1 M Tris-HCl, pH 7.5; 0.15 M NaCl; 0.05% Tween 20) at room temperature with 5 min interval. Coverslips were then incubated with Fluorophore Tyramide for 30 min at room temperature. Fluorophore Tyramide was 1:87.5 diluted in Amplification Diluent. After three times wash with TNT wash buffer, coverslips were counterstained with nuclear fluorescent Hoechst 33258 (Serva, 2 µg/ml in PBS) for 5 min at room

temperature. Cells were then washed with PBS for three times with 5 min interval and mounted with Mowiol.

2.10.6 Acquisition of Confocal Image Series

catFISH results were examined with Leica SP2 confocal microscope. The setting up for the confocal microscope was: 63x objective/Numerical aperture 1.32 oil, Zoom 2, 1024 x 1024 format, 8 bit resolution, xyz scan mode, 400 Hz speed, 1.0 airy pinhole, line average 2, frame average 1. Z dimension depth was defined with the Cy-3 signal and normally it spanned 7 to 10 µm. Intensity settings of photomultiplier tubes (PTM) for Hoechst and Cy-3 were set to get the minimal signal but not saturated for the highest. Signals from catFISH and Hoechst staining were scanned sequentially between frames with a ΔZ of 1 µm. For the quantitative analysis, confocal settings was adjust from above with the changes in: 40x objective, Zoom 1, 512 x 512 format, line average 1, and ΔZ 3 µm. These images were merged to get the maximal signal with ImageJ software and analyzed for positive *Arc* signal or signal location.

2.11 Data Analysis

All the imaging data were analyzed off-line with ImageJ [117] and Microsoft Excel™ (2010). Graphs were made with SigmaPlot™ or GraphPad Prism®. Images and graphs were processed and organized in Inkscape [69]. References were managed through JabRef [71]. Statistic analysis was performed with two-tailed homoscedastic Student's T test (n.s.: not significant; *: $p < 0.05$; **: $p < 0.01$; ***: $p < 0.001$).

Chapter 3

Results

Neuronal activity plays a critical role in neural development, in neural circuits formation and maintenance, and in learning and memory [32]. The regulation of gene transcription by neuronal activity is an integral part of the process that underlies learning and memory [40]. Electrical activation of neurons induces transient increases in the intracellular calcium (Ca^{2+}) concentration, which can propagate to the nucleus thereby linking synaptic stimulation to gene regulatory events [11]. However, it is unclear if and how different spatial-temporal patterns of activity give rise to distinct genomic responses. The first aim of my thesis was to use optogenetic methods to investigate activity dependent regulation of signaling pathways and gene expression in hippocampal neurons. Specifically, I expressed Channelrhodopsin (ChR2), a light-gated, cation-selective, small membrane channel in primary hippocampal neurons. ChR2 is a ion channel isolated from *Chlamydomonas reidhardtii* [99]. It is a nonselective cation channel with intrinsic light sensitivity and is widely used in the field of neuroscience research [118, 83, 48]. It is fully functional when expressed in the mammalian system without addition of a cofactor. ChR2 can be activated with blue LED pulses to reliably induce action potential firing.

I made a double mutant of ChR2 [154], C128A and T159C, termed ChR2-ab, which had a longer opening time and larger ion conductance compared to the wild type. Transfection or recombinant adeno-associated virus (rAAV)-mediated gene transfer were used to express ChR2-ab in cultured hippocampal neurons. Action potential bursts and associated Ca^{2+} transients were induced with bursts of blue light. The expression of immediately early genes, including many well-known activity regulated genes are robustly induced with specific blue light stimulation pattern in the ChR2-ab expression cells. The mechanism underlying ChR2-ab function was analyzed.

The second aim of my thesis was to target ChR2 onto the internal membrane system in order to directly evoke Ca^{2+} release from internal stores. Different endoplasmic reticulum (ER) and inner nuclear membrane (INM) targeting sequences were used and the subcellular location of ChR2 was imaged with high-resolution microscopy. Ca^{2+} imaging and electrophysiological recordings suggested that with ER and INM targeting sequences, ChR2 was localized away from the plasma membrane.

The regulation of gene transcription by neuronal activity is an integral part of the processes underlying learning and memory. The third aim of my thesis was to determine what is the minimal activity requirement for transcription initiation. To these ends, I used Bicuculline (Bic)-mediated stimulation of neuronal activity to analyze the minimal activity required for *Arc* transcription initiation. *Arc* was chosen as the model gene and catFISH was applied as the most sensitive method to detect the first transcripts of *Arc* mRNA, and detailed Ca^{2+} imaging was utilized to detect nuclear Ca^{2+} transients. Based on my data, I conclude that one nuclear Ca^{2+} transient is sufficient to initiate *Arc* gene transcription.

3.1 Manipulation of Neuronal Activity with ChR2

In the central nervous system, maintenance and upregulation of activity induces synaptogenesis, promotes dendritic morphogenesis, protects neurons and can enhance cognitive functioning. A decrease in or loss of neuronal activity leads to synapse loss, neuronal degeneration and malfunction of the whole system. One means by which activity regulates neuronal function is through activity regulated gene expression. Afferent stimuli trigger the release of neurotransmitter, which is sensed by the receptors or channels on the target cell's membrane. These signals are then transformed within the cells via intracellular signal transduction pathways. One of the most important second messengers in neurons is Ca^{2+}. Ca^{2+} transients occur at the plasma membrane where NMDA receptors and voltage-gated Ca^{2+} channels are activated and at the ER membrane when Ca^{2+} is released from intracellular stores. Ca^{2+} entering the cell by these means invades nuclei, where it can activate nuclear calcium signaling and lead to activity induced gene transcription. This can happen when nuclear Ca^{2+} binds to CaM, forming the Ca^{2+}/CaM complex, and the complex activates calcium/calmodulin-dependent protein kinase type IV (CaMKIV). CaMKIV phosphorylates CREB at Ser133 site, which then binds to its transcriptional co-activator CBP and initiates gene transcription. Here, ChR2-ab was used as a tool to induce neuronal activity. Activity dependent gene expression was triggered by ChR2-ab activation, ChR2-ab and the underlying mechanisms were analyzed.

3.1.1 Neuroprotective Effects of Synaptic Activity

Enhancing neuronal activity protects neurons against deleterious insults. For this work, I first confirmed the neuroprotective effect of electrical activity induced by Bicuculline (Bic), a competitive antagonist of $GABA_A$ receptors (γ-aminobutyric acid receptor, type A), in our cultured hippocampal neurons. As our hippocampal cultures contained about 10% inhibitory interneurons that imposed a tonic inhibition on the neuronal network, removal of $GABA_A$ergic inhibition with Bic led the neurons to fire synchronous bursts of action potentials. The Bic-induced bursts of action potentials occurred periodically and were associated with global calcium transients (Figures 3.1 A and B). Synaptic stimulation of cultured neurons induced gene expression and protected them against NMDA-mediated excitotoxicity. Here, neurons stimulated with Bic for different periods of

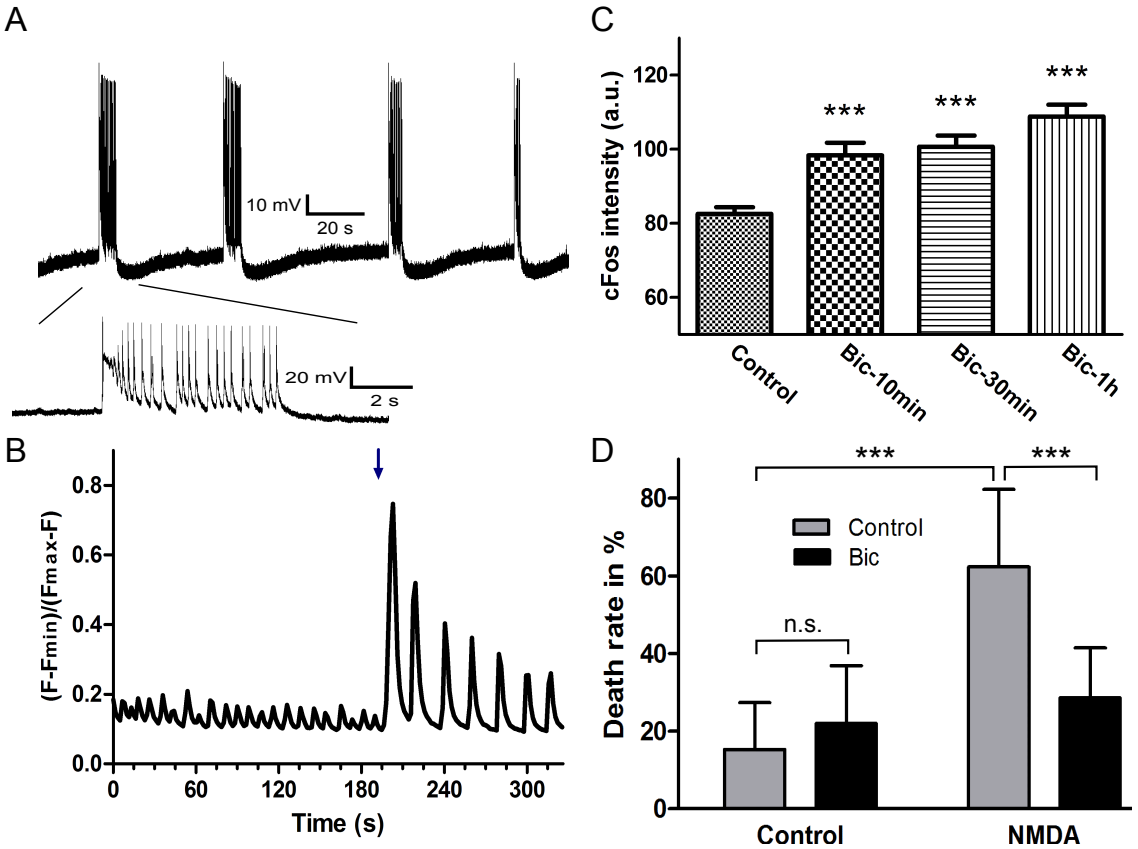

Figure 3.1: Bic treatment produces synaptic activation and protects neurons against deleterious challenge. (A) Electrophysiological recordings of current-clamped neurons treated with 750 µM Bic. Bursts of action potentials were recorded and the inserted trace amplifies a signal burst. (B) Imaging of global Ca^{2+} transients in hippocampal neurons in basal condition and exposure to Bic at marked point (blue arrow). (C) Immunocytochemistry analysis of cFos protein level before (Control) and different time periods of time after Bic stimulated (10 min, 30 min and 1 hour). C-fos level is represented with the staining intensity in arbitrary unit (a.u.). (D) Quantitative analysis of a cell death experiment induced by NMDA bath application (20 mM, 10 min) with and without Bic pre-treatment (50 µM, overnight). Data are represented as mean ± s.d. (n = 3 independent cell preparations).

time (10 min, 20 min and 1 hour) expressed increasing levels of *cFos*, a cellular proto-oncogene belonging to the IEG family of transcription factors (Figure 3.1 C).To verify the protective effect of activity, neurons were challenged with bath-applied NMDA (20 µM NMDA for 10 min), which led to around 60% cell death after 24 hours while the basal cell death rate was below 20%. Cells pre-treated with Bic overnight were more resistant to this deleterious insult (Figure 3.1 D).

3.1.2 ChR2 Induced Activity in Cultured Hippocampal Neurons

Wildtype (wt) ChR2 was used to set up all the stimulation, recording, and subsequent functional analysis used to investigate the possible activity induction function of ChR2 in neuronal cells. Hippocampal neurons were transfected with mCherry-tagged ChR2, and electrophysiological record-

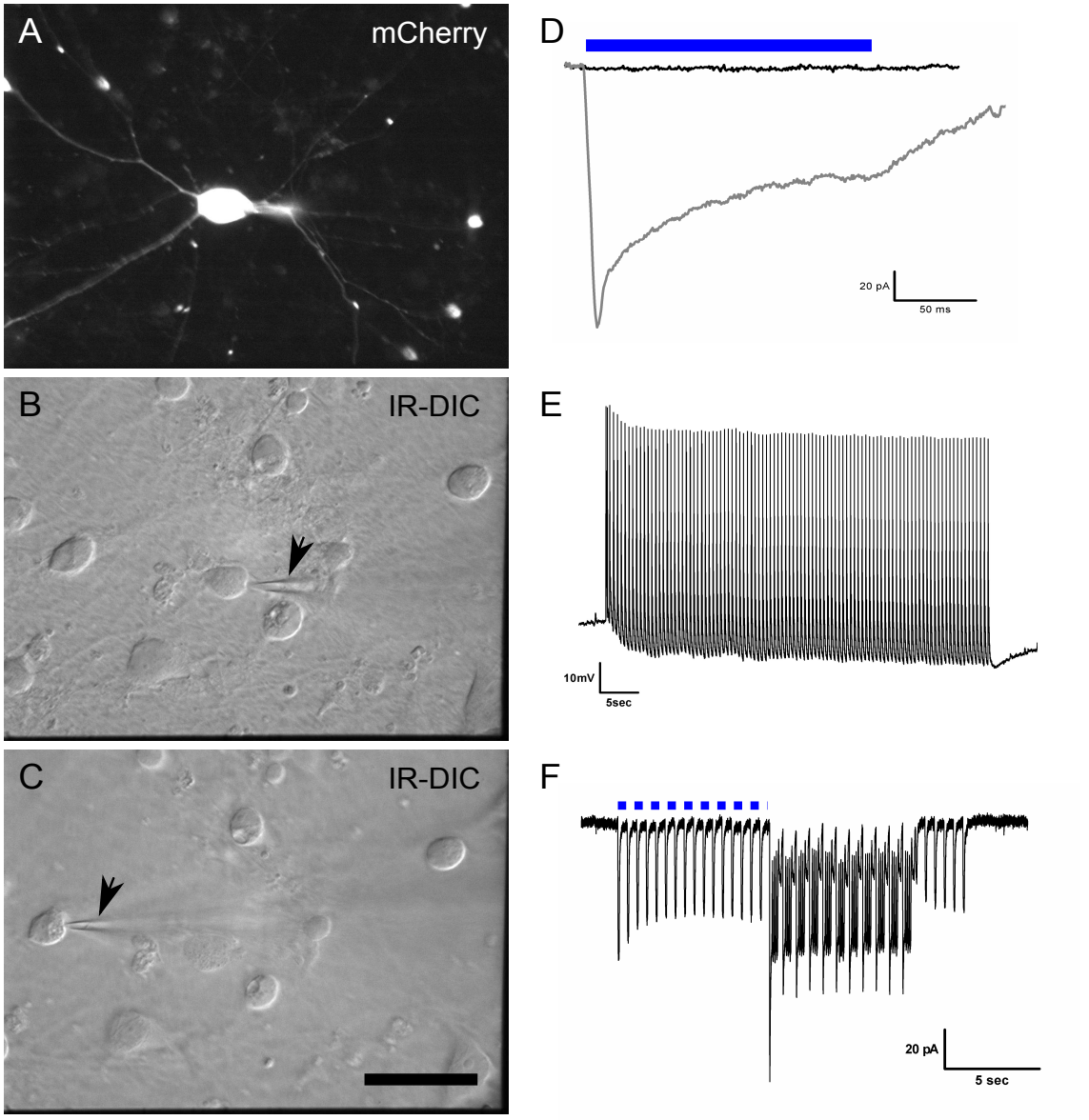

Figure 3.2: ChR2 expressing neurons show blue light specific inward current and action potential. (A) shows a neuron transfected with mCherry-tagged ChR2. (B) and (C) are the infra-red differential interference contrast (IF-DIC) pictures of the same field with pipette patching to the mCherry positive (B) and negative control cells (C). Arrows point to the tip of pipette. The scale bar represents 50 µm. (D) is the result of voltage-clamp showing current change of the negative cell (black line) and positive neuron (grey line) to blue light flash (blue bar). (E) represents voltage changes of the ChR2 expressing neuron to a burst of blue light flashes at 1 Hz with flash duration of 10 ms. (F) shows the current response of ChR2 positive neuron to low frequency (1 Hz with duration of 10 ms) of flashes and high frequency of light bursts (10 Hz with 10 ms duration for 8 sec). Blue bars indicate flashes, not time scaled.

ings were used to measure the light-induced currents triggered after 48 hours of expression. As a membrane protein, ChR2 distributes well all over the neurons, including the dendrites, and forms puncta at some branching points. Stimulation using the blue light evoked large inward currents in ChR2-expressing cells (Figure 3.2). Control cells exhibited no response to blue light as shown by the black line in (D). Neurons expressing ChR2 fired reliable action potentials to 1 Hz blue flashes for a prolonged time as shown in (E). When the flash frequency was increased, however, cells failed to resolve it, and instead exhibited a sustained negative current. I next examined the Ca^{2+} transients triggered by ChR2-induced activity. As the blue light used to visualize fluo-based small molecule Ca^{2+} probe activates ChR2, I chose to use Fura-2 and X-rhod-1 as calcium sensors. Fura-2 is a ratiometric calcium dye with excitation peaks at 340 and 380 nm. Because 380 nm is strong and closer to 470 nm (to activate the ChR2), I first did single-wavelength imaging using 340 nm. Ca^{2+} transients were indeed detected in concert with light flashes, but, as shown in Figure 3.3 (D), the amplitudes were very small. I next performed the imaging with 380 nm excitation. Fluorescence changes detected under these conditions were much larger than those observed with 340 nm. However, as the electrophysiological recordings shown in Figure 4.1 demonstrate, 380 nm light- and, to a lesser extend-340 nm light activated ChR2. Therefore I elected to use X-rhod-1 to detect Ca^{2+} changes as the activation light for X-rhod-1 (560-580 nm) did not appreciably activate ChR2 (data not shown). In this case, use of an mCherry tag would not be appropriate as its excitation spectrum lies within the band of wavelengths used to excite X-rhod-1. I therefore removed the mCherry tag from the original ChR2 construct and performed the Ca^{2+} imaging blindly. Figure 3.3 (F) shows the Ca^{2+} transients evoked by blue flashes in one representative neuron. Although the calcium imaging with ChR2 was not very successful, it was clear that activation of ChR2 did induce calcium transients. I therefore moved on to analyze the cellular functions of ChR2 activation in neurons.

3.1.3 Characterization of Different ChR2 Mutants

After the first identification of ChR2 and application into neuroscience research, the coding sequence of ChR2 was optimized to the human codon for better expression in human systems. I tested both the original algal sequence and the human codon optimized sequence, and did not observe any differences in expression. After some discussion with other labs, I decided to use the original ChR2 coding sequence.During the evolution of optogenetic methods, many mutations of ChR2 having different properties were developed. Two of them drew our interest. One was ChR2-C128A, also called step-function opsin (SFO) or bi-stable ChR2 [13]. The cysteine at residue 128 is mutated to alanine. It is called ChR2-a in this study and it has a longer opening time than the unmutated ChR2. ChR2-a can be activated with blue light and inactivated with green light, and is as such bi-stable. The other ChR2 mutant that drew our interest was ChR2-T159C, which we call ChR2-b. ChR2-b harbors a threonine to cysteine mutation at residue 159. ChR2-b is a high-efficiency channelrhodopsin and can mediate fast neuronal stimulation at low light levels [12]. In order to induce gene expression, we thought that a combination of these two mutants could make a cell-depolarizing tool (ChR2-ab). Figure 3.4 shows that all three mutants expressed well in neurons. Cultured hippocampal neurons were infected on DIV 4 and were fixed on DIV 11.

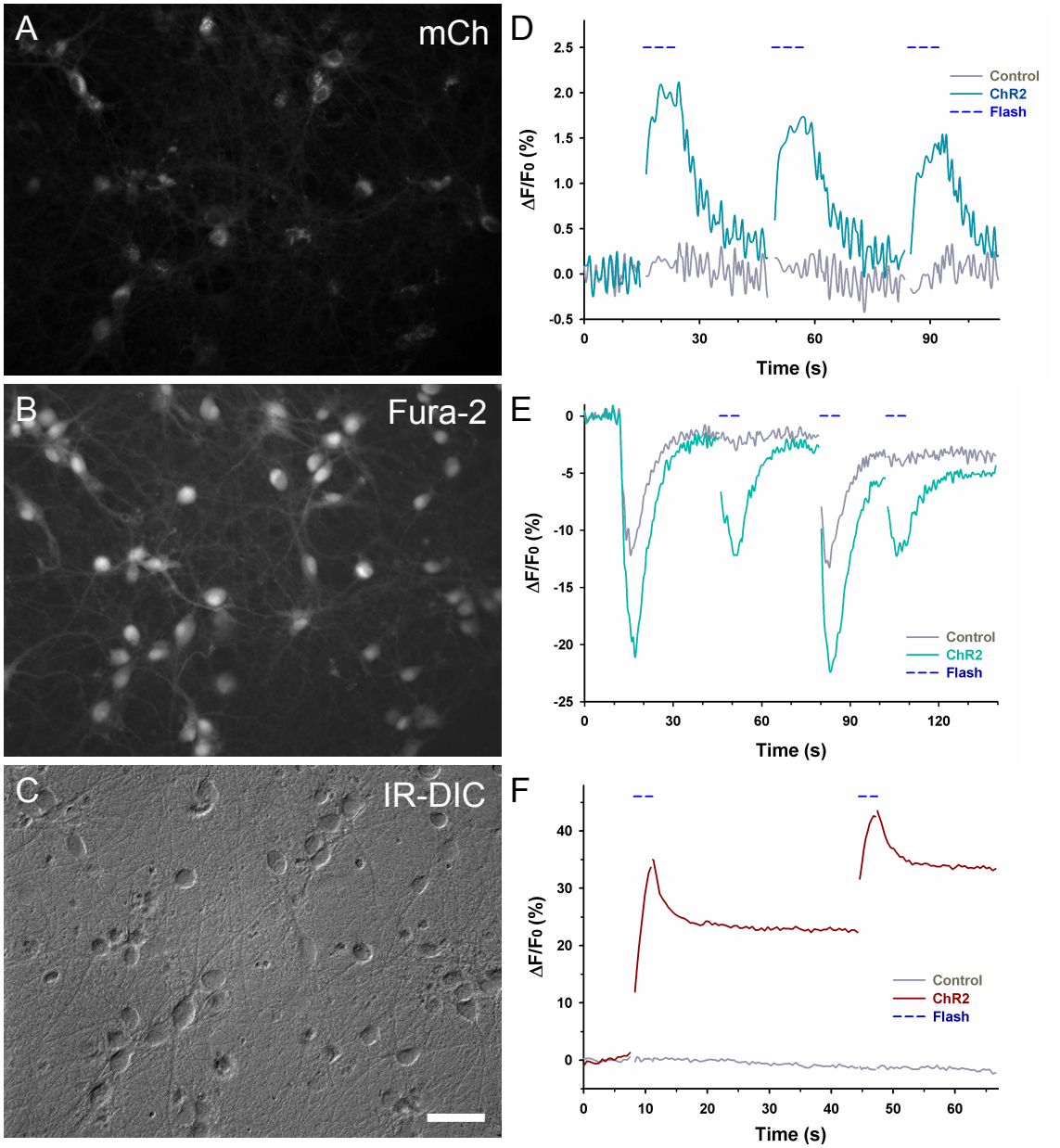

Figure 3.3: ChR2 activation causes Ca^{2+} transients in neurons. (A) shows the mCherry channel representing the infected neurons. (B) is the picture after Fura-2 loading taking with 380 nm excitation wavelength. (C) is infra-red differential interference contrast (IR-DIC) image of the cells in the same field. (D) and (E) are recording results from Fura-2 Ca^{2+} imaging made with 340 nm and 380 nm excitation, respectively. Note the different scale of Y-axis. (F) shows the X-rhod-1 imaging result. Grey lines are uninfected neurons and colored lines represent ChR2 expressing cells. The scale bar is 50 µm.

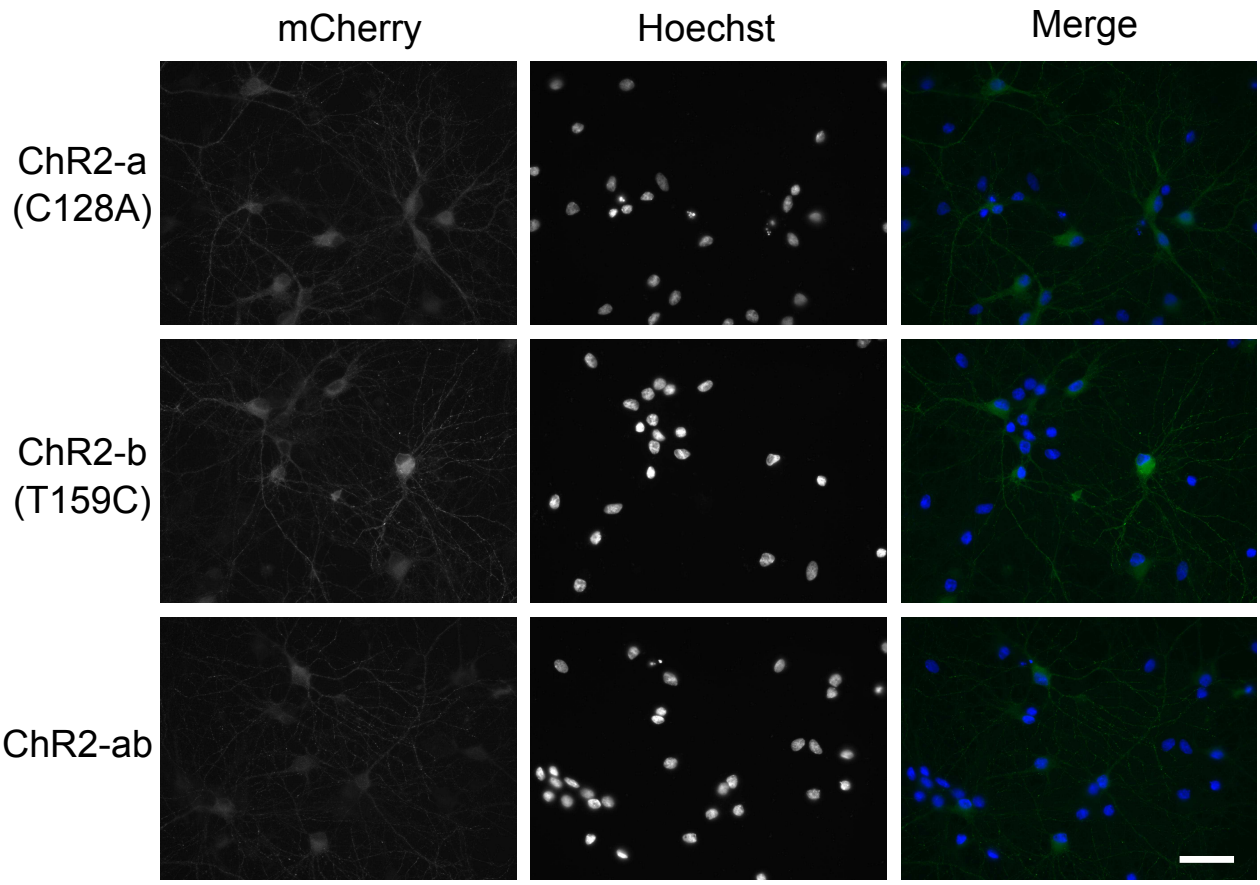

Figure 3.4: AAV mediated expression of different ChR2 mutants. Two single mutants, ChR2-a (C128A) and ChR2-b (T159C), and a double mutant, ChR2-ab (C128A+T159C), are shown. mCherry channel is the fluorescent tag showing the distribution of ChR2. Hoechst is the nucleus counter staining. The scale bar represents 50 μm.

3.1.4 Gene Induction Elicited by ChR2-ab

To investigate the potential cellular function of ChR2s, I performed quantitative PCR (Q-PCR) to analyze the expression level of activity regulated genes upon light-mediated activation of cultured neurons. For this experiment, neurons were infected with rAAV viruses carrying different versions of mCherry-tagged ChR2 coding sequences. Infection was chosen because the efficiency is much higher than transfection; about 30% in rat culture and reaching 80 to 90 % of the cell population in mouse culture. As a membrane protein, ChR2 needs a certain period of time to be expressed and inserted into the cell membrane to function properly. For this experiment, we therefore used mouse cultures and performed gene expression analysis nine to ten days after infection on DIV 13/14. The expression level of nine activity-regulated inhibitor of death (AID) genes [157] was analyzed in cells infected with ChR2-a, -b and -ab mutants stimulated with blue light for four hours. As shown in Figure 3.5, only ChR2-ab infected neurons responded. The raw data of 6 representative genes (gene level with and without LED light stimulation) show that expression is only induced in cells infected with ChR2-ab mutant (Figure 3.5 A-F). This result can be clearly seen when the light-stimulated gene expression levels are normalized to unstimulated gene expression levels from the same group of cultures (Figure 3.5 G). Except for *btg2*, which is induced with fast kinetics after AP bursting and peaks at 2 h instead of 4 h [157], all genes are significantly and specifically up-regulated in ChR2-ab infected cells with blue light stimulation.

Because of this obvious phenomenon of ChR2-ab, I then focused on verifying its function and the underlying mechanism.

3.1.5 Mechanism of ChR2-ab Function

Induced expression of the nine analyzed activity-dependent genes in ChR2-ab expressing neurons strongly suggested that artificial activity could be applied to neurons in a controlled manner and this exogenously introduced activity initiated endogenous cellular responses. But the underlying mechanism was still not clear. The next questions we asked were how ChR2-ab-mediated activity was transduced into cells, and which effectors were involved in the gene induction process. Pharmacological methods were used to identify whether other receptors or channels were involved in the function of ChR2-ab.

To investigate the involvement of NMDA receptors, AMPA receptors, L-type voltage dependent calcium channels (VDCC), and sodium channels, I treated hippocampal neurons with 10 μM MK801 plus 50 μM APV, 20 μM DNQX, 10 μM Nifedipine, and 1 μM TTX, respectively, for 30 minutes prior to and during stimulation with blue light. As shown in Figure 3.6, the induction was completely blocked when L-type VDCCs were inhibited. Unexpectedly, DNQX treatment resulted in the induction of some AID genes under basal conditions. This effect was enhanced the cells were stimulated with blue light. A similar effect has been reported for BDNF-mediated activity [113]. In particular, the BDNF-induced expression of *Arc* was enhanced in the presence of NBQX, another AMPA receptor blocker. Because of the effect of DNQX on basal gene expression, AMPA receptor involvement was not further analyzed in ChR2-ab function. From the normalized gene

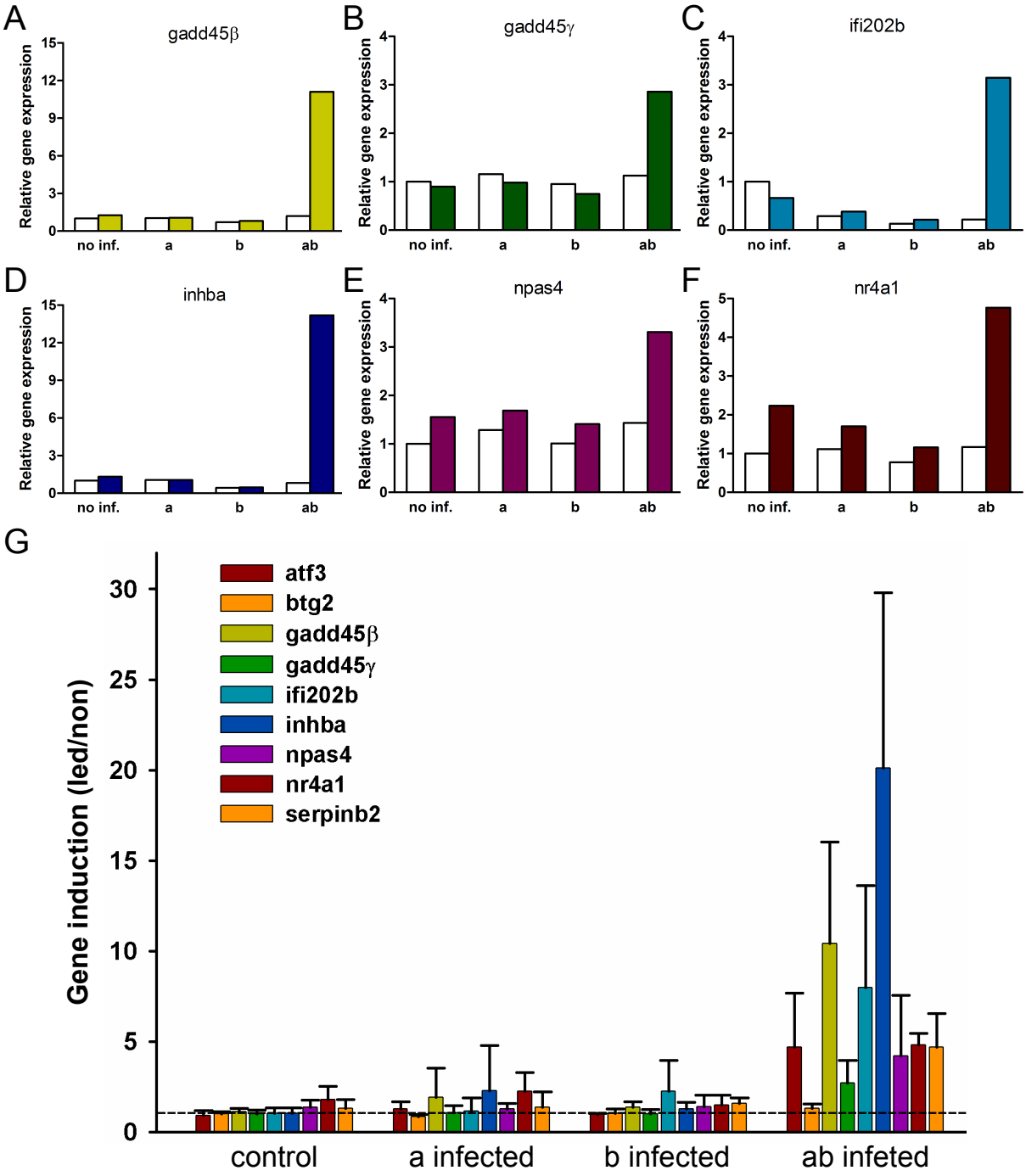

Figure 3.5: Gene level analysis of activity-regulated inhibitor of death (AID) genes with Q-PCR on control, ChR2-a infected, ChR2-b infected and ChR2-ab infected neurons. (A) to (F) Q-PCR analysis of relative gene expression of six representative genes in un-infected, ChR2-a-mCh, ChR2-b-mCh and ChR2-ab-mCh infected cultures (no inf., a, b and ab, respectively) with (colored bars) and without (blank bars) blue light treatment from one representative experiment. (G) Ratiomatric analysis of 9 AID gene expression level between LED light stimulated and non-treatment conditions with the respective infection. Dotted line marks no gene induction (1 fold). Except for *btg2*, all other 8 genes in "ab infected" group were significantly higher than control. Data are represented as mean ± s.d. (n = 3 independent cell preparations).

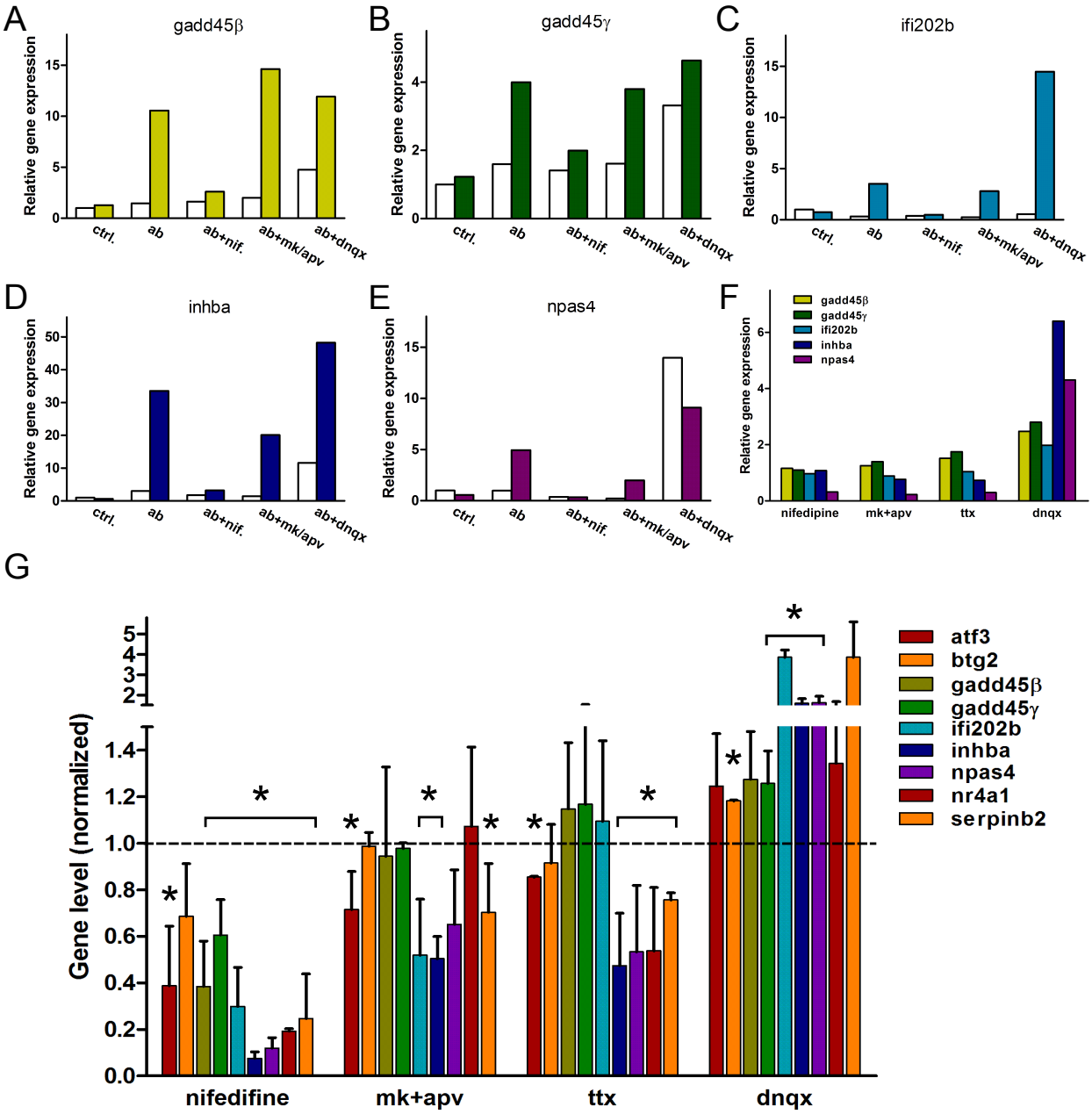

Figure 3.6: ChR2-mediated gene induction is mainly dependent on L-type VDCC. (A) to (E) are Q-PCR analysis results showing raw data of relative gene levels of *gadd45β, gadd45γ, ifi202b, inhba* and *npas4* in control (ctrl.) and ChR2-ab infected (ab) cells with and without LED stimulation in the absence and presence of 10 μM nifedipine (nif.), 10 μM MK801 + 50 μM APV (mk/apv) and 20 μM DNQX (dnqx) of one representative experiment. Blank bars represent no light stimulation and colored bars are with LED treatment for 4 hours. (F) is Q-PCR results showing the level of the same 5 genes in the basal condition without LED treatment but in the presence of nifedipine, MK801+APV, TTX (1 μM, ttx) and DNQX in control cells after 4.5 hours treatment (0.5 hour pretreatment). Note that DNQX treatment itself already potentiates gene expression. (G) is normalized Q-PCR results of activity-regulated inhibitor of death (AID) genes between light stimulated ChR2-ab infected neurons with and without blocker pretreatment. Dotted line marks no gene induction (1 fold). Data are presented as mean ± s.d. and n=3.

expression analysis, ChR2-mediated, light-induced expression of *atf3, inhba* and *serpinb2* were L-type VDCC, NMDA receptor, and sodium channel dependent. As mentioned above, four hour stimulation was not the optimal time point for analyzing the induction level of *btg2*, and it did not show any dependency on any receptor/channel here. Except for *btg2*, ChR2-ab mediated induction of all other 8 AID genes was significantly inhibited when L-type VDCCs were blocked with Nifedipine. Excepting *gadd45*β and *gadd45*γ, AID gene induction was also blocked by pharmacological antagonism of NMDA receptors or sodium channels. These results indicate that L-type VDCCs play an essential role in ChR2-ab mediated gene induction.

Previous data have shown that nuclear calcium plays a particularly important role in activity-dependent transcription. To investigate the potential role of nuclear calcium signaling in ChR2-ab-mediated gene transcription, calmodulin binding protein 4 (CaMBP4) was used to inhibit nuclear calcium function. CaMBP4 is a nuclearly localized protein that contains four repeats of the M13 calmodulin binding peptide derived from the rabbit skeletal muscle myosin light chain kinase. It binds to and inactivates the nuclear calcium/calmodulin (Ca^{2+}/CaM) complex [144]. As shown in Figure 3.7 A, four example genes (*arc, bdnf, c-fos* and *inhba*) whose expression are dependent on nuclear calcium signaling [156], were induced with LED light stimulation in ChR2-ab-infected neurons. This induction was blocked when the cells were co-infected with viruses harboring CaMBP4. The gene induction levels of nine AID genes were analyzed in this experiment. In Figure 3.7 B, basal level 1.0 means CaMBP4 has no blocking effect and numbers smaller than 1.0 mean that nuclear calcium function inhibition blocked the gene induction. In this case, all nine AID genes show nuclear calcium dependency as the gene induction level after normalization was lower than 1.0.

Given the importance of CREB and its co-activator CREB binding protein (CBP) in mediating transcriptional activation by synaptic activity and nuclear calcium signaling, and in light of the critical role of CREB/CBP in neuronal survival, I next tested the role of CBP in ChR2-ab induced gene expression. In these experiments, I used a protein called E1A to interfere with the function of CBP. E1A is an adenovirus protein whose major role is to induce cell entry into the S phase of the cell cycle. It thus provides an optimal environment for viral replication [100]. E1A achieves this effect by interacting with a number of cellular proteins, including the CBP/p300 family of transcription coactivators. E1A binds to CBP via its amino terminal-conserved region 1 (CR1) and disrupts its function by competitively inhibiting the interaction between CBP and cellular transcription factors [6]. As expected, rAVV-mediated expression of E1A blocked the ChR2-ab induced expression of *c-fos* (Figure 3.8 B), a known target of the CREB/CBP transcription factor complex [28]. Expression of E1A also blocked the light-mediated induction of most AID genes. Expression of a mutant version of E1A lacking the CR1 domain (E1AΔCR1) that fails to interact with CBP had no effect on *bdnf, c-fos, gadd45*β or *inhba* regulation. When these data examining the role CBP are analyzed in the same way as were the data for CaMBP4, it can be clearly seen that E1A blocked ChR2-ab-mediated, light-induced, expression of *arc, bdnf, c-fos, gadd45*β*, gadd45*γ*, ifi202b, inhba* and *nr4a1*. These results indicate that CBP plays an essential role in ChR2-ab-induced gene induction.

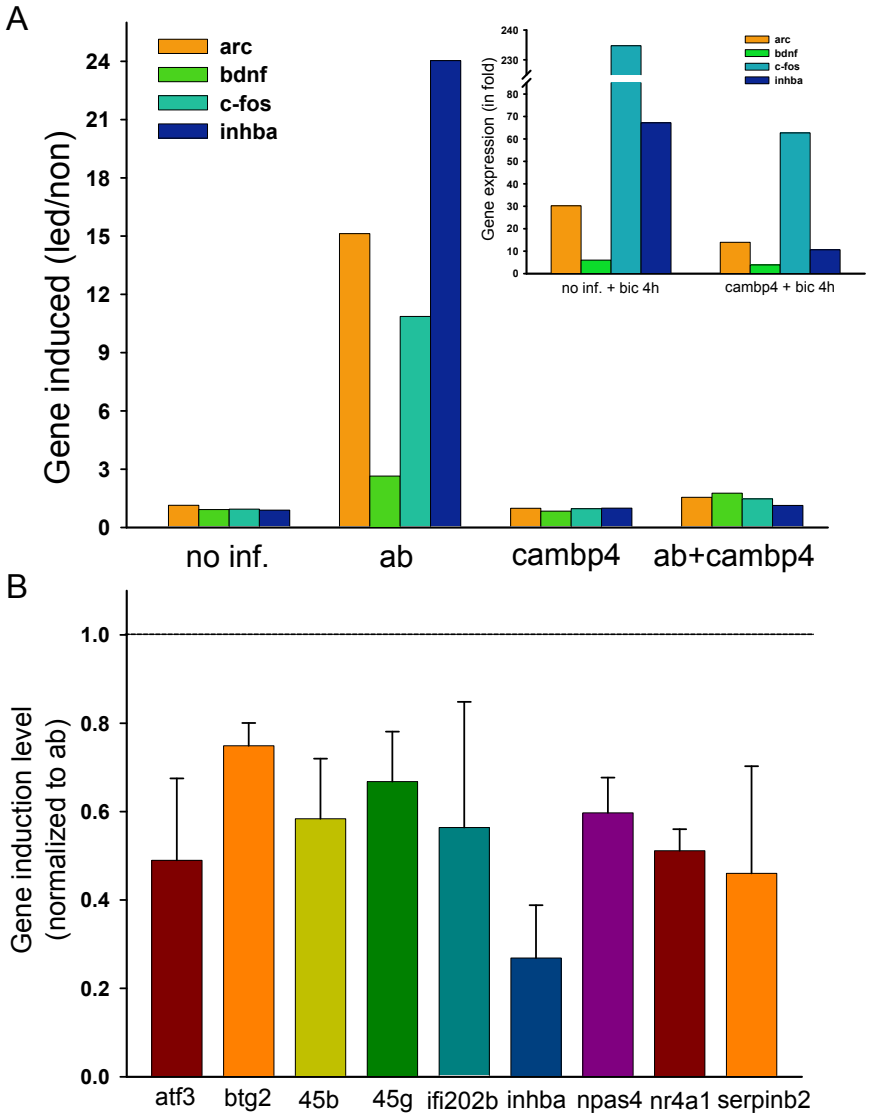

Figure 3.7: ChR2-ab mediated gene induction is dependent on nuclear Ca^{2+}. (A) is four representative genes showing the expression level (ratio between LED stimulated and non-treated conditions, led/non) in no infected (no inf.), ChR2-ab infected (ab), CaMBP4 infected (cambp4) and double infected with ChR2-ab and CaMBP4 (ab+cambp4) conditions of one representative experiment. Inset is the same four genes induced with Bic stimulation for 4 hours and this Bic mediated gene induction is blocked when the cells are infected with CaMBP4. (B) is the normalized induction level of 9 AID genes showing the effect of CaMBP4. A ratio of gene level between light stimulated double infected (ChR2-ab and CaMBP4) and ChR2-ab single infected cultures is made and level 1.0 indicates the gene induction is not effected by CaMBP4. Light induced, ChR2-ab mediated induction of all 9 AID genes are significantly inhibited by CaMBP4 expression (n=4).

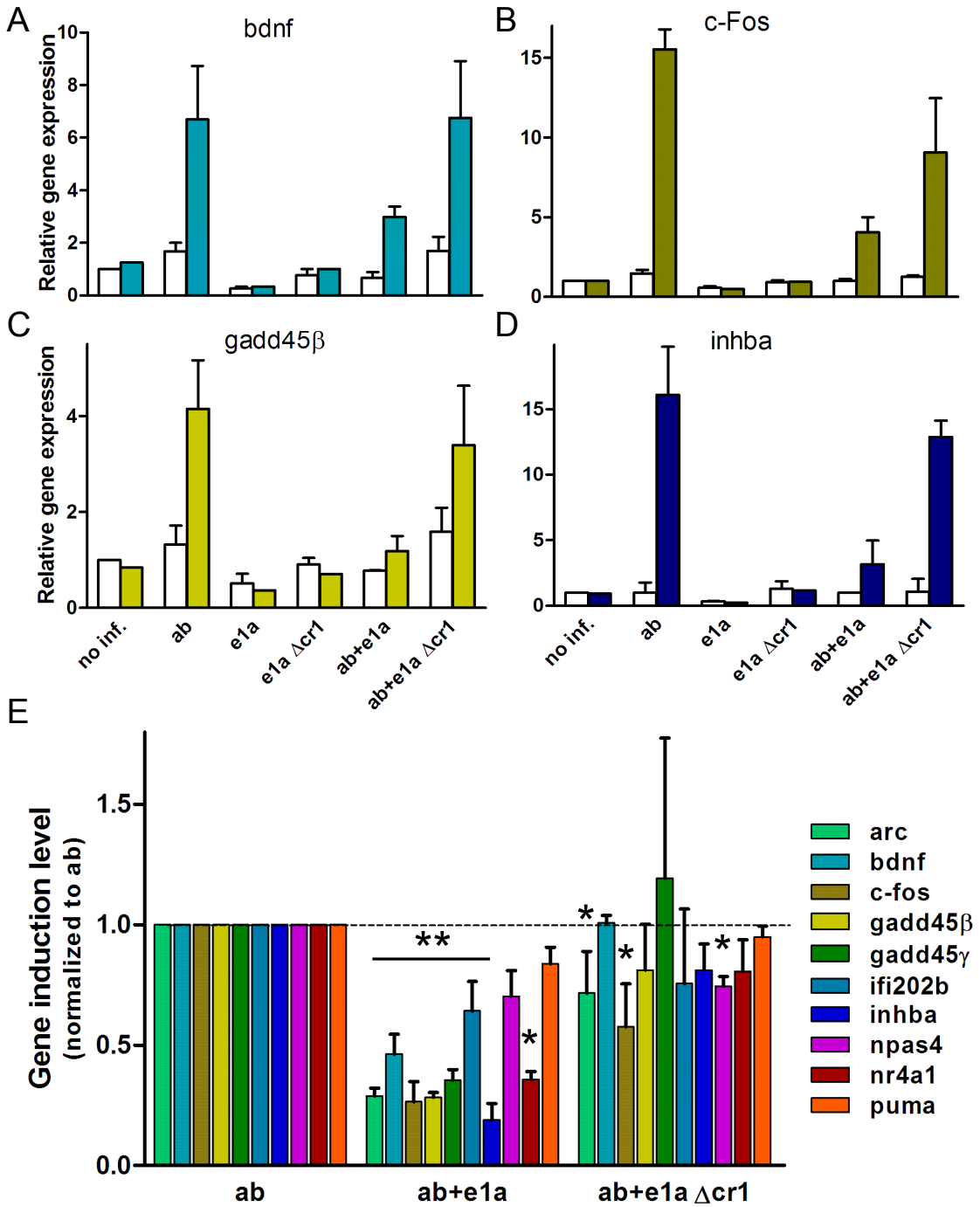

Figure 3.8: Disruption of CBP function inhibits light induced gene expression in ChR2-ab infected neurons. (A) to (D) are Q-PCR analysis of four representative genes showing the raw data with and without LED light stimulation for 4 hours. Cells were not infected (no inf.), infected with viruses expressing ChR2-ab (ab), E1A (e1a), E1AΔCR1 (e1aΔcr1) and double infected. (E) shows the effect of E1A on gene induction. Q-PCR analysis of 10 genes with double infection are normalized to ChR2-ab single infection (n=3).

3.1.6 Signaling pathways activated with ChR2-ab-mediated activity

I next investigated the signaling mechanisms through which ChR2-ab induces gene expression upon light activation. Whole cell lysates from cultured hippocampal neurons infected with AAV-ChR2-ab and stimulated with blue light were subjected to immunoblot analysis using antibodies specific for phosphorylated-CREB (pCREB, at Ser133 site) and phosphorylated-ERK1/2 (pERK, dually phosphorylated at Thr202 and Tyr204 of ERK1, Thr185 and Tyr187 of ERK2). To our surprise, the basal levels of pCREB and pERK were elevated in ChR2-ab-expressing neurons and they were reduced following 10 min light stimulation. In a control experiment, we found that light stimulation did not affect CREB or ERK phosphorylation in uninfected neurons (Figure 3.9 A). Previous work has shown that calcium entry through extrasynaptic NMDA receptors activates a general and dominant CREB shut-off pathway [62]. I therefore used MK801 and APV to examine whether extrasynaptic NMDA receptors mediated CREB shut-off was the case in ChR2-ab-expressing cells. MK801 is a non-competitive and APV is a competitive antagonist of NMDA receptors. They were used together to block both synaptic and extrasynaptic NMDA receptors. As shown in Figure 3.9 A, B and C, pre-incubation of neurons with MK/APV only partially blocked the decrease in CREB phosphorylation upon LED stimulation. We therefore turned to another way of investigating the involvement of extrasynaptic NMDA receptors in light-induced CREB de-phosphorylation: in uninfected neurons, 50 mM KCl was used for 20 min to promote phosphorylation of CREB. When NMDA was then bath applied for 10 min, pCREB level was reduced. Stimulation with blue light mimicked the effect achieved with NMDA bath application; both NMDA treatment and light stimulation resulted in decreased pCREB levels in ChR2-ab-infected cells. Any further treatment (KCl, KCl+NMDA or KCl+LED) decreased pCREB level in ChR2-ab infected cells (3.9 D). These results indicate that light-induced, ChR2-ab-mediated CREB shut-off is achieved through activation of extrasynaptic NMDA receptors.

3.1.7 Increased basal activity in ChR2-ab infected neurons

Network neuronal activity is critical for signal transduction and gene induction. To study the causal element for elevated basal pCREB in ChR2-ab expressing neurons, I performed whole-cell patch clamp recordings and measured the miniature excitatory postsynaptic currents (mEPSP). The particular aim of these experiments was to determine whether ChR2-ab infection had any effect on the electrical properties of the neurons. As a control for potential artifacts resulting from the overexpression of a membrane protein, ChR2-b was included in this experiment. As shown in Figure 3.10, ChR2-ab-infected neurons resulted in a markedly increased basal activity, which was evident in the strongly decreased inter event interval (IEI). By contrast, expression of ChR2-b had no influence on the IEI (Figure 3.10 G). The membrane resistance of ChR2-ab infected neurons was significantly lower than that measured in uninfected cells (Figure 3.10 D). This might be due to the decreased IEI. Other electrical properties, including membrane capacitance (Cm), mEPSC rise time and decay time, mEPSC amplitude, and access resistance (Ra) for patching were not different from that measured in uninfected neurons. Furthermore, no difference was found between uninfected,

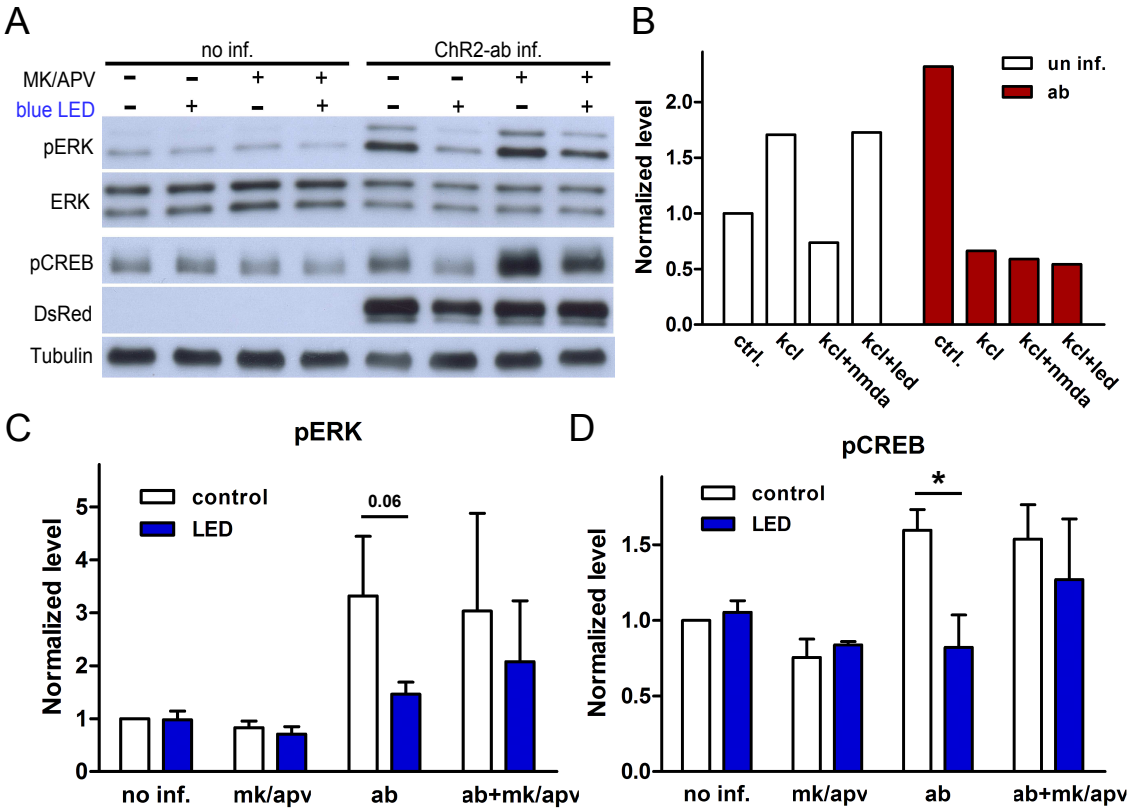

Figure 3.9: Activation of CREB and ERK are elevated in ChR2-ab expressing neurons and light stimulation decreases it. (A) is the western-blot analysis by using CREB and ERK phosphospecific antibodies (pCREb and pERK) in uninfected (no inf.) or AAV-ChR2-ab infected (ChR2-ab inf.) hippocampal neurons with and without LED light stimulation in the presence or absence of 10 μM MK801 and 50 μM APV. ERK is the internal protein level control for pERK. DsRed blots mCherry tag to show the presence of ChR2-ab. Tubulin is used as loading control. (B) shows the responses of control (un inf.) and ChR2-ab infected (ab) neurons to 20 μM NMDA (kcl+nmda) and LED (kcl+led) with and without pretreatment with 50 mM KCl for 20 min (kcl).(C) and (D) are quantitative analysis of pERK and pCREB levels. Blank bars present control condition and blue bars are the LED stimulated ones. Data are presented as mean ± s.e.m. and n = 3 independent preparations.

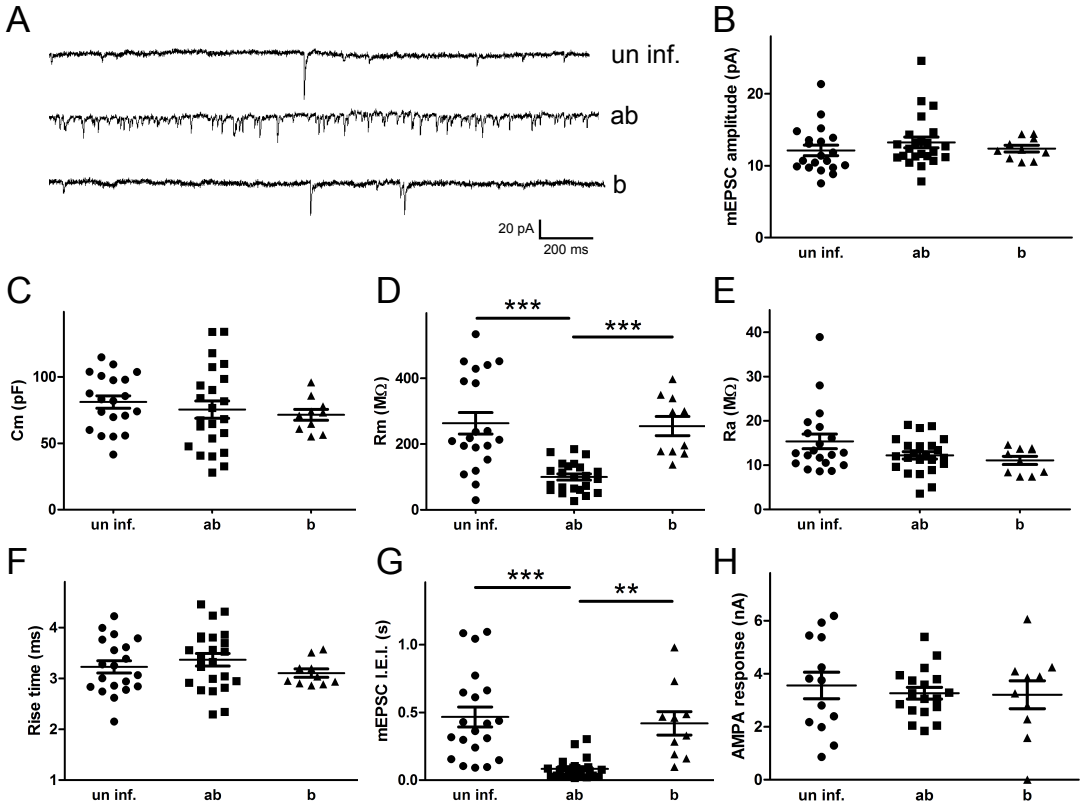

Figure 3.10: Patch-clamp analysis reveals that ChR2-ab expressing neurons show higher basal activity. (A) is representative traces of mEPSC recording with un-infected and infected neurons with ChR2-ab and ChR2-b. (B) to (H) are scatter plots showing the distribution and mean ± s.e.m. (horizontal bars) of mEPSC amplitude (B), membrane capacitance (Cm) (C), membrane resistance (Rm) (D), access resistance (Ra) (E), rise time of mEPSC (F), inter event interval of mEPSC (I.E.I.) (G) and amplitude of AMPA responses (H). Data are presented as mean ± s.d.. Each dot is one cell in one coverslip and 5 cell preparations are included.

ChR2-b-infected, and ChR2-ab-infected neurons with regards to the total number of AMPA receptors, which was measured via the amplitude of the depolarizing response to bath-applied AMPA (Figure 3.10 H). These results indicate that the expression of ChR2-ab in neurons increases their basal activity level without altering the number of AMPA receptors, quantal size or the gross membrane properties.

3.1.8 ChR2-ab in cell death

Induction of the AID genes in ChR2-ab-expressing neurons strongly suggests its potential as a tool to protect neurons from death. To investigate the role of light-induced activity in neuronal survival, I carried out a cell death assay in which bath application of NMDA or staurosporine (STS) were used to induce cell death in cultured hippocampal neurons. To our surprise, stimulation of ChR2-ab did not show any protective effect, but instead induced massive cell death. I then turned to analyze the basal cell death 20 hours after 4 hour LED activation on DIV 10 and DIV 14. As neurons developed *in vitro*, the basal cell death rate increased, both in un-infected and in ChR2-ab-infected cultures (Figure 3.11 E, compare DIV 10 and DIV 14 in control condition). On DIV 14, stimulation with blue light led to significantly more cell death in ChR2-ab-infected than in control neurons. These findings, together with our observations that ChR2-ab stimulation leads to CREB shut-off and an increase in basal activity, led us to conclude that activating ChR2-ab in neurons partially activated extrasynaptic NMDA receptors; and that this effect dominated the beneficial synaptic activation, leading to cell death.

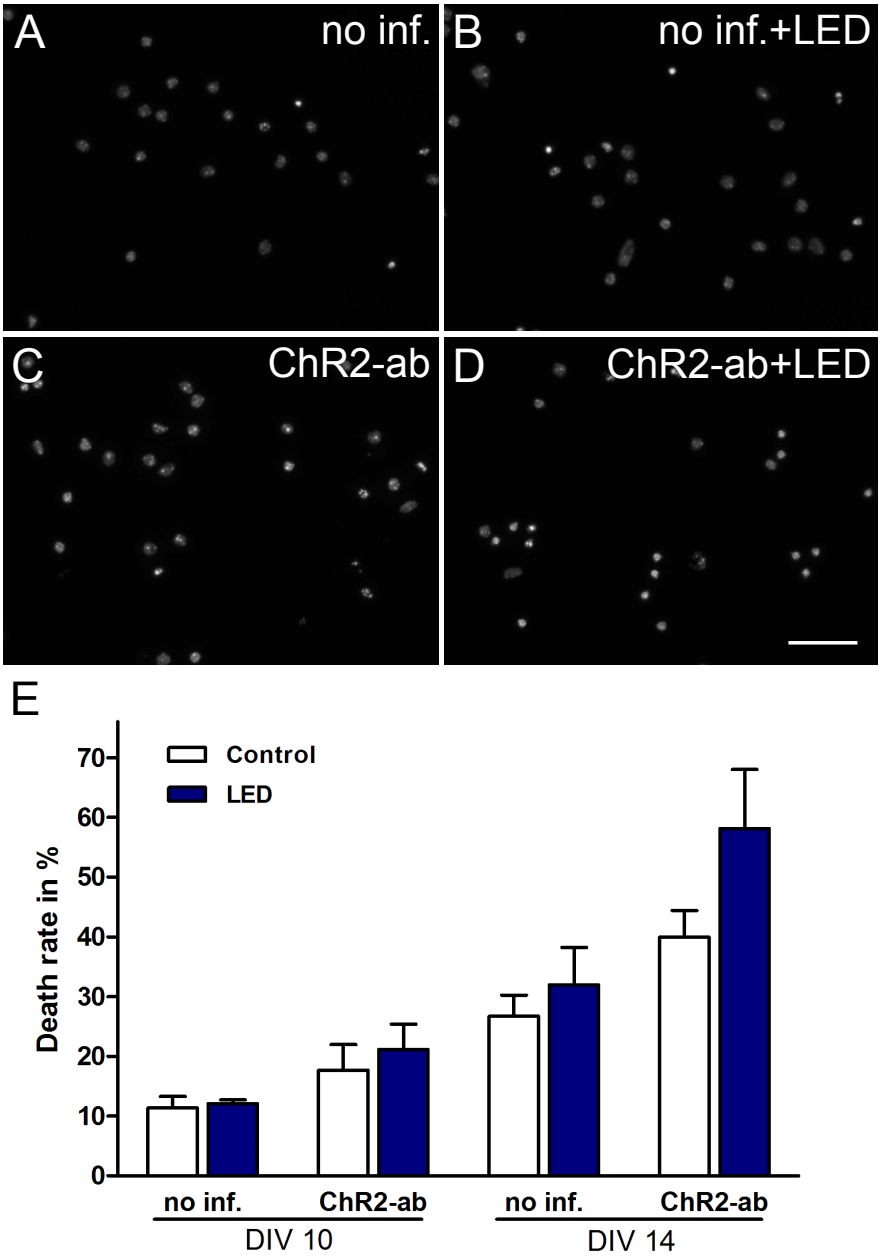

Figure 3.11: LED induced cell death in ChR2-ab infected culture. (A) to (D) are pictures of Hoechst staining from DIV 14 of non-infected (no inf.) and ChR2-ab infected (ab) cells with and without LED stimulation. Concentrated and bright nuclei represent dead cells. (E) is the quantitative analysis of cell mortality on both DIV 10 and 14 with blank bars for control and blue bars for LED stimulated conditions. Data are presented as mean ± s.e.m. and from 4 independent cell preparations. Scale bar is 50 µm.

3.2 Targeting of ChR2

The nuclear Ca^{2+} pool can decode neuronal impulse patterns and may specify transcriptional responses. Buffering the nuclear Ca^{2+} by microinjecting BAPTA-D70 specifically reduced nuclear Ca^{2+} rises induced by high KCl treatment and inhibited gene expression mediated by CREB [61]. However, whether nuclear Ca^{2+} itself is sufficient to activate CREB and induce gene transcription is not yet clear. Recent reports show that the nuclear envelop (NE), which is contiguous with the ER lumen, serves as a Ca^{2+} store, and that Ca^{2+} release can be induced from it [109]. To directly test whether nuclear Ca^{2+} is sufficient to initiate gene transcription, we aimed at targeting ChR2 onto the inner nuclear membrane (INM) in order to guide Ca^{2+} entry into nuclei from the ER. ChR2 is Ca^{2+} permeable and when the driving force of Ca^{2+} is high enough, opening of INM-targeted ChR2 with light should induce Ca^{2+} transients in the nuclei.

3.2.1 Targeting sequences

ChR2 is a membrane protein harboring seven transmembrane domains and it has the amino-terminal (N-) facing the extracellular space. According to its topology, ChR2 belongs to type IV-B class of integral transmembrane proteins, which are multiple pass molecules and have their N-terminal domains targeted to the ER lumen.

Table 3.1: ChR2 targeting sequences

Name	Description	Reference
(Non-targeted)		
ChR2-mCh	mCherry tagged ChR2	
ChR2-eGFP	eGFP tagged ChR2	
ChR2A-tDimer	cleavable tDimer	[134]
(ER lumen comtrol)		
ChR2-mCh-KDEL	ER lumen targeting	[135]
(ER-targeted)		
ChR2-mCh-7aa	KLRRRRI	[94]
ChR2-mCh-6aa	FLKKYL	[152]
ChR2-mCh-36aa	RKR motif from Kir6.2	[153]
(INM-targeted)		
LBRN-ChR2-mCh	Lamin-B receptor N-term	[126]
ChR2-mCh-gB6aa	DRLRHR	[93]
ChR2-mCh-GNAEGR	N-term of lamin C2	[5]
ChR2-mCh-ARΔ11	AREG-cyto deleting last 11 aa	[70]
ChR2-mCh-HB-EGFΔC	185-198 aa of human HB-EGF	[64]
ChR2-LR2-215-h2nls-mCh	long unfolded linker	[92]

As the INM is continuous with ER membrane and the nuclear Ca^{2+} transients originate to a large extent from the ER, I first tried using a number of different ER retention signals to target

ChR2 onto the ER membrane. This strategy is based on the lateral diffusion of membrane proteins between the ER and nuclear membranes. Once ER targeting was achieved, the second step would be to trap ChR2 in the nuclear membrane. "KDEL," the classic sequence targeting proteins to the ER, works perfectly with soluble proteins, but would not target a membrane protein to ER, so it was used here as a control. For ER membrane targeting, three sequences rich in arginine or lysine (R or K), which had been shown to have ER retention/retrieval functions, were attached to the C terminus of ChR2-mCherry (Table 3.1). The localization of these targeted proteins was investigated with spinning-disk confocal microscopy.

As there are no established INM targeting sequences, I tried several possible sequences for INM targeting of ChR2. The Lamin-B receptor localizes to the inner membrane of the nuclear envelope and anchors the lamina and the heterochromatin to the membrane. The N-terminal domain of the Lamin-B receptor was found to function as a nuclear envelope targeting signal [126]. Amphiregulin (AR; official symbol AREG) is synthesized as a type I transmembrane protein and is expressed on the plasma membrane. Staining results, however, suggested that it translocated from the plasma membrane to the ER or nuclear envelope. Its C-terminal lacking the last 11 residues, which exposed the RKKL motif at the very C-terminal showed obvious nuclear envelope guidance function [70]. Heparin-binding EGF-like growth factor (HB-EGF) is also synthesized as a type I transmembrane protein and is expressed on the cell surface. After exposure to ectodomain-shedding stimuli, it translocates to the nuclear envelope. Studies show that a short sequence element within the cytoplasmic domain of HB-EGF (residue 185-198 of human HB-EGF) allows this transmembrane protein to localize to the nuclear envelope [64]. Another study showed that a short sequence element within the cytoplasmic tail of human cytomegalovirus glycoprotein B (DRLRHR, abbreviated as gB-6aa here) was sufficient to induce translocation of the membrane protein CD8 to the INM [93]. The unique N-terminal hexapeptide GNAEGR from meiotic lamin C2 was also shown to be essential for nuclear envelope association [5].

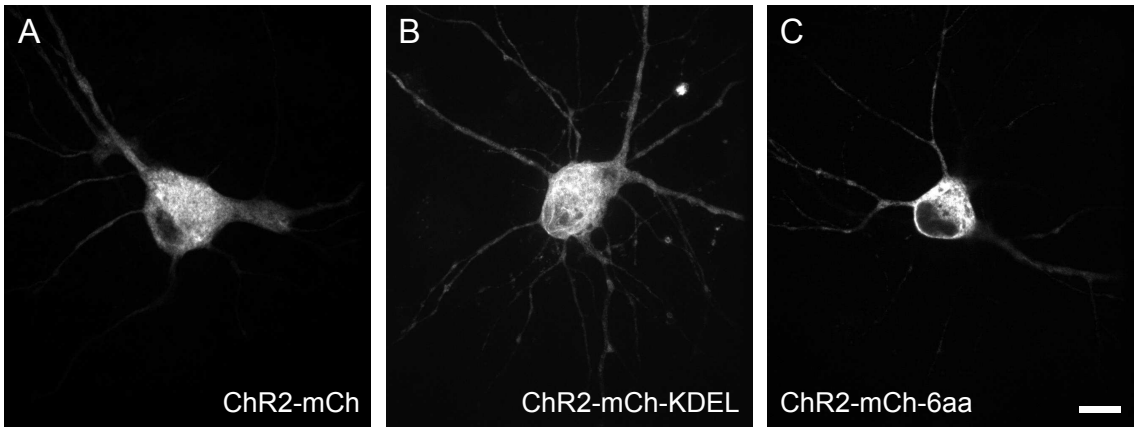

Figure 3.12: Differently targeted ChR2 expressed in neurons. Maximal stacked spinning-disk confocal images of transfected neurons with wild type ChR2-mCh (A), ChR2-mCh tagged with ER lumen targeting sequence KDEL (B) and ChR2-mCh tagged with lysine rich ER retention peptide FLKKYL (6aa, C). Scale bar is 10 μm.

The ER system in neurons extends into the dendrites, and it is difficult to exam the fine distribution of ChR2 (Figure 3.12). I thus used AtT20 cells, a cell line of mouse pituitary tumor, which is flat and thus makes it easier to distinguish the plasma membrane from internal organs, and to exam the distribution of targeted ChR2s. As shown in Figure 3.13, wild type ChR2 tagged with mCherry or eGFP depicted the boundary of AtT20 cells with fine protrusions. As expected, the distribution of ChR2-mCh-KDEL was similar to that of ChR2-mCh. ChR2A-tDimer harbors an auto-cleavable peptide between ChR2 and the tDimer tag that becomes cleaved after translation. The soluble tDimer showed a cytoplasmic fluorescence distribution. In contrast, ChR2-mCh-7aa/6aa showed a distinct distribution, which was neither on the plasma membrane, like ChR2-mCh-KDEL, nor in the cytosol, like ChR2A-tDimer. Mcherry signal from ChR2-mCh-7aa/6aa was excluded from nuclei and exhibited a web-like distribution similar to that of the ER (ChR2-mCh-36aa showed a localization similar to ChR2-mCh-7aa, and is not shown here).

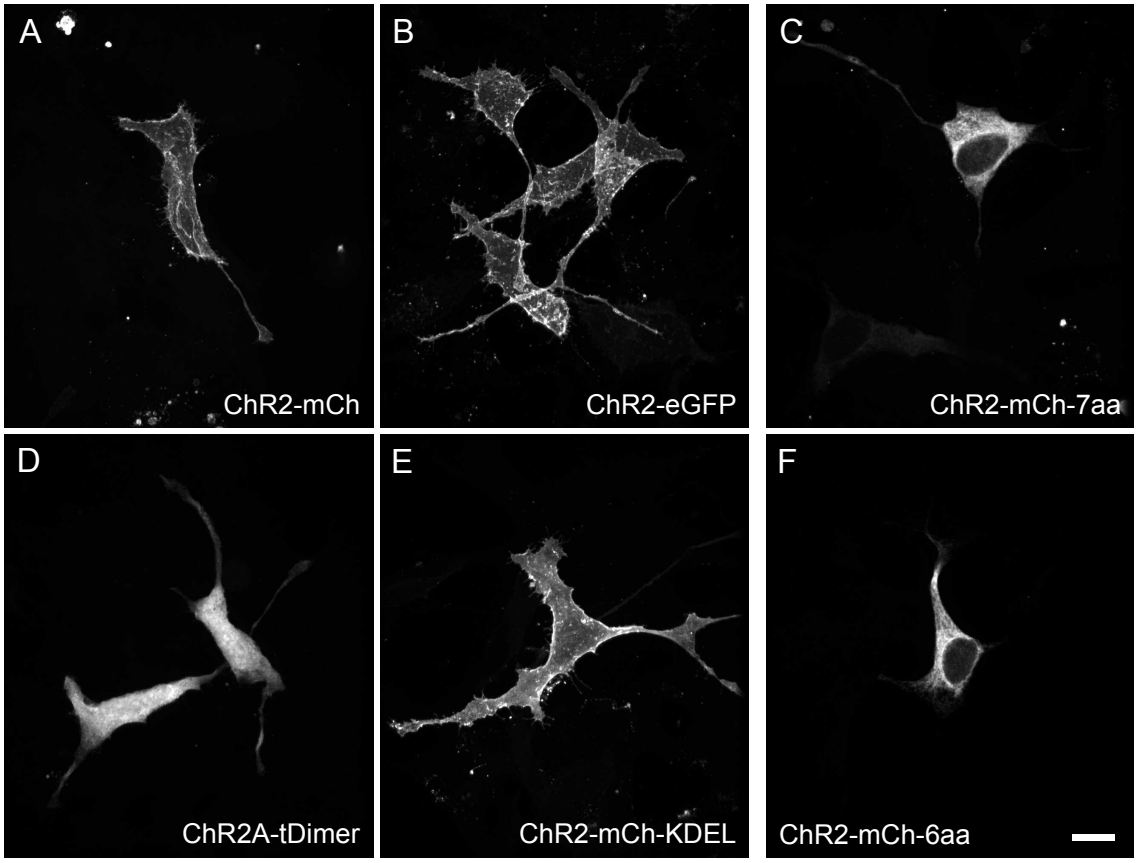

Figure 3.13: Differentially targeted ChR2s expressed in AtT 20 cells. Maximal stacked spinning-disk confocal images of wild type ChR2 tagged with mCherry (A), eGFP (B), cleavable 2A peptide followed with tDimer (D), mCherry and KDEL sequence (E), arginine-rich peptide KLRRRRI (7aa, C) and lysine-rich peptide FLKKYL (6aa, F). Scale bar is 10 μm.

The attempt to use INM targeting sequences was not successful. As shown in Figure 3.14, LBRN and 6aa combination exhibited similar distributions to that achieved with 6aa alone, and were mostly visible in the ER. All other sequences tested were found on the plasma membrane, similar to the wild type ChR2.

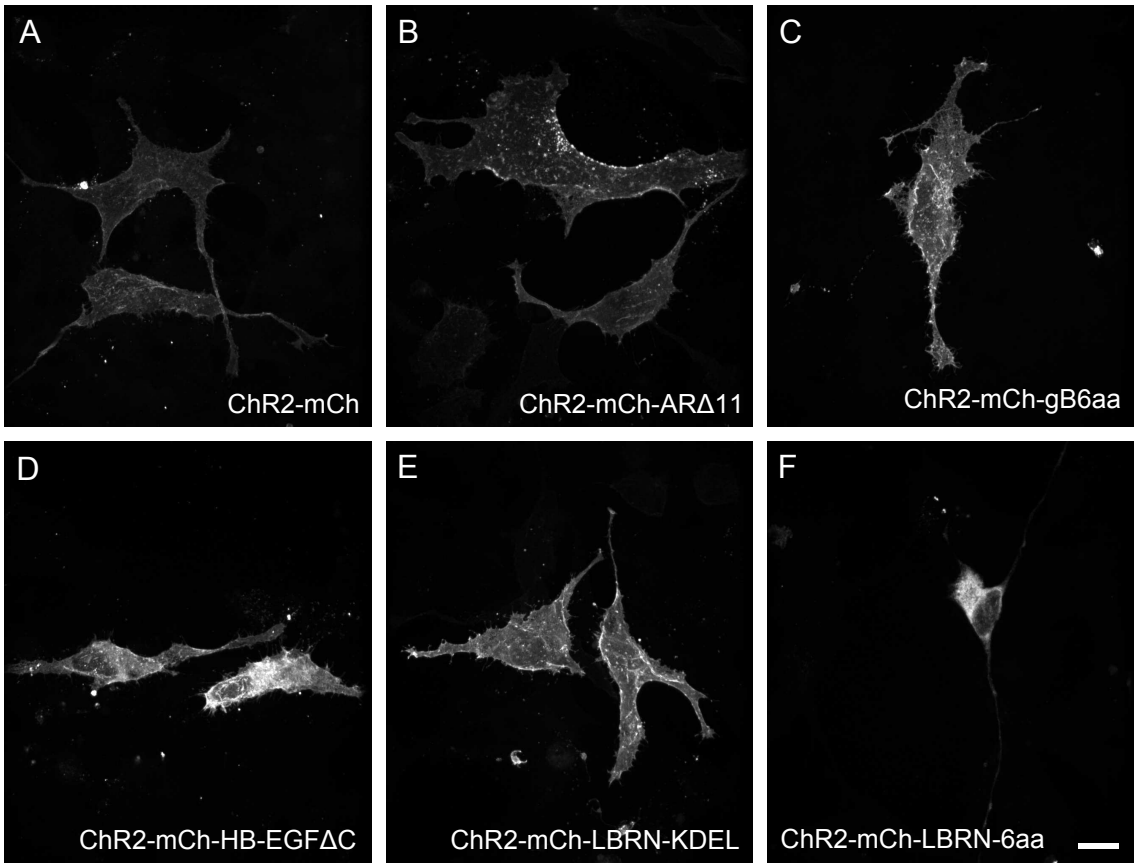

Figure 3.14: INM targeting sequences with ChR2-mCh expressed in AtT20 cells. Maximal stacked spinning-disk confocal images of wild type ChR2-mCherry (A) and ChR2-mCherry followed with AREG cytoplasmic domain without the last 11 residues (ARΔ11, B), DRLRHR motif from human cytomegalo-virus glycoprotein B (gB6aa, C), cytoplasmic segment of heparin-binding EGF-like protein deleting the very C-terminal (HB-EGFΔC, D), N-terminal of LaminB receptor followed by KDEL sequence (LBRN-KDEL, E) and FLKKYL (LBRN-6aa, F). Scale bar is 10 μm.

3.2.2 Characterization of targeted ChR2

Targeting of ChR2 to ER with the arginine and lysine rich sequence was promising from the image results, and I continued to test their function with Ca^{2+} imaging and electrophysiological recordings. Fura-2 imaging results indicated that blue light stimulation of ER-targeted ChR2 did not evoke any apparent cytoplasmic Ca^{2+} transients. Stimulation of wild-type ChR2-infected neurons, on the other hand, reliably and reproducibly evoked cytoplasmic Ca^{2+} signals in time with the stimulation (Figure 3.15 A and B). From voltage clamp recordings, I found that wild-type ChR2 and KDEL-tagged ChR2 exhibited similar inward currents in response to blue light stimulation, and that these currents were remarkably decreased when ChR2 was targeted to ER with the 6aa (FLKKYL) peptide (Figure 3.15 C).

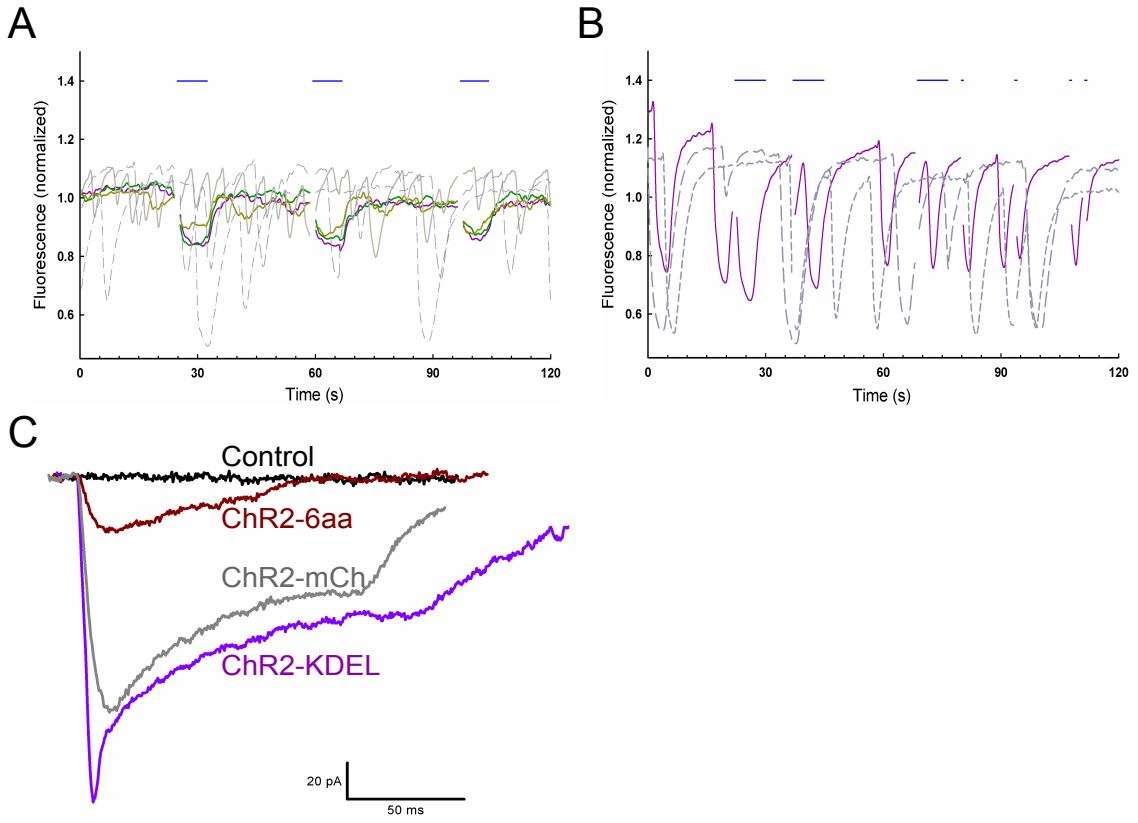

Figure 3.15: ER targeted ChR2 does not induce Ca^{2+} transients upon light stimulation and mediates smaller inward current. (A) is Fura-2 Ca^{2+} imaging with 380 nm excitation result of ChR2-mCh infected coverslip. Blue line represents LED stimulation. Colored traces are mCherry positive neurons and grey lines are negative ones. (B) is Fura-2 Ca^{2+} imaging result of ChR2-mCh-7aa infected coverslip. Blue line represents LED stimulation. Colored traces are mCherry positive neurons and grey lines are negative ones. (C) is recording of current with voltage-clamp from control, ChR2-mCherry-6aa, ChR2-mCherry and ChR2-mCherry-KDEL infected neurons.

3.3 Minimal Activity Requirement for Gene Transcription

To investigate the minimal activity requirement for gene transcription initiation, we chose the widely studied *arc* gene, which plays a critical role in mediating the formation of long term memory, as our model gene, and used Bicuculline (Bic) stimulation to induce neuronal activity in cultured hippocampal neurons. This protocol uses a brief Bic treatment to produce synchronized bursts of action potentials and then TTX, a sodium channel blocker, to stop bursting. To verify rapid *arc* transcription, we used an RNA probe against mature *arc* mRNA and performed cellular compartment analysis of temporal activity by fluorescent *in situ* hybridization (catFISH). CatFISH uses the long RNA probe transcribed *in vitro* from the full length cDNA for the *arc* gene to detect mature mRNA. In the first experiment, I stimulated mouse and rat hippocampal cells with Bic for 10 min,

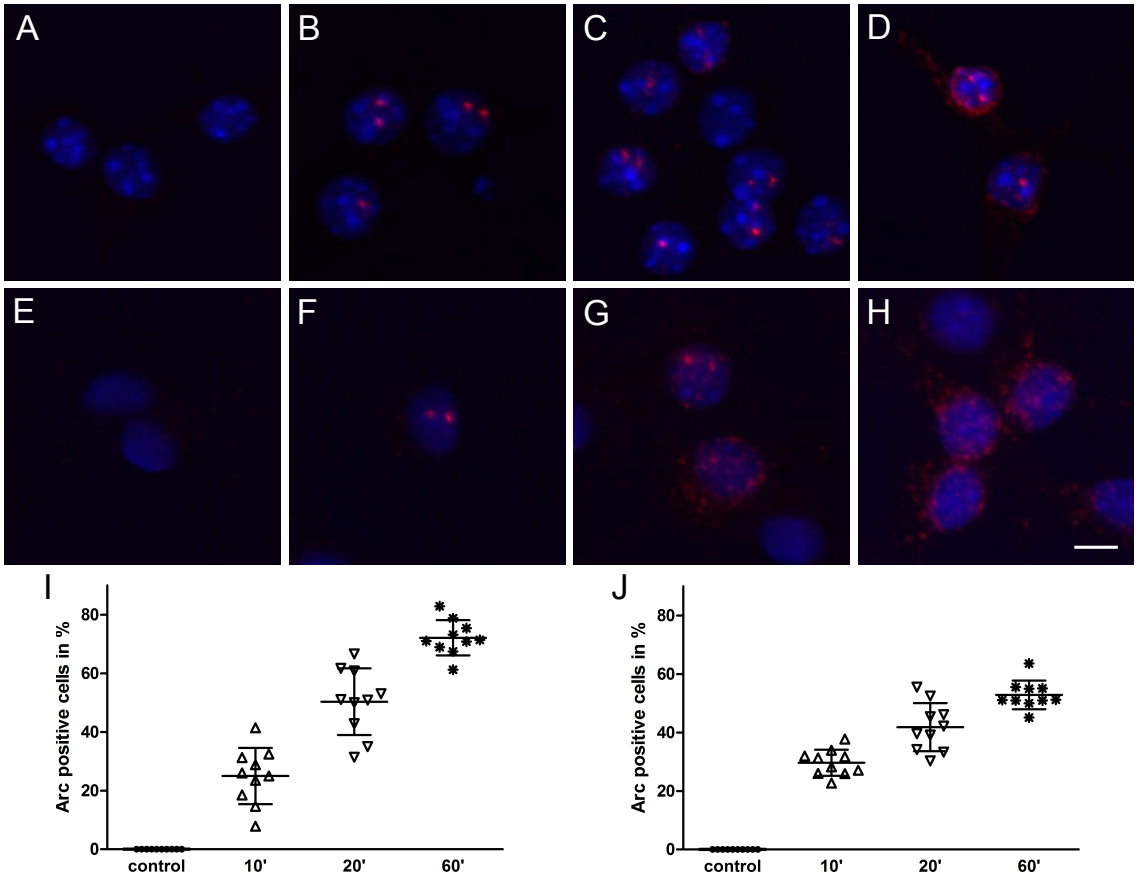

Figure 3.16: Electrical activation of neurons with Bic stimulation leads to *arc* transcription. (A) to (H) are color merged maximal stacked confocal images of Hoechst staining (in blue) and Cy3 signals from catFISH (in red). (A) to (D) are from mouse hippocampal neurons and (E) to (H) are from rat hippocampal neurons. (A) is control condition without stimulation hybridized with anti-sense probe against *arc* gene. (E) is from Bic treated for 20 min and hybridized with sense *arc* probe. (B) and (F) are cells treated with Bic for 10 min, (C) and (G) for 20 min and (D) and (H) for 1 hours. Scale bar represents 10 µm. (I) an (J) are quantitative results of scatter graph (mean ± s.d.) showing percentage of counted nuclei positive for *arc* mRNA signal for each time point from mouse and rat cultures, respectively.

20 min and 1 hour, and fixed the cells immediately after these time points for *in situ* hybridization. For 10 min Bic activation, *arc* mRNA was found only in nuclei in localized foci (Figure 3.16 B and F for mouse and rat neurons, respectively). After 20 min of increased neuronal activity, *arc* mRNA was transported into the cytosol and the hybridization signal appeared in the perinuclear domain (Figure 3.16 C and G for mouse and rat neurons, respectively). With an activation longer than 1 hour, *arc* mRNA diffused into the cytosol and dendrites (Figure 3.16 D and H for mouse and rat neurons, respectively) and the signal was less localized than for brief stimulations. No positive *arc* mRNA signal was detected for the unstimulated control condition and negative control hybridized with sense probe (Figure 3.16 A and E). For quantitative analysis, *arc* mRNA signal was categorized as present or absent, without taking into account the location of the signal. As shown in Figure 3.16 I and J, for mouse culture and rat culture respectively, Bic progressively induced *arc* gene transcription. Because rat cells were easier to obtain and generally had lower basal activity, they were used for the subsequent studies (mouse cells: 10': 24.97 $\pm$ 9.59%, mean $\pm$ s.d.; 20': 50.35 $\pm$ 11.36%; 60': 72.14 $\pm$ 6.01% and rat cells: 10': 29.67 $\pm$ 4.48%; 20': 41.85 $\pm$ 8.22%; 60': 52.86 $\pm$ 4.88%).

Next, I shortened the time window for Bic treatment to investigate the relation between the duration of activation and the levels of *arc* transcription. As a positive control, 10 min stimulation was chosen because it gave clear discrete intranuclear foci of *arc* mRNA. As shown in Figure 3.17

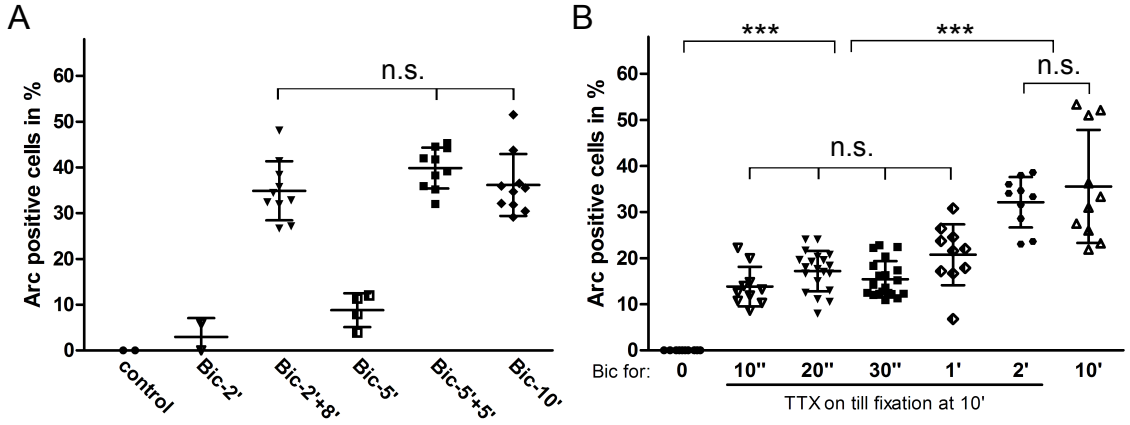

Figure 3.17: Bic stimulation for 10 seconds initiates *arc* transcription. (A) is catFISH result showing scatter graph for percent of *arc* signal positive cells after different Bic stimulation periods. Bic-2' and Bic-5' mean that cells were treated with Bic for 2 and 5 min respectively and fixed immediately afterwards. Bic-2'+8' and Bic-5'+5' mean that cells were treated with Bic for 2 and 5 min, respectively, and then TTX was put on for 8 and 5 min, respectively (to make a total of 10 min). Bic-10' means cells were treated continuously for 10 min and fixed straight after it. (B) is catFISH result of shorter Bic stimulation conditions. X-axis is the time periods for Bic treatment. The middle five conditions were applied with TTX after Bic and fixed at 10 min time point. Data are presented as mean $\pm$ s.d..

A, rat neurons were stimulated for 2 min, 5 min or 10min. Cells were either fixed immediately after Bic treatment (Bic-2' and Bic-5') or 1 µM TTX was applied, and cells were fixed 10 min after stimulation (Bic-2'+8' and Bic-5'+5'). When cells were fixed immediately after 2 min or 5 min Bic stimulation, *arc* mRNA positive cells were not significantly different from the control condition.

For cells fixed 10 min after the start of stimulation, however, cultures stimulated with Bic for 10 sec, 20 sec, 30 sec and 1 min showed a similar proportion of positive cells (Figure 3.17 B). 2 min stimulation plus 8 min TTX was not significantly different from 10 min Bic treatment. These data indicate that *arc* gene transcription can be initiated by very brief stimuli.

Ca^{2+} transients are the effectors in the transmission of electrical stimulation to the nuclei to initiate gene expression, which in turn is essential for the maintenance of plasticity-associated changes. We therefor used Ca^{2+} imaging to monitor Ca^{2+} transients in stimulated neurons. Fluo-3 was used to measure whole cell Ca^{2+} transients and GCaMP3nls, comprised of the genetically encoded Ca^{2+} indicator GCaMP3 [136] targeted to nucleus with an NLS peptide, was used to measure nuclear Ca^{2+} changes. The same stimulation protocol as for *arc* gene analysis was used for Ca^{2+} imaging:

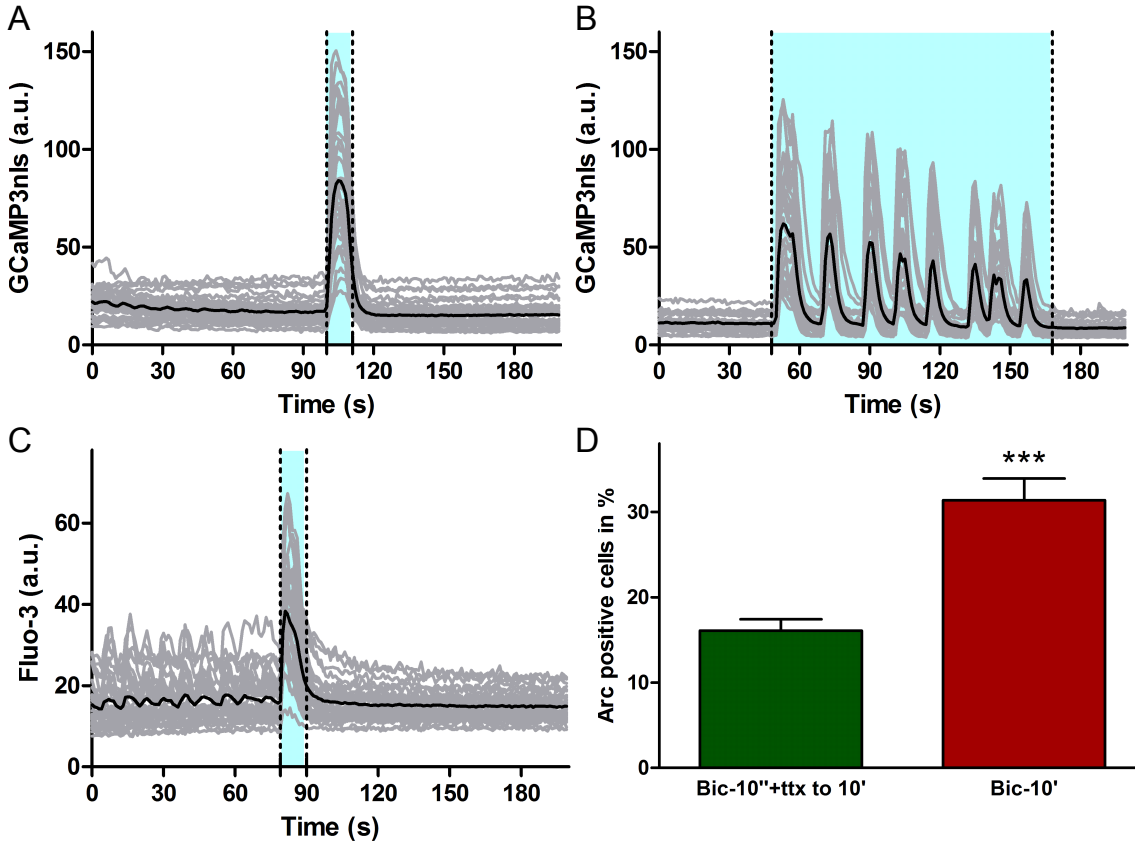

Figure 3.18: Bic stimulation for 10 seconds initiates *arc* transcription. (A) and (B) are Ca^{2+} imaging recording in rat cultures infected with GCaMP3nls. Bic was put on cells for 10 sec or 2 min (colored part between dotted lines in A and B, respectively) and then TTX was applied. (C) is the same as (A) except that Fluo-3 was used to monitor Ca^{2+} change. (D) is quantitative analysis of catFISH with *arc* gene. Percentage of *arc* positive cells in 10 sec and 10 min Bic stimulated conditions are shown in green($16.08 \pm 1.338\%$) and red bars ($31.35 \pm 2.555\%$, mean $\pm$ s.e.m.). n= 6 independent culture preparations.

Bic was applied to cells and TTX was added after different time windows. As shown in Figure 3.18, Bic induced synchronized Ca^{2+} transients that decayed slowly over time and in which the first transient had the largest amplitude (3.18 B). TTX efficiently blocked these Ca^{2+} rises immediately

after its application (3.18 A and C). 10 sec Bic stimulation induced only one Ca^{2+} transient. These findings indicate that very brief stimuli with a single nuclear Ca^{2+} transient is sufficient to initiate *arc* gene transcription.

Chapter 4

Discussion

In this study, I used ChR2 as a tool to manipulate neuronal activity. A double mutant variant of ChR2, ChR2-ab, was made, characterized and its cellular functions were studied. The goal was to investigate whether intrinsic activity could be mimicked in a controllable way and if yes, how this was achieved. The results indicated that ChR2-ab inherited the properties from its previous single mutants, being more sensitive, longer opening and bi-stable. rAAV mediated expression of ChR2-ab in neurons reached 80% in hippocampal culture. Endogenous activity could be mimicked with ChR2-mediated, light-induced membrane depolarization. A pool of activity dependent genes (AID genes) were induced in ChR2-ab-expressing neurons. The gene induction effect on AID genes of ChR2-ab was L-type voltage-dependent Ca^{2+} channel dependent as it was completely blocked with L-type VDCC antagonist nifedifine. Induction with *atf3, ifi202b, inhba* and *serpinb2* was inhibited with NMDA receptor blockers MK801 and APV. When synaptic activity was inhibited with Na^{+} channel blocker TTX to prevent action potential firing, ChR2-ab-mediated induction of *atf3, inhba, npas4, nr4a1* and *serpinb2* was also restrained. ChR2-ab-mediated gene induction was nuclear Ca^{2+} dependent as when the function of nuclear Ca^{2+}/CaM complex was impaired with CaMBP4, gene induction was blocked. Interfering the function of CREB/CBP transcription complex with E1A protein diminished gene expression induced with ChR2-ab. Whole-cell patch clamp and signaling pathway analysis revealed that neurons expressing ChR2-ab showed higher basal activity, represented with more frequent mEPSC and higher level of pCREB and pERK. More cells died after light application in ChR2-ab-infected condition on DIV 14. Pharmacological analysis suggested that this was due to activation of extra-synaptic NMDA receptors during ChR2-ab activation. In another strategy of inducing activity, ChR2 was targeted to endoplasmic reticulum membrane with various targeting sequences with the goal to directly introduce Ca^{2+} release from internal Ca^{2+} stores. Additionally, transcription analysis with catFISH method revealed that a single nuclear Ca^{2+} transient induced with Bic treatment was capable of initiating transcription of *Arc* gene.

4.1 ChR2 Mediated Activity and Gene Expression

4.1.1 Choosing the ChR2 Variant

When using ChR2s to manipulate neuronal activity, the ideal should be instantaneous and predictable membrane potential change. As mentioned in the Introduction 1.4.3, various ChR2 variants were used for divergent purposes [82]. ChR2-ab was chosen to be made for this study because of its unique properties. ChR2-b has the most recently identified property of higher cation conductance and increased sensitivity to light; ChR2-a has the mutation prolonging the opening of the channel. ChR2-ab maintains blue light activation around 480 nm wavelength light and can be de-activated with green light. Opening of the channels upon blue light is prolonged to minute scale and cells expressing them were depolarized. This mimics the persistent neuronal activity effect of KCl stimulation. Previous results showed that KCl mediated depolarization markedly increased dendritic growth and branching [114, 150]. Membrane depolarization would induce a secondary response, activating the L-type voltage dependent Ca^{2+} channels. Neuronal activity mediated with high concentration of extracellular K^+ was reported to be able to induce CREB/CBP-dependent gene expression [60]. ChR2-ab mediated depolarization was reasoned to account for its function in gene induction when stimulated with blue light. At the very beginning of this project, blue light was applied through an optic fiber to each dish manually, trying to keep the stimulation the same for all conditions. Later this was automated through a stimulator (S48 Square Pulse Stimulator, Grass Technologies). To analyze the population effect in gene induction, blue light through a microscope objective or a optic fiber is way from enough, so a customized LED plate had to be built up. Thanks to the electronic workshop of Heidelberg University (Fachabteilung Elektronik), a LED array plate with diameter of $\sim$13 cm was built for all the light mediated gene analysis experiments. The LED units were from LUMITRONIX® (Item No. 54401, 50 lm) which dominated at 467 nm with a viewing angle of 100° . With rAAV infection, above 80% of the cell population expressed ChR2-ab. With the LED array, cells in 35 mm diameter dish was all covered by blue light illumination.

There is another similar variant of ChR2, ChR2-ad (also called SSFO, Super Step Function Opsin, obtained from SfN meeting, 2012) harboring mutants of C128A and D156A. This mutant was shown to depolarize neurons more than ChR2-a, and probably less than ChR2-ab. Cells expressing ChR2-ad did not show any mortality problem and was found to be able to enhance endogenous firing upon light activation. If the cell death resulted from ChR2-ab was due to its over depolarization in cell culture, ChR2-ad would be a better alternative for this purpose. However, when we consider using this tool to generally increase activity *in vivo*, for example in Alzheimer's disease (AD) there is a significant loss of activity and neurons in cerebral cortex and certain subcortical regions, due to the restrict transmission of blue light in brain tissue, ChR2-ab might be a better choice. So the first thing to continue for ChR2-ab usage, I will stereotactic inject ChR2-ab virus into hippocampus and check the cell survival situation. If cell death caused by ChR2-ab is not the case in the brain, it will be used to increase circuit activity to rescue the cell loss in AD model.

4.1.2 ChR2-ab Mediated Neuronal Activity and Its Function

Natural activity stimulation *in vivo* [53] and pharmacological induced synaptic activity *in vitro* [157] have been shown to induce gene transcription. In this study, I used a controllable, exogenous tool to induce and mimic neuronal activity. MEA recording revealed that blue LED light induced bursts of spikes in ChR2-ab infected culture (Figure 4.4, data from Dr. H. Eckehard Freitag). The light-dependent bursts stood out significantly from uninfected control cultures. This activity achieved physiological function, activity-dependent gene induction. This gene induction was observed only in ChR2-ab expressing cells but not in ChR2-a or ChR2-b infected cells (see Figure 3.5). Considering the characteristics of these three ChR2 variants, depolarization mediated by ChR2-a opening probably was not big enough to initiate gene responses. Gene analysis in this thesis was all done at 4 hour time point, which is well established with Bic treatment in the lab [156]. Previous data showed that 4 hour high KCl treatment induced expression of Dnmt3a2 [105] which indicated that ChR2-a mediated depolarization did not reach the threshold to activate L-type VDCC which started the downstream effects. ChR2-b itself mediated much bigger current and much more sensitive to blue light, meaning less intensity of blue light would activate it. When ChR2-ab was activated, the membrane depolarization was similar to that induced with KCl. And this depolarization would last into time scale of minute. So the stimulation pattern used in gene induction experiments was shed blue light every 30 second for a train of flashes (10 ms duration) at 20 Hz for 6 seconds. This pattern was maintain from Micro-Electrode-Arrays (MEA) recording of Bic stimulated neurons.

Apart from the 9 AID genes stated in the result part, 7 other genes were studied for their responses to ChR2-ab mediated activity. These were *arc, bdnf, c-fos, dnmt3a1, dnmt3a2, egr1* and *puma*. As shown in Figure 4.2 in Appendix, except for *dnmt3a1* and *puma*, others were also robust induced in ChR2-ab expressing neurons. *Dnmt3a1* was not up regulated by Bic induced electrical activity [105] and it was the same with ChR2-ab mediated activity in this work. *Puma* (also know as *bbc3*) was shown to be down regulated with AP bursting activity [80] and it stayed unchanged here. During performing the mRNA level analysis with Q-PCR protocol, I noticed that some genes, including *atf3, egr1, ifi202b* and *serpinb2* were significantly down regulated only by rAAV infection. This seems to be a common phenomenon in the lab and it may due to some side effects of the virus infection itself. However, light treatment could induce robust expression of these genes.

Since virus did not infect all the cells in the population, we had infected and uninfected neurons in the same dish.Evoked excitatory postsynaptic current (eEPSC) was recorded in uninfected neurons in a ChR2 sparsely infected coverslips (unpublished data from Dr. C. Peter Bengtson). This results indicate that synaptic transmission from ChR2 expressing neurons to downstream uninfected cells indeed happen upon light activation. So the gene induction effect I observe probably came from a direct response in ChR2-ab expressing neurons and a secondary response in postsynaptic neurons. To investigate the direct and secondary effect of ChR2-ab, I used a post-synaptic density (PSD) targeting sequence to guide ChR2-ab to localize in the PSD (ChR2-ab-psd, [49]). Immunocytochemistry with antibody against c-fos protein was used to detect its level in individual neurons. When coverslips were analyzed as a unit, the one infected with ChR2-ab-psd and illuminated with blue LED light showed much higher level of c-fos staining (Figure 4.5 A). When I

separately analyzed infected (mCh positive) and uninfected (mCh negative) cells in the same coverslip, ChR2-ab-psd expressing neurons without light activation already showed higher c-fos level. In the LED activated coverslip, ChR2-ab-psd positive neurons had remarkably increased level of c-fos (Figure 4.5 B). Interestingly, uninfected neurons in the LED treated coverslip also had higher intensity of c-fos staining compared to those in the un-illuminated coverslip. This indicated that there was a secondary response at the network level in ChR2-ab-psd infected coverslip.

4.1.3 Restrictions on ChR2-ab Use

ChR2-ab did inherit the special properties from the single mutants: long opening, high sensitivity and large ion conductance. All these characteristics also made ChR2-ab not suitable for precise neuronal activity manipulation. When it was activated, cells expressing it would be depolarized for up to a minute with slow decay. This depolarization could be reversed to with green light which closed the channel immediately. Probably ambient light can already activate it. So the cells that have ChR2-ab correctly expressed on cell membrane would be under sustained depolarization situation. This may account for the significant decrease in the inter event interval of mEPSC recording (Figure 3.10 D) suggesting that under basal condition (without light activation), ChR2-ab is a bit "leaky". This might be the reason for the high level of pERK and pCREB in ChR2-ab expressing neurons (Figure 3.9). In fact, the higher basal pCREB level was also detected with ChR2-a expressing neurons, to a less extend. Light stimulation pulled it down. This was contrary to previous report in which cells transduced with lentivirus carrying ChR2-EYFP had significantly elevated Ser 133 pCREB with blue light delivery compared with sham-treated neurons [49]. I checked whether ambient light would cause channel activation by putting cells under the aluminium foil directly after virus infection and keeping the tissue culture hood dark during medium change or other treatments. But still, the high pCREB level was detected. Decrease of pCREB upon LED stimulation in ChR2-ab expressing neurons was also out of our expect. Taking the bi-stable property (blue light activate it and green light close it) of ChR2-ab into account, the ideal culturing condition would be putting cells in a green light environment after infection, giving ChR2-ab no chance to be activated in any unintended way. In this case, ChR2-ab would be activated only when the blue light is applied as designed. It can be achieved with a blue/green mixed LED array (with the help of a two-output-channel stimulator) or two separate LED arrays used under different circumstances.

One explanation for high pCREB and pERK level in ChR2-ab expressing neurons without light stimulation is that the leaky channel led to micro Ca^{2+} domain close to the cell membrane. Previous work had shown that this was enough to switch on ERK signaling pathway. Once activated, ERK pathway propagated in a Ca^{2+}-independent way to the nucleus and resulted in CREB activation [56]. However, in the case with ChR2-ab expressing neurons, any further treatments (LED light, NMDA and KCl application) on those cells led to dramatic decrease on the high basal pCREB and pERK level. In control uninfected cells, NMDA or KCl treatments would induce phosphorylation of CREB and NMDA on top of KCl would de-phosphorylate CREB owing to activation of extrasynaptic NMDA receptors [62]. While in ChR2-ab infected cells, even KCl decreased the original

high level of pCREB. The mechanism beneath still needs to be studied. Monitoring the Ca^{2+} concentration change would give us more information. Unfortunately, because of the sensitivity of ChR2-ab to a broad spectra of light, Ca^{2+} imaging to recording the Ca^{2+} change in those infected cells was not feasible. Fura-2 and X-rhod-1, which have excitation light (from LEDs which were wavelength specific) far from blue light could still activate the channel, to variable extends.

Regarding the contribution of other receptors or channels in ChR2-ab mediated gene induction effect, L-type VDCC was the most important one. Blockade of it prevented the gene induction mediated by ChR2-ab. This was in agreement with our proposal that ChR2-ab activation causes membrane depolarization which then activates L-type VDCC and downstream signaling pathways. NMDA receptor blockade did not interfere the induction of *btg2, gadd45*β*, gadd45*γ*, npas4* and *nr4a1* by ChR2-ab. And the induction of *btg2, gadd45*β*, gadd45*γ*, npas4* and *ifi202b* was not action potential dependent as preventing neuron firing by Na^+ channel blocker TTX did not have any effect on ChR2-ab mediated induction of these genes. This pharmacological analysis revealed that ChR2-ab mediated gene induction generally required corporation from L-type VDCC, NMDA receptor and Na^+ channel.

The fact observed in this work that more cells died after blue light stimulation in ChR2-ab infected condition indicated that these cells might have a failure in mitochondrial function because of the channel expression. I tested this hypothesis by measuring the ATP level of uninfected and ChR2-ab infected conditions with and without LED treatment. The results showed no difference within condition with light stimulation. But there was a significantly decrease of ATP level in infected condition (see Figure 4.3 in Appendix). This might due to the side effect of virus infection as expression of the viral machinery took use of host cell energy to express exogenous proteins. This effect became especially strong when cells were cultured longer than two weeks.

4.1.4 Conclusion and Outlook

Optogenetics has been broadly applied to various aspects of neuroscience research. Results from this study presented a sign that ChRs can be deleterious. Many strategies have been used to increase the expression level of ChRs in mammalian cells: mammalian codons substitution, stronger promoter, ER exporting sequence to increase membrane insertion *et al.*, but is the overwhelming expression of a membrane protein good for cells, or can they bear it? More cells died over the culturing process indicated that too many functional channels on the cell membrane might lead to deleterious effect to cells.

Results from mEPSC recording provided a hint that ChR2-ab infected neurons had no difference in AMPA receptor number per synapse as the amplitude of mEPSC was similar to non-infected cells. However, they might have more spines as they had more frequent mEPSCs. The morphological change of ChR2-ab infected neurons still needs to be studied. Gene induction mediated by ChR2-ab indicates that it can be used as a cell depolarization tool to induce neuronal activity. Considering its super light sensitivity, *in vivo* application would be feasible and benefit substantially to those suffering from decreased or lost neural network activity.

4.2 ChR2 Targeting

Full length channelrhodopsin 2 has 737 residues and the N-term 315 amino acids were hypothesized to be a 7-TM helices. When expressed in oocytes of *X. laevis*, in the presence of *all-trans* retinal, identical photocurrent and very similar current-voltage relationships were obtained with the full-length and the first 315aa ChR2s. This allowed for the conclusion that the N-term 7 TM helices mediated the channel current [99]. So the topology of ChR2 was predicted to be 7 TM domain with the N-terminal facing extracellular side and C- terminal in the intracellular side. It was confirmed by crystal structure analysis of ChRs resolved at 2.3 Å resolution [73]. This high-resolution information revealed that ChR architecture to be very specific and different from many other known transmembrane proteins. N-term in the extracellular side means that during he synthesis process, there should be a stop-transfer anchor sequence and the N-term would stay inside the lumen of ER before transferred on to plasma membrane. For the first try to guide ChR2 onto the inner nuclear membrane (INM), I checked a typical INM locating protein, LBR. Lamin-B receptor (LBR) is a polytopic integral membrane protein localized exclusively in the INM domain of the nuclear envelop. LBR has 8 TM locating on the INM and has its N-terminal in the intranuclear compartment [104]. The first membrane spanning region of LBR was shown to be sufficient for sorting to the INM [125]. At the same time, the amino-terminal domain of LBR was reported to be a nuclear envelope targeting signal [126]. LBRN-GFP actually was shown to distribute equal and random in ER and ONM but highly concentrated in the INM [38]. So I used the N-term and N-term plus the first TM of LBR (LBRN-TM1) at the N-term of ChR2 and analyzed its distribution with high resolution microscope. Unfortunately, both showed similar distribution pattern as the wild type ChR2. Because integral proteins of the INM are synthesized as membrane-integrated proteins on the peripheral ER, transport from ER to INM involved lateral diffusion in the lipid bilayer around the nuclear pore membrane [101], I then turned to use ER retention sequences to target ChR2 onto the ER membrane as the first step. As ER membrane system is in the continuality with outer nuclear membrane (ONM), it is possible that a ER membrane protein could accumulate in the nucleus by lateral diffusion and designed ligand binding (nuclear trap strategy).

Many ER retention/retrievial signals were used (see Table 3.1) and the ones with arginine-rich or lysine-rich motif (7aa-KLRRRRI and 6aa-FLKKYL) worked well. Targeted ChR2 showed distinct distribution from plasma membrane bound one and it depicted the internal membrane system. Ca^{2+} imaging recording revealed that no synchronized Ca^{2+} transients were induced with ER targeted ChR2 according to light stimulation. Whole-cell patch clamp result represented that the current mediated by ER-targeted ChR2 was greatly diminished compared to normal plasm membrane-bound one. The small remaining current upon light stimulation might be accounted for by a secondary effect of internal cation release from ER. Alternatively, it was conceivable that a tiny fraction of ChR2 still inserted onto the cell membrane. In any case, these data indicated that ER targeting of ChR2 was successful. However, the Ca^{2+} imaging result on the other hand was disappointing because another purpose with ER targeted ChR2 was that I wanted to directly induce Ca^{2+} release from ER. This result suggested that with wild type ChR2, which had little permeability to Ca^{2+}, it would not be suitable for this goal. As mentioned in Introduction 1.4.3, ChR2-c harbored enhanced Ca^{2+} permeability and was shown to have superior properties [74]. So the immediate next

step would be: to exchange ChR2-c for ChR2 in ER targeted constructs and check for Ca^{2+} release from the ER.

4.3 Minimal Activity Requirement for Gene Transcription

New synthesized protein is crucial for sustained neuronal functional change and formation of long-term memories. So we set off to investigate the minimal activity requirement for gene transcription initiation. The very original idea was to use ChR2-b as the controllable activity tool to explore this question. ChR2-b can be activated with as low as 1.9 mW/mm^2 light intensity and as high as 60 Hz blue flashes to produce reliable action potentials [12]. But no gene transcription was detected even with high frequency flashes in ChR2-b infected neurons. In contrast, Bic induced bursts of action potentials, although with lower firing frequency, induced robust gene transcription. This suggested that it may not be the frequency or number of action potentials leading to the transcription. Downstream effectors, possibly Ca^{2+} signals which invade into the nuclei, are still needed to be explored. As mentioned above, fine Ca^{2+} imaging with ChR2 is still a problem, especially with ChR2-b. In this sense, ChR2-b is a bit too sensitive as it can be activated with most other wavelength of Ca^{2+} imaging lights.

I chose *arc* as the model gene because its expression is tightly activity regulated and it plays very important role in activity mediated learning and memory [122]. *Arc* is one of the few immediate early genes which get transcribed at the very early state. It was massively induced 5 min after the rat being put into a novel environment [142]. *Arc* transcripts first stay in the nuclei as very concentrated foci and then translocated into cytosol and dendrites. In this body of work, I made use of the first stage of activity regulated *arc* transcription. A very sensitive method, catFISH, was used to detect *arc* transcripts at the mRNA level. Ten minutes Bic stimulation point was chosen for most of the experiments because it gave the best intranuclear foci signal. But during the progress of this study, some technique problem came up: *arc* signal became blur and not concentrated; counter staining of nucleus with Hoechst also lost its structure and had fuzzy boundary. Many control experiments were planned and executed and the hybridization solution at 56°C was found to be the cause of it. The pH of hybridization buffer dropped massively when it is heated up to 56 °C in a formamide humidified chamber while it stayed around pH7 when it was kept in a closed eppentube. The acid environment came from the oxygenation of formamide at high temperature and oxygen rich atmosphere. It was the acid solution stripped the nuclear structure and led to the blurring detecting results.

The results showed that a single nuclear Ca^{2+} transient, within 10 seconds, was sufficient to initiate *arc* gene transcription. But it took longer for it to be detected. This matches with the working mechanism of the molecular transcription machinery. Transcription initiation needs polymerase II (Pol II), general transcription factors (*TFIIA, TFIIB, etc.*), gene specific transcription factors (e.g. CREB) and co-factors (e.g. CBP). Once Pol II starts transcribing from the template DNA, this process is not activity dependent. But it takes time for those already-started transcripts to be finished. That is probably why in Figure 3.17 A (Bic-2' and Bic-5'), when cell were fixed immediately after

2 or 5 min Bic stimulation, no significant *arc* transcript signals were detected in any cell. However, if cells were given some time to finish the already-started transcription (Bic-2'+8' and Bic-5'+5'), about 15% cells showed *arc* mRNA signals. The percentage of *arc* positive cells was comparable to that of continuous 10 min Bic stimulation. Results from this study add to the fact that *arc* is one of the very first transcribed IEGs and its transcription initiation requires minimal one Ca^{2+} transient. Percent of Arc positive cells increased along with the stimulation periods and it reached 72% of the population after one hour. This accumulative result suggests that some cells in the culture are more sensitive than the others to activity change and respond immediately.

Detection of the first *arc* transcripts to some extend relied on the very low basal activity during the culturing and handling. To minimize the basal activity of the culture, I used rat hippocampal neurons cultured in a L-15 medium (Leibovitz) based growth medium (no Glutamine L-15 75.85%, $NaHCO_3$ 0.2%, SVM 0.45%, Progesterone 1mM, 112 2.4%, ITS 0.5%, Putrescine 1.6 mg/ml, Transferring 5 mg/ml, rat serum 1%, B27 2%). According to the experience and recording from MEA, rat cells in this medium show much less spontaneous activities. And in this set of experiments, no *arc in situ* hybridization signal was detected in control untreated condition.

Appendix

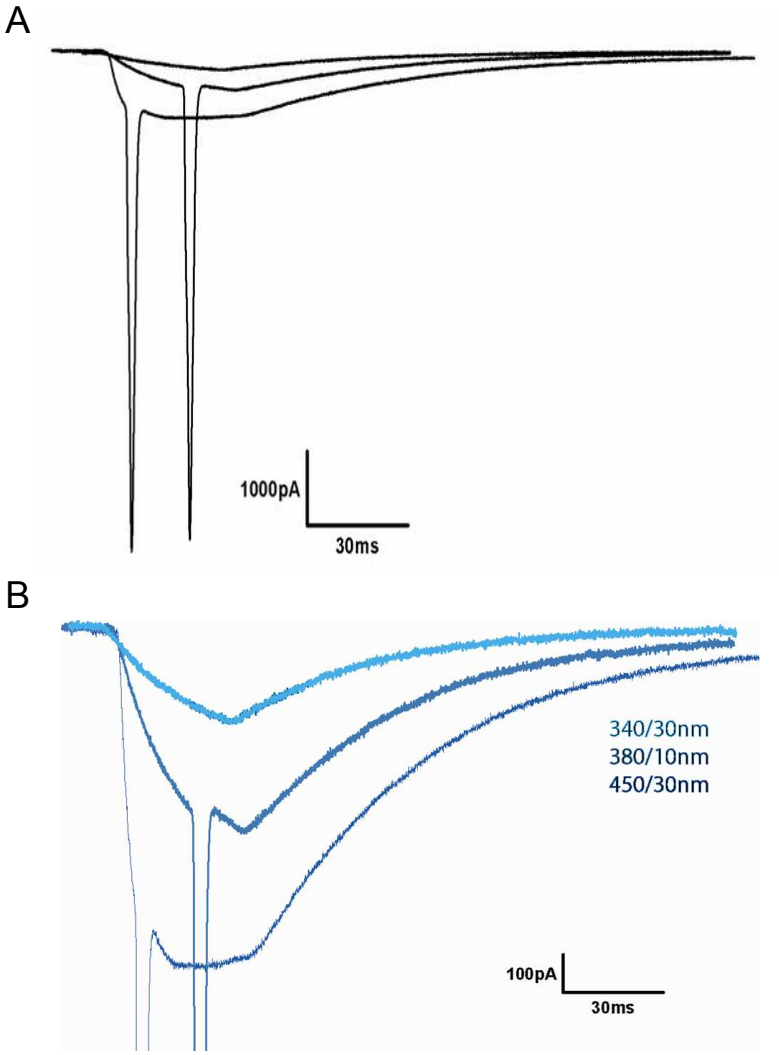

Figure 4.1: ChR2-b is activated by a broad spectra of lights. (A) is the overview of the responses of ChR2-b illuminated with Fura-2 excitation lights (340/30 nm and 380/10 nm) and normal channel activation light (450/30nm). Note that in voltage clamp, both 450/30 nm and 380/10nm caused a breakthrough of the cells, represented by the huge sharp inward current. (B) is a zoomed-in image showing the currents mediated by channel. Basically, both excitation light of Fura-2 could activate ChR2-b, just to different extends. This is also true for X-rhod-1 excitation light.

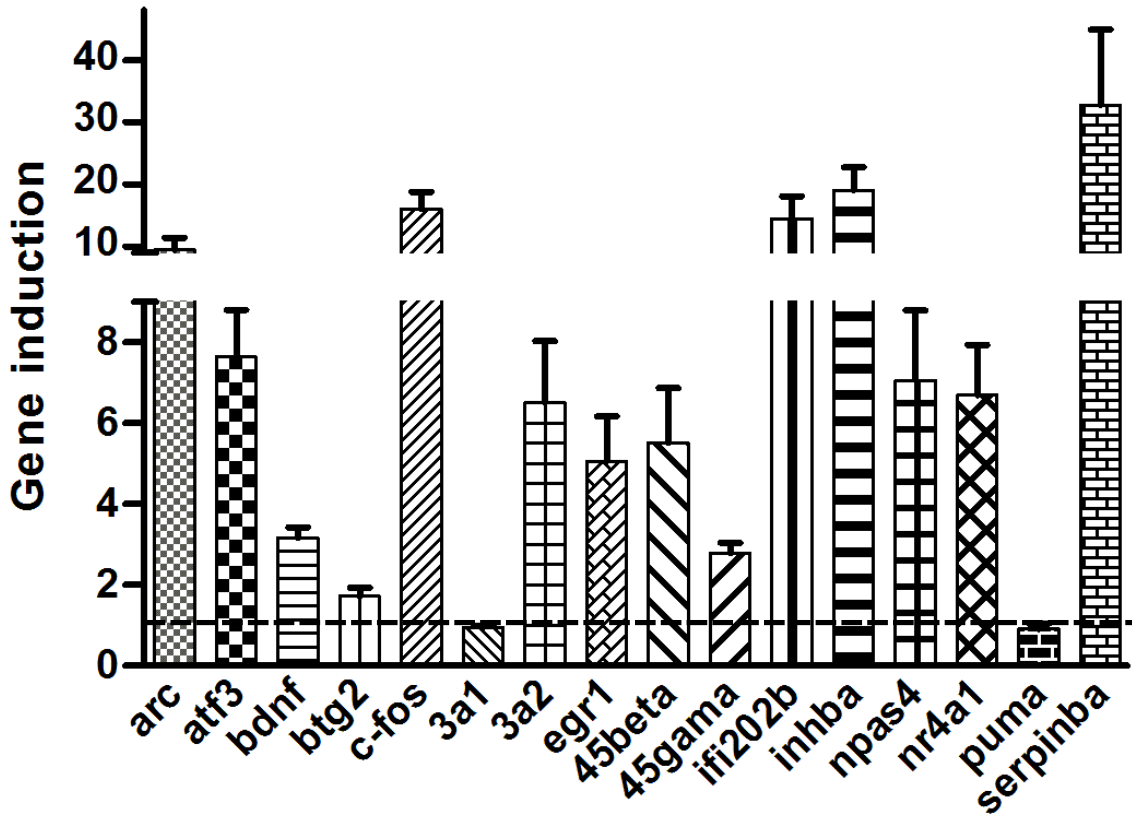

Figure 4.2: Summary of gene induction effect on 16 genes by ChR2-ab-mCh mediated activity. Q-PCR analysis of relative gene expression of total 16 genes analyzed in this study of cells infected with virus carrying ChR2-ab-mCh construct after 4 hour blue LED light stimulation ($n \geq 12$ independent cell preparations). Dotted line represents 1, which means those genes were not induced.

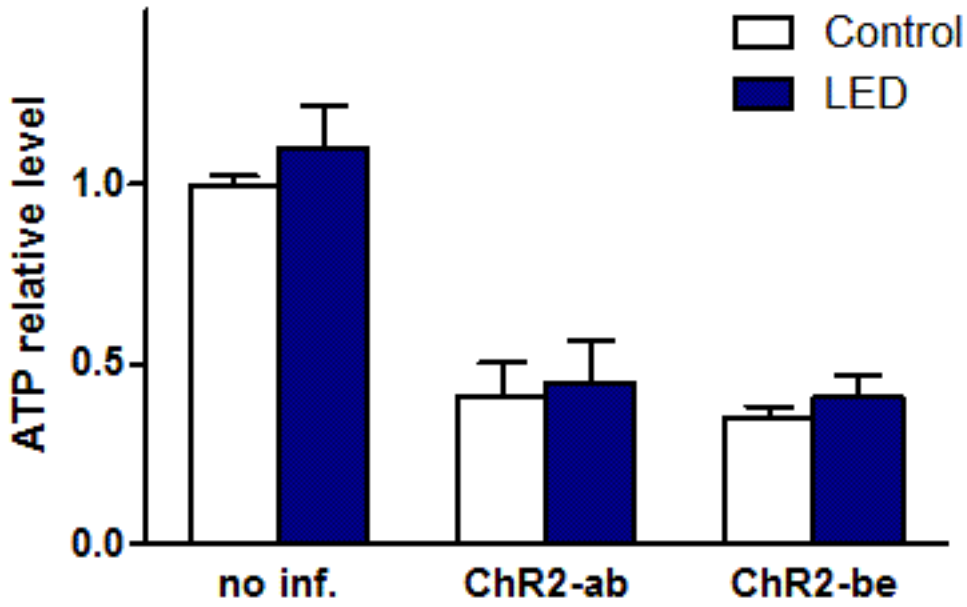

Figure 4.3: No change in ATP production with and without light in ChR2-ab expressing cells. Cells were infected with ChR2-ab-mCh (ab) or ChR2-be-mCh (be, as a channel control) or not infected (no inf.). On DIV 14, TM was changed to CO_2-independent SGG (140.1 mM NaCl, 5.3 mM KCl, 1 mM $MgCl_2$, 2 mM $CaCl_2$, 10 mM HEPES, 1 mM glycine, 30 mM glucose and 0.5 mM sodium pyruvate) prior to experiment. After 4 hour blue LED light stimulation, cells were lysated and applied to ATP detection assay "ATPlite 1step Luminescence ATP Detection Assay System" (PerkinElmer®) according to the manufacturer's instructions (n = 2 independent cell preparations). The measurement was performed at room temperature. ATP level was normalized to control condition without LED treatment. No difference was detected within the same infection group with or without LED; but a significate decrease of ATP level was noted between the uninfected and infected groups.

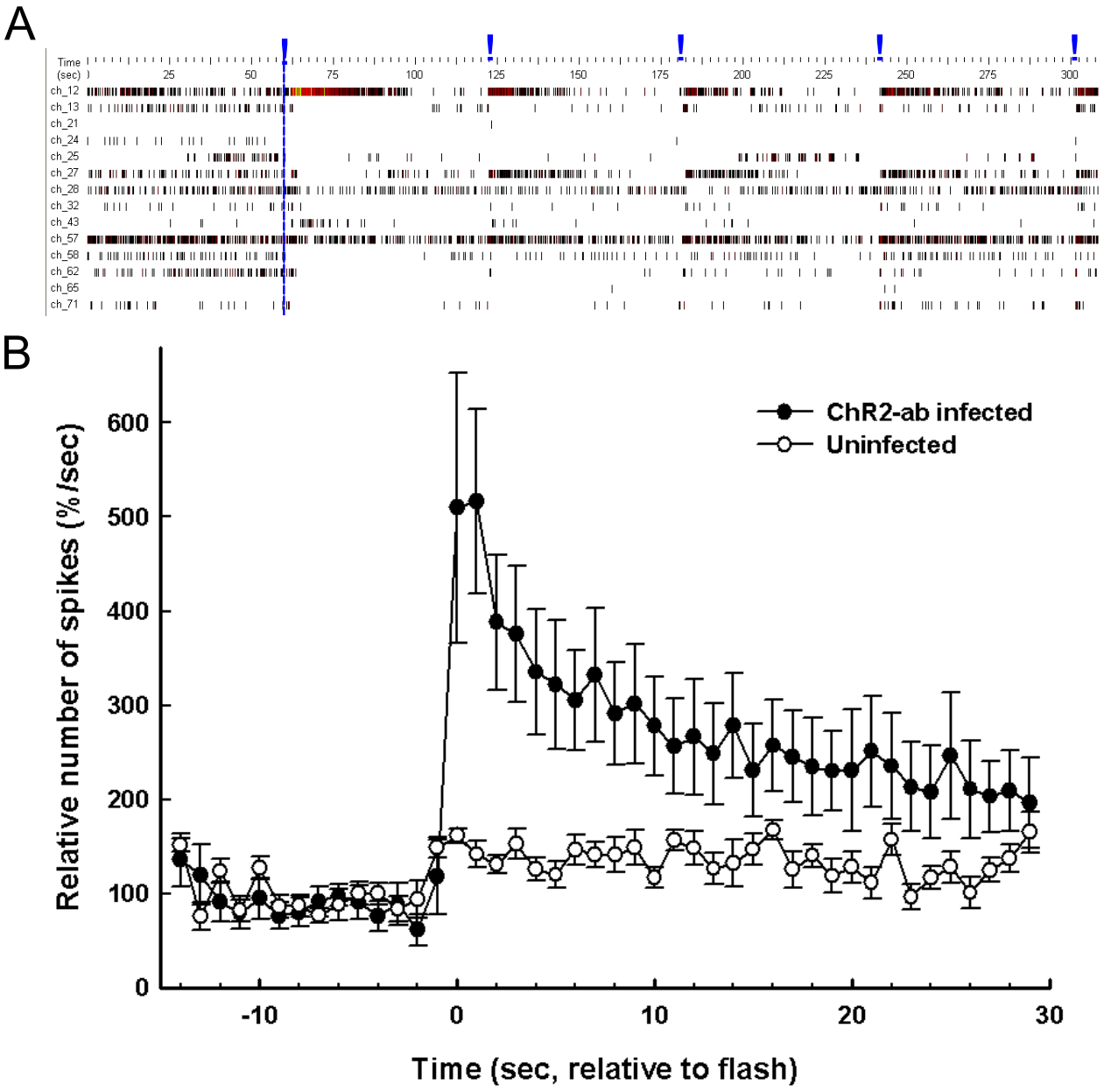

Figure 4.4: Bursts of spikes induced with blue light in ChR2-ab infected multi-electrode array (MEA) culture. Rat hippocampal neurons were cultured on MEA and recording was performed on DIV 10. As shown in (A), cells were illuminated every minute for 1 second with a fiber optic guided light from a blue LED. The blue line represents the first LED stimulation. Following blue dots above the graph indicate the 1 s light on every 60 seconds. The relative number of spikes was plotted against time. ChR2-ab infected culture (solid circle) responded robustly to light stimulation compared to uninfected condition (hollow circle). Time scale was adjusted to have light flash positioned at 0 point. Data from Dr. H Eckehard Freitag.

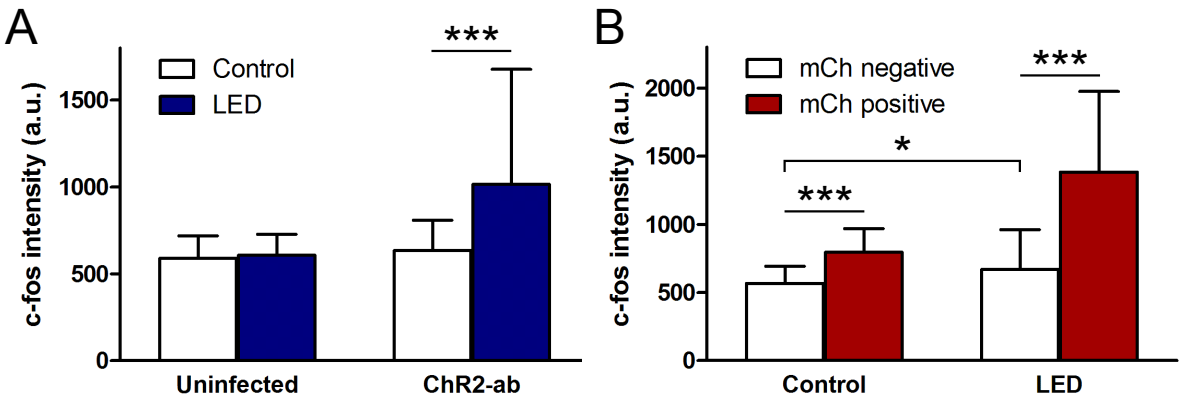

Figure 4.5: Blue light stimulation induced expression of c-fos in both infection positive and negative neurons in ChR2-ab-psd infected culture. (A) shows immunocytochemistry (ICC) analysis of c-fos protein level in uninfected and ChR2-ab infected groups with and without LED treatment. C-fos level is represented with the staining intensity in arbitrary unit (a.u.). C-fos increase was detected only in the infected condition with light stimulation. (B) represents c-fos level only from ChR2-ab infected conditions, with (LED) or without (Control) light treatment. Uninfected (mCh negative, blank bars) and ChR2-ab infected (mCh positive, red bars) cells in the same coverslip were analyzed separately. ChR2-ab expressing cells without light treatment already have higher level of c-fos staining and this was robustly induced with blue light stimulation. ChR2-ab negative cells in the LED treated condition also show significant higher level compared to those in un-illuminated condition.

References

[1] S. M. Aamodt and M. Constantine-Paton. The role of neural activity in synaptic development and its implications for adult brain function. *Adv Neurol*, 79:133–144, 1999.

[2] K. Abe. Neural activity-dependent regulation of gene expression in developing and mature neurons. *Dev Growth Differ*, 50(4):261–271, May 2008.

[3] C. M. Alberini. The role of protein synthesis during the labile phases of memory: revisiting the skepticism. *Neurobiol Learn Mem*, 89(3):234–246, Mar 2008.

[4] C. M. Alberini. Transcription factors in long-term memory and synaptic plasticity. *Physiol Rev*, 89(1):121–145, Jan 2009.

[5] M. Alsheimer, E. von Glasenapp, M. Schnolzer, H. Heid, and R. Benavente. Meiotic lamin C2: the unique amino-terminal hexapeptide GNAEGR is essential for nuclear envelope association. *Proc Natl Acad Sci U S A*, 97(24):13120–13125, Nov 2000.

[6] Z. Arany, D. Newsome, E. Oldread, D. M. Livingston, and R. Eckner. A family of transcriptional adaptor proteins targeted by the E1A oncoprotein. *Nature*, 374(6517):81–84, Mar 1995.

[7] B. R. Arenkiel, J. Peca, I. G. Davison, C. Feliciano, K. Deisseroth, G. J. Augustine, M. D. Ehlers, and G. Feng. In vivo light-induced activation of neural circuitry in transgenic mice expressing channelrhodopsin-2. *Neuron*, 54(2):205–218, Apr 2007.

[8] N. Axmacher, F. Mormann, G. FernÃ¡ndez, C. E. Elger, and J. Fell. Memory formation by neuronal synchronization. *Brain Res Rev*, 52(1):170–182, Aug 2006.

[9] H. Bading. Transcription-dependent neuronal plasticity the nuclear calcium hypothesis. *European Journal of Biochemistry*, 267(17):5280–5283, Sep 2000.

[10] C. Bamann, R. Gueta, S. Kleinlogel, G. Nagel, and E. Bamberg. Structural guidance of the photocycle of channelrhodopsin-2 by an interhelical hydrogen bond. *Biochemistry*, 49(2):267–278, Jan 2010.

[11] C. P. Bengtson and H. Bading. Nuclear calcium signaling. *Adv Exp Med Biol*, 970:377–405, 2012.

[12] A. Berndt, P. Schoenenberger, J. Mattis, K. M. Tye, K. Deisseroth, P. Hegemann, and T. G. Oertner. High-efficiency channelrhodopsins for fast neuronal stimulation at low light levels. *Proc Natl Acad Sci U S A*, 108(18):7595–7600, May 2011.

[13] A. Berndt, O. Yizhar, L. A. Gunaydin, P. Hegemann, and K. Deisseroth. Bi-stable neural state switches. *Nat Neurosci*, 12(2):229–234, Feb 2009.

[14] M. J. Berridge. Inositol trisphosphate and calcium signalling. *Nature*, 361(6410):315–325, Jan 1993.

[15] M. J. Berridge. Calcium signalling and cell proliferation. *Bioessays*, 17(6):491–500, Jun 1995.

[16] M. J. Berridge. Inositol trisphosphate and calcium signalling mechanisms. *Biochim Biophys Acta*, 1793(6):933–940, Jun 2009.

[17] M. J. Berridge, M. D. Bootman, and H. L. Roderick. Calcium signalling: dynamics, homeostasis and remodelling. *Nat Rev Mol Cell Biol*, 4(7):517–529, Jul 2003.

[18] M. J. Berridge, P. Lipp, and M. D. Bootman. The versatility and universality of calcium signalling. *Nature Reviews Molecular Cell Biology*, 1(1):11–21, Oct 2000.

[19] T. V. Bliss and G. L. Collingridge. A synaptic model of memory: long-term potentiation in the hippocampus. *Nature*, 361(6407):31–39, Jan 1993.

[20] T. V. Bliss and T. Lomo. Long-lasting potentiation of synaptic transmission in the dentate area of the anaesthetized rabbit following stimulation of the perforant path. *J Physiol*, 232(2):331–356, Jul 1973.

[21] A. Bonni, A. Brunet, A. E. West, S. R. Datta, M. A. Takasu, and M. E. Greenberg. Cell survival promoted by the Ras-MAPK signaling pathway by transcription-dependent and -independent mechanisms. *Science*, 286(5443):1358–1362, Nov 1999.

[22] R. Bourtchuladze, B. Frenguelli, J. Blendy, D. Cioffi, G. Schutz, and A. Silva. Deficient long-term memory in mice with a targeted mutation of the cAMP-responsive element-binding protein. *Cell*, 79(1):59–68, 1994.

[23] E. S. Boyden, F. Zhang, E. Bamberg, G. Nagel, and K. Deisseroth. Millisecond-timescale, genetically targeted optical control of neural activity. *Nature Neuroscience*, 8(9):1263–1268, Sep 2005.

[24] A. B. Brillantes, K. Ondrias, A. Scott, E. Kobrinsky, E. Ondriasová, M. C. Moschella, T. Jayaraman, M. Landers, B. E. Ehrlich, and A. R. Marks. Stabilization of calcium release channel (ryanodine receptor) function by FK506-binding protein. *Cell*, 77(4):513–523, May 1994.

[25] M. E. Cardenas and J. Heitman. Role of calcium in T-lymphocyte activation. *Advances in Second Messenger and Phosphoprotein Research*, 30:281–298, 1995.

[26] D. C. Chang and C. Meng. A localized elevation of cytosolic free calcium is associated with cytokinesis in the zebrafish embryo. *The Journal of Cell Biology*, 131(6 Pt 1):1539–1545, Dec 1995.

[27] S. Chawla and H. Bading. CREB/CBP and SRE-interacting transcriptional regulators are fast on-off switches: duration of calcium transients specifies the magnitude of transcriptional responses. *J Neurochem*, 79(4):849–858, Nov 2001.

[28] S. Chawla, G. E. Hardingham, D. R. Quinn, and H. Bading. CBP: a signal-regulated transcriptional coactivator controlled by nuclear calcium and CaM kinase IV. *Science*, 281(5382):1505–1509, Sep 1998.

[29] D. W. Choi. Glutamate neurotoxicity and diseases of the nervous system. *Neuron*, 1(8):623–634, Oct 1988.

[30] S. Chowdhury, J. D. Shepherd, H. Okuno, G. Lyford, R. S. Petralia, N. Plath, D. Kuhl, R. L. Huganir, and P. F. Worley. Arc/Arg3.1 interacts with the endocytic machinery to regulate AMPA receptor trafficking. *Neuron*, 52(3):445–459, Nov 2006.

[31] H. T. Cline. Dendritic arbor development and synaptogenesis. *Curr Opin Neurobiol*, 11(1):118–126, Feb 2001.

[32] S. Cohen and M. E. Greenberg. Communication between the synapse and the nucleus in neuronal development, plasticity, and disease. *Annu Rev Cell Dev Biol*, 24:183–209, 2008.

[33] S. F. Cooke and T. V. P. Bliss. Plasticity in the human central nervous system. *Brain*, 129(Pt 7):1659–1673, Jul 2006.

[34] D. A. Costa, J. R. Cracchiolo, A. D. Bachstetter, T. F. Hughes, K. R. Bales, S. M. Paul, R. F. Mervis, G. W. Arendash, and H. Potter. Enrichment improves cognition in AD mice by amyloid-related and unrelated mechanisms. *Neurobiol Aging*, 28(6):831–844, Jun 2007.

[35] J. R. Cottrell, G. R. DubÃ©, C. Egles, and G. Liu. Distribution, density, and clustering of functional glutamate receptors before and after synaptogenesis in hippocampal neurons. *J Neurophysiol*, 84(3):1573–1587, Sep 2000.

[36] F. H. Crick. Thinking about the brain. *Scientific American*, 241(3):219–232, Sep 1979.

[37] F. H. Cruzalegui and H. Bading. Calcium-regulated protein kinase cascades and their transcription factor targets. *Cellular and Molecular Life Sciences*, 57(3):402–410, Mar 2000.

[38] J. Ellenberg, E. D. Siggia, J. E. Moreira, C. L. Smith, J. F. Presley, H. J. Worman, and J. Lippincott-Schwartz. Nuclear membrane dynamics and reassembly in living cells: targeting of an inner nuclear membrane protein in interphase and mitosis. *J Cell Biol*, 138(6):1193–1206, Sep 1997.

[39] H. Enslen, P. Sun, D. Brickey, S. H. Soderling, E. Klamo, and T. R. Soderling. Characterization of Ca^{2+}/calmodulin-dependent protein kinase IV. Role in transcriptional regulation. *J Biol Chem*, 269(22):15520–15527, Jun 1994.

[40] S. W. Flavell and M. E. Greenberg. Signaling mechanisms linking neuronal activity to gene expression and plasticity of the nervous system. *Annu Rev Neurosci*, 31:563–590, 2008.

[41] J. K. Foskett, C. White, K.-H. Cheung, and D.-O. D. Mak. Inositol trisphosphate receptor Ca2+ release channels. *Physiol Rev*, 87(2):593–658, Apr 2007.

[42] D. Gall, F. Prestori, E. Sola, A. D'Errico, C. Roussel, L. Forti, P. Rossi, and E. D'Angelo. Intracellular calcium regulation by burst discharge determines bidirectional long-term synaptic plasticity at the cerebellum input stage. *J Neurosci*, 25(19):4813–4822, May 2005.

[43] J. Gariépy and R. S. Hodges. Primary sequence analysis and folding behavior of EF hands in relation to the mechanism of action of troponin C and calmodulin. *FEBS Lett*, 160(1-2):1–6, Aug 1983.

[44] A. Ghosh, D. D. Ginty, H. Bading, and M. E. Greenberg. Calcium regulation of gene expression in neuronal cells. *J Neurobiol*, 25(3):294–303, Mar 1994.

[45] M. D. Glitsch. Spontaneous neurotransmitter release and Ca2+–how spontaneous is spontaneous neurotransmitter release? *Cell Calcium*, 43(1):9–15, Jan 2008.

[46] N. Gogolla, I. Galimberti, Y. Deguchi, and P. Caroni. Wnt signaling mediates experience-related regulation of synapse numbers and mossy fiber connectivities in the adult hippocampus. *Neuron*, 62(4):510–525, May 2009.

[47] G. A. Gonzalez and M. R. Montminy. Cyclic AMP stimulates somatostatin gene transcription by phosphorylation of CREB at serine 133. *Cell*, 59(4):675–680, Nov 1989.

[48] I. Goshen, M. Brodsky, R. Prakash, J. Wallace, V. Gradinaru, C. Ramakrishnan, and K. Deisseroth. Dynamics of retrieval strategies for remote memories. *Cell*, 147(3):678–689, Oct 2011.

[49] V. Gradinaru, K. R. Thompson, F. Zhang, M. Mogri, K. Kay, M. B. Schneider, and K. Deisseroth. Targeting and readout strategies for fast optical neural control in vitro and in vivo. *J Neurosci*, 27(52):14231–14238, Dec 2007.

[50] U. F. Greber and L. Gerace. Depletion of calcium from the lumen of endoplasmic reticulum reversibly inhibits passive diffusion and signal-mediated transport into the nucleus. *J Cell Biol*, 128(1-2):5–14, Jan 1995.

[51] G. Grynkiewicz, M. Poenie, and R. Y. Tsien. A new generation of Ca^{2+} indicators with greatly improved fluorescence properties. *J Biol Chem*, 260(6):3440–3450, Mar 1985.

[52] L. A. Gunaydin, O. Yizhar, A. Berndt, V. S. Sohal, K. Deisseroth, and P. Hegemann. Ultrafast optogenetic control. *Nat Neurosci*, 13(3):387–392, Mar 2010.

[53] J. F. Guzowski, B. L. McNaughton, C. A. Barnes, and P. F. Worley. Environment-specific expression of the immediate-early gene Arc in hippocampal neuronal ensembles. *Nat Neurosci*, 2(12):1120–1124, Dec 1999.

[54] J. F. Guzowski and P. F. Worley. Cellular compartment analysis of temporal activity by fluorescence in situ hybridization (catFISH). *Current Protocols in Neuroscience*, Chapter 1:Unit 1.8, Aug 2001.

[55] A. M. Hagenston and H. Bading. Calcium signaling in synapse-to-nucleus communication. *Cold Spring Harb Perspect Biol*, 3(11):a004564, Nov 2011.

[56] G. E. Hardingham, F. J. Arnold, and H. Bading. A calcium microdomain near NMDA receptors: on switch for ERK-dependent synapse-to-nucleus communication. *Nat Neurosci*, 4(6):565–566, Jun 2001.

[57] G. E. Hardingham and H. Bading. Coupling of extrasynaptic NMDA receptors to a CREB shut-off pathway is developmentally regulated. *Biochim Biophys Acta*, 1600(1-2):148–153, Nov 2002.

[58] G. E. Hardingham and H. Bading. The Yin and Yang of NMDA receptor signalling. *Trends Neurosci*, 26(2):81–89, Feb 2003.

[59] G. E. Hardingham and H. Bading. Synaptic versus extrasynaptic NMDA receptor signalling: implications for neurodegenerative disorders. *Nat Rev Neurosci*, 11(10):682–696, Oct 2010.

[60] G. E. Hardingham, S. Chawla, F. H. Cruzalegui, and H. Bading. Control of recruitment and transcription-activating function of CBP determines gene regulation by NMDA receptors and L-type calcium channels. *Neuron*, 22(4):789–798, Apr 1999.

[61] G. E. Hardingham, S. Chawla, C. M. Johnson, and H. Bading. Distinct functions of nuclear and cytoplasmic calcium in the control of gene expression. *Nature*, 385(6613):260–265, Jan 1997.

[62] G. E. Hardingham, Y. Fukunaga, and H. Bading. Extrasynaptic NMDARs oppose synaptic NMDARs by triggering CREB shut-off and cell death pathways. *Nat Neurosci*, 5(5):405–414, May 2002.

[63] Y. Hayashi, M. M. Zviman, J. G. Brand, J. H. Teeter, and D. Restrepo. Measurement of membrane potential and [Ca^{2+}]i in cell ensembles: application to the study of glutamate taste in mice. *Biophys J*, 71(2):1057–1070, Aug 1996.

[64] M. Hieda, M. Isokane, M. Koizumi, C. Higashi, T. Tachibana, M. Shudou, T. Taguchi, Y. Hieda, and S. Higashiyama. Membrane-anchored growth factor, HB-EGF, on the cell surface targeted to the inner nuclear membrane. *J Cell Biol*, 180(4):763–769, Feb 2008.

[65] M. Hollmann and S. Heinemann. Cloned glutamate receptors. *Annu Rev Neurosci*, 17:31–108, 1994.

[66] Y.-S. Hu, P. Xu, G. Pigino, S. T. Brady, J. Larson, and O. Lazarov. Complex environment experience rescues impaired neurogenesis, enhances synaptic plasticity, and attenuates neuropathology in familial Alzheimer's disease-linked APPswe/PS1DeltaE9 mice. *FASEB J*, 24(6):1667–1681, Jun 2010.

[67] J. R. Hughes. Post-tetanic potentiation. *Physiol Rev*, 38(1):91–113, Jan 1958.

[68] C. Ikonomidou, F. Bosch, M. Miksa, P. Bittigau, J. Vöckler, K. Dikranian, T. I. Tenkova, V. Stefovska, L. Turski, and J. W. Olney. Blockade of NMDA receptors and apoptotic neurodegeneration in the developing brain. *Science*, 283(5398):70–74, Jan 1999.

[69] Inkscape Community. *Inkscape 0.48*, 2012.

[70] M. Isokane, M. Hieda, S. Hirakawa, M. Shudou, K. Nakashiro, K. Hashimoto, H. Hamakawa, and S. Higashiyama. Plasma-membrane-anchored growth factor pro-amphiregulin binds A-type lamin and regulates global transcription. *J Cell Sci*, 121(Pt 21):3608–3618, Nov 2008.

[71] JabRef Development Team. *JabRef*, 2013.

[72] J. L. Jankowsky, G. Xu, D. Fromholt, V. Gonzales, and D. R. Borchelt. Environmental enrichment exacerbates amyloid plaque formation in a transgenic mouse model of Alzheimer disease. *J Neuropathol Exp Neurol*, 62(12):1220–1227, Dec 2003.

[73] H. E. Kato, F. Zhang, O. Yizhar, C. Ramakrishnan, T. Nishizawa, K. Hirata, J. Ito, Y. Aita, T. Tsukazaki, S. Hayashi, P. Hegemann, A. D. Maturana, R. Ishitani, K. Deisseroth, and O. Nureki. Crystal structure of the channelrhodopsin light-gated cation channel. *Nature*, 482(7385):369–374, Feb 2012.

[74] S. Kleinlogel, K. Feldbauer, R. E. Dempski, H. Fotis, P. G. Wood, C. Bamann, and E. Bamberg. Ultra light-sensitive and fast neuronal activation with the Ca^{2+}-permeable channelrhodopsin CatCh. *Nat Neurosci*, 14(4):513–518, Apr 2011.

[75] M. Knobloch and I. M. Mansuy. Dendritic spine loss and synaptic alterations in Alzheimer's disease. *Mol Neurobiol*, 37(1):73–82, Feb 2008.

[76] T. Kono, K. T. Jones, A. Bos-Mikich, D. G. Whittingham, and J. Carroll. A cell cycle-associated change in Ca^{2+} releasing activity leads to the generation of Ca^{2+} transients in mouse embryos during the first mitotic division. *Journal of Cell Biology*, 132(5):915–923, Mar 1996.

[77] E. Korzus, M. G. Rosenfeld, and M. Mayford. CBP histone acetyltransferase activity is a critical component of memory consolidation. *Neuron*, 42(6):961–972, Jun 2004.

[78] R. P. Kwok, J. R. Lundblad, J. C. Chrivia, J. P. Richards, H. P. Bächinger, R. G. Brennan, S. G. Roberts, M. R. Green, and R. H. Goodman. Nuclear protein CBP is a coactivator for the transcription factor CREB. *Nature*, 370(6486):223–226, Jul 1994.

[79] A. Lanahan and P. Worley. Immediate-early genes and synaptic function. *Neurobiol Learn Mem*, 70(1-2):37–43, 1998.

[80] D. Lau and H. Bading. Synaptic activity-mediated suppression of p53 and induction of nuclear calcium-regulated neuroprotective genes promote survival through inhibition of mitochondrial permeability transition. *Journal of Neuroscience*, 29(14):4420–4429, Apr 2009.

[81] W. Li, J. Llopis, M. Whitney, G. Zlokarnik, and R. Y. Tsien. Cell-permeant caged InsP3 ester shows that Ca^{2+} spike frequency can optimize gene expression. *Nature*, 392(6679):936–941, Apr 1998.

[82] J. Y. Lin. A user's guide to channelrhodopsin variants: features, limitations and future developments. *Exp Physiol*, 96(1):19–25, Jan 2011.

[83] X. Liu, S. Ramirez, P. T. Pang, C. B. Puryear, A. Govindarajan, K. Deisseroth, and S. Tonegawa. Optogenetic stimulation of a hippocampal engram activates fear memory recall. *Nature*, 484(7394):381–385, Apr 2012.

[84] B. E. Lonze and D. D. Ginty. Function and regulation of CREB family transcription factors in the nervous system. *Neuron*, 35(4):605–623, Aug 2002.

[85] G. L. Lyford, K. Yamagata, W. E. Kaufmann, C. A. Barnes, L. K. Sanders, N. G. Copeland, D. J. Gilbert, N. A. Jenkins, A. A. Lanahan, and P. F. Worley. Arc, a growth factor and activity-regulated gene, encodes a novel cytoskeleton-associated protein that is enriched in neuronal dendrites. *Neuron*, 14(2):433–445, Feb 1995.

[86] G. Lynch, D. Muller, P. Seubert, and J. Larson. Long-term potentiation: persisting problems and recent results. *Brain Res Bull*, 21(3):363–372, Sep 1988.

[87] M. Maletic-Savatic, R. Malinow, and K. Svoboda. Rapid dendritic morphogenesis in CA1 hippocampal dendrites induced by synaptic activity. *Science*, 283(5409):1923–1927, Mar 1999.

[88] T. Mantamadiotis, T. Lemberger, S. C. Bleckmann, H. Kern, O. Kretz, A. Martin Villalba, F. Tronche, C. Kellendonk, D. Gau, J. Kapfhammer, C. Otto, W. Schmid, and G. Schütz. Disruption of CREB function in brain leads to neurodegeneration. *Nat Genet*, 31(1):47–54, May 2002.

[89] A. Matsuno-Yagi and Y. Mukohata. Two possible roles of bacteriorhodopsin; a comparative study of strains of Halobacterium halobium differing in pigmentation. *Biochem Biophys Res Commun*, 78(1):237–243, Sep 1977.

[90] R. P. Matthews, C. R. Guthrie, L. M. Wailes, X. Zhao, A. R. Means, and G. S. McKnight. Calcium/calmodulin-dependent protein kinase types II and IV differentially regulate CREB-dependent gene expression. *Mol Cell Biol*, 14(9):6107–6116, Sep 1994.

[91] T. J. McCown, X. Xiao, J. Li, G. R. Breese, and R. J. Samulski. Differential and persistent expression patterns of CNS gene transfer by an adeno-associated virus (AAV) vector. *Brain Research*, 713(1-2):99–107, Mar 1996.

[92] A. C. Meinema, J. K. Laba, R. A. Hapsari, R. Otten, F. A. A. Mulder, A. Kralt, G. van den Bogaart, C. P. Lusk, B. Poolman, and L. M. Veenhoff. Long unfolded linkers facilitate membrane protein import through the nuclear pore complex. *Science*, 333(6038):90–93, Jul 2011.

[93] G. A. Meyer and K. D. Radsak. Identification of a novel signal sequence that targets transmembrane proteins to the nuclear envelope inner membrane. *J Biol Chem*, 275(6):3857–3866, Feb 2000.

[94] K. Michelsen, V. Schmid, J. Metz, K. Heusser, U. Liebel, T. Schwede, A. Spang, and B. Schwappach. Novel cargo-binding site in the beta and delta subunits of coatomer. *J Cell Biol*, 179(2):209–217, Oct 2007.

[95] M. R. Montminy and L. M. Bilezikjian. Binding of a nuclear protein to the cyclic-AMP response element of the somatostatin gene. *Nature*, 328(6126):175–178, 1987.

[96] J. I. Morgan and T. Curran. Stimulus-transcription coupling in the nervous system: involvement of the inducible proto-oncogenes fos and jun. *Annu Rev Neurosci*, 14:421–451, 1991.

[97] G. Nagel, M. Brauner, J. F. Liewald, N. Adeishvili, E. Bamberg, and A. Gottschalk. Light activation of channelrhodopsin-2 in excitable cells of Caenorhabditis elegans triggers rapid behavioral responses. *Curr Biol*, 15(24):2279–2284, Dec 2005.

[98] G. Nagel, D. Ollig, M. Fuhrmann, S. Kateriya, A. M. Musti, E. Bamberg, and P. Hegemann. Channelrhodopsin-1: a light-gated proton channel in green algae. *Science*, 296(5577):2395–2398, Jun 2002.

[99] G. Nagel, T. Szellas, W. Huhn, S. Kateriya, N. Adeishvili, P. Berthold, D. Ollig, P. Hegemann, and E. Bamberg. Channelrhodopsin-2, a directly light-gated cation-selective membrane channel. *Proceedings of the National Academy of Sciences*, 100(24):13940–13945, Nov 2003.

[100] M. J. O'Connor, H. Zimmermann, S. Nielsen, H. U. Bernard, and T. Kouzarides. Characterization of an E1A-CBP interaction defines a novel transcriptional adapter motif (TRAM) in CBP/p300. *J Virol*, 73(5):3574–3581, May 1999.

[101] T. Ohba, E. C. Schirmer, T. Nishimoto, and L. Gerace. Energy- and temperature-dependent transport of integral proteins to the inner nuclear membrane via the nuclear pore. *J Cell Biol*, 167(6):1051–1062, Dec 2004.

[102] S.-i. Okamoto, M. A. Pouladi, M. Talantova, D. Yao, P. Xia, D. E. Ehrnhoefer, R. Zaidi, A. Clemente, M. Kaul, R. K. Graham, D. Zhang, H.-S. Vincent Chen, G. Tong, M. R. Hayden, and S. A. Lipton. Balance between synaptic versus extrasynaptic NMDA receptor activity influences inclusions and neurotoxicity of mutant huntingtin. *Nat Med*, 15(12):1407–1413, Dec 2009.

[103] H. Okuno. Regulation and function of immediate-early genes in the brain: beyond neuronal activity markers. *Neurosci Res*, 69(3):175–186, Mar 2011.

[104] A. L. Olins, G. Rhodes, D. B. M. Welch, M. Zwerger, and D. E. Olins. Lamin B receptor: multi-tasking at the nuclear envelope. *Nucleus*, 1(1):53–70, 2010.

[105] A. M. M. Oliveira, T. J. Hemstedt, and H. Bading. Rescue of aging-associated decline in Dnmt3a2 expression restores cognitive abilities. *Nat Neurosci*, 15(8):1111–1113, Aug 2012.

[106] S. Papadia, F. X. Soriano, F. Léveillé, M.-A. Martel, K. A. Dakin, H. H. Hansen, A. Kaindl, M. Sifringer, J. Fowler, V. Stefovska, G. McKenzie, M. Craigon, R. Corriveau, P. Ghazal, K. Horsburgh, B. A. Yankner, D. J. A. Wyllie, C. Ikonomidou, and G. E. Hardingham. Synaptic NMDA receptor activity boosts intrinsic antioxidant defenses. *Nat Neurosci*, 11(4):476–487, Apr 2008.

[107] S. Papadia, P. Stevenson, N. R. Hardingham, H. Bading, and G. E. Hardingham. Nuclear Ca2+ and the cAMP response element-binding protein family mediate a late phase of activity-dependent neuroprotection. *J Neurosci*, 25(17):4279–4287, Apr 2005.

[108] A. A. Penn and C. J. Shatz. Brain waves and brain wiring: the role of endogenous and sensory-driven neural activity in development. *Pediatr Res*, 45(4 Pt 1):447–458, Apr 1999.

[109] O. H. Petersen, O. V. Gerasimenko, J. V. Gerasimenko, H. Mogami, and A. V. Tepikin. The calcium store in the nuclear envelope. *Cell Calcium*, 23(2-3):87–90, 1998.

[110] B. Potier, F. Poindessous-Jazat, P. Dutar, and J. M. Billard. NMDA receptor activation in the aged rat hippocampus. *Experimental Gerontology*, 35(9-10):1185–1199, Dec 2000.

[111] K. Qing, C. Mah, J. Hansen, S. Zhou, V. Dwarki, and A. Srivastava. Human fibroblast growth factor receptor 1 is a co-receptor for infection by adeno-associated virus 2. *Nature Medicine*, 5(1):71–77, Jan 1999.

[112] E. Racker and W. Stoeckenius. Reconstitution of purple membrane vesicles catalyzing light-driven proton uptake and adenosine triphosphate formation. *J Biol Chem*, 249(2):662–663, Jan 1974.

[113] V. R. Rao, S. A. Pintchovski, J. Chin, C. L. Peebles, S. Mitra, and S. Finkbeiner. AMPA receptors regulate transcription of the plasticity-related immediate-early gene Arc. *Nat Neurosci*, 9(7):887–895, Jul 2006.

[114] L. Redmond, A. H. Kashani, and A. Ghosh. Calcium regulation of dendritic growth via CaM kinase IV and CREB-mediated transcription. *Neuron*, 34(6):999–1010, Jun 2002.

[115] E. M. Rial Verde, J. Lee-Osbourne, P. F. Worley, R. Malinow, and H. T. Cline. Increased expression of the immediate-early gene arc/arg3.1 reduces AMPA receptor-mediated synaptic transmission. *Neuron*, 52(3):461–474, Nov 2006.

[116] C. A. Ross, J. Meldolesi, T. A. Milner, T. Satoh, S. Supattapone, and S. H. Snyder. Inositol 1,4,5-trisphosphate receptor localized to endoplasmic reticulum in cerebellar Purkinje neurons. *Nature*, 339(6224):468–470, Jun 1989.

[117] C. A. Schneider, W. S. Rasband, and K. W. Eliceiri. NIH Image to ImageJ: 25 years of image analysis. *Nat Methods*, 9(7):671–675, Jul 2012.

[118] P. Schoenenberger, D. Gerosa, and T. G. Oertner. Temporal control of immediate early gene induction by light. *PLoS One*, 4(12):e8185, 2009.

[119] G. M. Shankar, B. L. Bloodgood, M. Townsend, D. M. Walsh, D. J. Selkoe, and B. L. Sabatini. Natural oligomers of the Alzheimer amyloid-beta protein induce reversible synapse loss by modulating an NMDA-type glutamate receptor-dependent signaling pathway. *The Journal of Neuroscience*, 27(11):2866–2875, Mar 2007.

[120] A. J. Shaywitz and M. E. Greenberg. CREB: a stimulus-induced transcription factor activated by a diverse array of extracellular signals. *Annual Review of Biochemistry*, 68:821–861, 1999.

[121] M. Sheng, M. A. Thompson, and M. E. Greenberg. CREB: a Ca^{2+}-regulated transcription factor phosphorylated by calmodulin-dependent kinases. *Science*, 252(5011):1427–1430, Jun 1991.

[122] J. D. Shepherd and M. F. Bear. New views of Arc, a master regulator of synaptic plasticity. *Nat Neurosci*, 14(3):279–284, Mar 2011.

[123] J. D. Shepherd, G. Rumbaugh, J. Wu, S. Chowdhury, N. Plath, D. Kuhl, R. L. Huganir, and P. F. Worley. Arc/Arg3.1 mediates homeostatic synaptic scaling of AMPA receptors. *Neuron*, 52(3):475–484, Nov 2006.

[124] O. Sineshchekov, K. Jung, and J. Spudich. Two rhodopsins mediate phototaxis to low-and high-intensity light in Chlamydomonas reinhardtii. *Proceedings of the National Academy of Sciences*, 99(13):8689, 2002.

[125] S. Smith and G. Blobel. The first membrane spanning region of the lamin B receptor is sufficient for sorting to the inner nuclear membrane. *J Cell Biol*, 120(3):631–637, Feb 1993.

[126] B. Soullam and H. J. Worman. The amino-terminal domain of the lamin B receptor is a nuclear envelope targeting signal. *J Cell Biol*, 120(5):1093–1100, Mar 1993.

[127] O. Steward, C. S. Wallace, G. L. Lyford, and P. F. Worley. Synaptic activation causes the mRNA for the IEG Arc to localize selectively near activated postsynaptic sites on dendrites. *Neuron*, 21(4):741–751, Oct 1998.

[128] C. Summerford, J. S. Bartlett, and R. J. Samulski. AlphaVbeta5 integrin: a co-receptor for adeno-associated virus type 2 infection. *Nature Medicine*, 5(1):78–82, Jan 1999.

[129] C. Summerford and R. J. Samulski. Membrane-associated heparan sulfate proteoglycan is a receptor for adeno-associated virus type 2 virions. *Journal of Virology*, 72(2):1438–1445, Feb 1998.

[130] P. Sun, H. Enslen, P. S. Myung, and R. A. Maurer. Differential activation of CREB by Ca^{2+}/calmodulin-dependent protein kinases type II and type IV involves phosphorylation of a site that negatively regulates activity. *Genes & development*, 8(21):2527–2539, Nov 1994.

[131] M. A. Sutton and E. M. Schuman. Dendritic protein synthesis, synaptic plasticity, and memory. *Cell*, 127(1):49–58, Oct 2006.

[132] T. Suzuki, K. Yamasaki, S. Fujita, K. Oda, M. Iseki, K. Yoshida, M. Watanabe, H. Daiyasu, H. Toh, E. Asamizu, S. Tabata, K. Miura, H. Fukuzawa, S. Nakamura, and T. Takahashi. Archaeal-type rhodopsins in Chlamydomonas: model structure and intracellular localization. *Biochemical and Biophysical Research Communications*, 301(3):711–717, Feb 2003.

[133] D. F. Swaab. Reactivation of atrophic neurons in Alzheimer's disease. *Neurological Research*, 25(6):652–660, Sep 2003.

[134] W. Tang, I. Ehrlich, S. B. E. Wolff, A.-M. Michalski, S. Wölfl, M. T. Hasan, A. Lüthi, and R. Sprengel. Faithful expression of multiple proteins via 2A-peptide self-processing: a versatile and reliable method for manipulating brain circuits. *J Neurosci*, 29(27):8621–8629, Jul 2009.

[135] R. D. Teasdale and M. R. Jackson. Signal-mediated sorting of membrane proteins between the endoplasmic reticulum and the golgi apparatus. *Annu Rev Cell Dev Biol*, 12:27–54, 1996.

[136] L. Tian, S. A. Hires, T. Mao, D. Huber, M. E. Chiappe, S. H. Chalasani, L. Petreanu, J. Akerboom, S. A. McKinney, E. R. Schreiter, C. I. Bargmann, V. Jayaraman, K. Svoboda, and L. L. Looger. Imaging neural activity in worms, flies and mice with improved GCaMP calcium indicators. *Nat Methods*, 6(12):875–881, Dec 2009.

[137] W. Tischmeyer and R. Grimm. Activation of immediate early genes and memory formation. *Cell Mol Life Sci*, 55(4):564–574, Apr 1999.

[138] K. R. Tovar and G. L. Westbrook. The incorporation of NMDA receptors with a distinct subunit composition at nascent hippocampal synapses in vitro. *J Neurosci*, 19(10):4180–4188, May 1999.

[139] P. Vanhoutte and H. Bading. Opposing roles of synaptic and extrasynaptic NMDA receptors in neuronal calcium signalling and BDNF gene regulation. *Current Opinion in Neurobiology*, 13(3):366–371, Jun 2003.

[140] A. Vasileva and R. Jessberger. Precise hit: adeno-associated virus in gene targeting. *Nature Reviews Microbiology*, 3(11):837–847, Nov 2005.

[141] M. Vasiljevic, F. F. Heisler, T. J. Hausrat, S. Fehr, I. Milenkovic, M. Kneussel, and W. Sieghart. Spatio-temporal expression analysis of the calcium-binding protein calumenin in the rodent brain. *Neuroscience*, 202:29–41, Jan 2012.

[142] A. Vazdarjanova, B. L. McNaughton, C. A. Barnes, P. F. Worley, and J. F. Guzowski. Experience-dependent coincident expression of the effector immediate-early genes arc and Homer 1a in hippocampal and neocortical neuronal networks. *J Neurosci*, 22(23):10067–10071, Dec 2002.

[143] N. Venable, V. Fernández, E. Díaz, and T. Pinto-Hamuy. Effects of preweaning environmental enrichment on basilar dendrites of pyramidal neurons in occipital cortex: a Golgi study. *Brain Res Dev Brain Res*, 49(1):140–144, Sep 1989.

[144] J. Wang, B. Campos, G. Jamieson, Jr, M. A. Kaetzel, and J. R. Dedman. Functional elimination of calmodulin within the nucleus by targeted expression of an inhibitor peptide. *J Biol Chem*, 270(51):30245–30248, Dec 1995.

[145] T. N. Wiesel. Postnatal development of the visual cortex and the influence of environment. *Nature*, 299(5884):583–591, Oct 1982.

[146] Z. H. Yao, J. J. Zhang, and X. F. Xie. Enriched environment prevents cognitive impairment and tau hyperphosphorylation after chronic cerebral hypoperfusion. *Curr Neurovasc Res*, 9(3):176–184, Aug 2012.

[147] O. Yizhar, L. E. Fenno, T. J. Davidson, M. Mogri, and K. Deisseroth. Optogenetics in neural systems. *Neuron*, 71(1):9–34, Jul 2011.

[148] Y. Yoshida and S. Imai. Structure and function of inositol 1,4,5-trisphosphate receptor. *Jpn J Pharmacol*, 74(2):125–137, Jun 1997.

[149] D. Young, P. A. Lawlor, P. Leone, M. Dragunow, and M. J. During. Environmental enrichment inhibits spontaneous apoptosis, prevents seizures and is neuroprotective. *Nat Med*, 5(4):448–453, Apr 1999.

[150] X. Yu and R. C. Malenka. Beta-catenin is critical for dendritic morphogenesis. *Nat Neurosci*, 6(11):1169–1177, Nov 2003.

[151] R. Yuste and T. Bonhoeffer. Morphological changes in dendritic spines associated with long-term synaptic plasticity. *Annu Rev Neurosci*, 24:1071–1089, 2001.

[152] N. Zerangue, M. J. Malan, S. R. Fried, P. F. Dazin, Y. N. Jan, L. Y. Jan, and B. Schwappach. Analysis of endoplasmic reticulum trafficking signals by combinatorial screening in mammalian cells. *Proc Natl Acad Sci U S A*, 98(5):2431–2436, Feb 2001.

[153] N. Zerangue, B. Schwappach, Y. N. Jan, and L. Y. Jan. A new ER trafficking signal regulates the subunit stoichiometry of plasma membrane K(ATP) channels. *Neuron*, 22(3):537–548, Mar 1999.

[154] F. Zhang, L.-P. Wang, E. S. Boyden, and K. Deisseroth. Channelrhodopsin-2 and optical control of excitable cells. *Nat Methods*, 3(10):785–792, Oct 2006.

[155] L. I. Zhang and M. M. Poo. Electrical activity and development of neural circuits. *Nat Neurosci*, 4 Suppl:1207–1214, Nov 2001.

[156] S.-J. Zhang, M. N. Steijaert, D. Lau, G. Schätz, C. Delucinge-Vivier, P. Descombes, and H. Bading. Decoding NMDA receptor signaling: identification of genomic programs specifying neuronal survival and death. *Neuron*, 53(4):549–562, Feb 2007.

[157] S.-J. Zhang, M. Zou, L. Lu, D. Lau, D. A. W. Ditzel, C. Delucinge-Vivier, Y. Aso, P. Descombes, and H. Bading. Nuclear calcium signaling controls expression of a large gene pool: identification of a gene program for acquired neuroprotection induced by synaptic activity. *PLoS Genet*, 5(8):e1000604, Aug 2009.

[158] J.-P. Zhao and M. Constantine-Paton. NR2A$^{-/-}$ mice lack long-term potentiation but retain NMDA receptor and L-type Ca^{2+} channel-dependent long-term depression in the juvenile superior colliculus. *J Neurosci*, 27(50):13649–13654, Dec 2007.

[159] F. Zorzato, J. Fujii, K. Otsu, M. Phillips, N. M. Green, F. A. Lai, G. Meissner, and D. H. MacLennan. Molecular cloning of cDNA encoding human and rabbit forms of the Ca^{2+} release channel (ryanodine receptor) of skeletal muscle sarcoplasmic reticulum. *J Biol Chem*, 265(4):2244–2256, Feb 1990.

[160] R. S. Zucker. Calcium- and activity-dependent synaptic plasticity. *Curr Opin Neurobiol*, 9(3):305–313, Jun 1999.